AN EXPERIMENTAL AND MODELING STUDY OF THE PHOTOCHEMICAL OZONE REACTIVITY OF ACETONE

Final Report to

Chemical Manufacturers Association
Contract No. KET-ACE-CRC-2.0

by

William P. L. Carter,
Dongmin Luo, Irina L. Malkina and John A. Pirece

December 10, 1993

Statewide Air Pollution Research Center, and
College of Engineering Center for Environmental Research and Technology
University of California
Riverside, California 92521

SUMMARY

A series of environmental chamber experiments and computer model simulations were carried out to assess the tendency of acetone to promote ozone formation in photochemical smog. The experiments consisted of NO_x - air photolysis of acetone by itself, and determinations of the effect of adding acetone on ozone formation in model photochemical smog systems. Indoor chambers using either fluorescent blacklight or xenon arc light sources and an outdoor chamber utilizing sunlight were employed. Similar experiments utilizing acetaldehyde were carried out for comparison and control purposes. The gas-phase photochemical mechanism for the atmospheric reactions of acetone was updated and was evaluated by model simulations of the results of these experiments. The mechanism was found to overpredict the effect of acetone on ozone formation and radical levels in the indoor chamber experiments with the blacklight light source and in some of the outdoor chamber runs, but fit the results of other outdoor chamber runs and the experiments runs using the xenon arc light source reasonably well. An adjusted mechanism which gave better agreement with the blacklight experiments and with some of the outdoor runs was developed.

The updated and adjusted acetone mechanisms were then used in model calculations to assess the effects of acetone on ozone formation under atmospheric conditions. This was done by calculating its incremental reactivity (defined as amount of additional ozone formed caused by adding acetone to the emissions, divided by the amount added) in model scenarios representing ozone episodes in 39 urban areas around the United States. The incremental reactivities of ethane and a mixture representing total emissions reactive organic gases from all sources were also calculated for comparison. The results indicate that acetone forms 10-15% as much ozone on a per mass basis as total ROG emissions, while ethane forms 6-20% as much ozone, depending on conditions. The implications of these results on the question of whether acetone should be exempt from regulation as an ozone precursor are discussed.

ACKNOWLEDGEMENTS AND DISCLAIMERS

The authors wish to acknowledge and thank our project officer, Dr. David Morgott of Eastman Kodak Co. for many helpful discussions and his support of this work. We also acknowledge Mr. William Long for valuable assistance in carrying out the experiments, Mr. Ken Sasaki for assistance in developing the outdoor chamber light model, Mr. Dennis Fitz for assisting in the management of this program and reviewing parts of this report, Ms. Kathalena Smihula, Mr. Armando Avallone, Mr. Patrick Sekera, and Mr. Jeff Friend for assisting in carrying out the experiments, and to Dr. Joseph Norbeck, the director of the College of Engineering, Center for Environmental Research and Technology, for supporting the student assistants working on this program and for providing some of the equipment which was used.

The experiments with acetone were funded by the CMA in part through providing support to Coordinating Research Council Project No. ME-9, and in part through Contract No. KET-ACE-CRC-2.0. Some of the base case and control experiments used in the data analysis and modeling for this program were obtained under funding from the California Air Resources Board Contract No. A032-0692 and Coordinated Research Council Project No. ME-9. In addition, the xenon arc light source used in this study was funded by the National Renewable Energy Laboratory through Contract No. XZ-2-12075-1, and the modular building where most of the experiments were conducted were provided by the California South Coast Air Quality Management District through Contract No. C91323. We wish to thank these agencies for their support of our programs.

The opinions and conclusions in this report are entirely those of the primary author, Dr. William P. L. Carter. Mention of trade names or commercial products do not constitute endorsement or recommendation for use.

EXECUTIVE SUMMARY

Background

Photochemical ozone formation is caused by the gas phase reactions of volatile organic compounds (VOCs) with oxides of nitrogen (NO_x) in the presence of sunlight. To reduce ground level ozone and achieve air quality standards, emissions of both NO_x and VOCs are subject to controls. However, VOCs are not equal in the amount of ozone formation they cause. If a VOC can be shown to make a negligible contribution to ozone formation when it is emitted into the atmosphere, the United States Environmental Protection Agency (EPA) can exempt it from regulation as an ozone precursor. Although the EPA has no formal policy as to what constitutes "negligible" reactivity, it has the informal policy of using the reactivity of ethane as the standard because ethane is the most rapidly reacting of the compounds which has already been exempted. Thus if a compound forms comparable or less ozone on a per gram emitted basis than ethane it can be considered for exemption.

Acetone is an important solvent species which reacts sufficiently slowly that it might reasonably be considered as a candidate for exemption. Its net atmospheric reaction rate, on a mass basis, has been estimated to be slightly less than that of ethane. However, the rate at which a VOC reacts is not the only factor which determine its effect on ozone. Unlike ethane, acetone undergoes photodecomposition in the atmosphere to form radicals, and increasing radical levels tends to cause increased rates of ozone formation from the other VOCs present. If this effect were sufficiently important, it would mean that acetone would cause more ozone formation than ethane.

The most direct quantitative measure of the degree to which a VOC contributes to ozone formation in a photochemical air pollution episode is its "incremental reactivity" for that episode. This is defined as the amount of additional ozone formation resulting from the addition of a small amount of the VOC to the emissions in the episode, divided by the amount of compound added. This measure of reactivity takes into account all of the factors by which a VOC affects ozone formation, including the effect of the environment where the VOC reacts. The latter is important because the amount of ozone formation caused by the reactions of a VOC depends significantly on how much NO_x is present.

We have previously investigated methods for ranking photochemical reactivities of various VOCs by calculating incremental reactivities of different VOCs under varying NO_x conditions in model scenarios representing various urban areas in the United States. Depending on the NO_x conditions used, acetone was calculated to be of comparable or greater reactivity than ethane. However, the chemical mechanism used for acetone in these calculations has not been adequately experimentally verified, and thus it would

not be appropriate to use these previous results as a basis for deciding whether it is appropriate to exempt acetone from regulation as an ozone precursor.

This report describes a study designed to provide experimental data necessary to test and improve the reliability of the atmospheric chemical mechanism for acetone, and then use the experimentally-verified mechanism to re-evaluate the atmospheric reactivity of acetone relative to those of ethane and other VOCs.

Experimental Approach

A number of different types of environmental chamber experiments were carried out to evaluate various aspects of acetone's atmospheric reaction mechanism. These are summarized below:

Acetone - NO_x experiments consisted of irradiations where acetone was the only compound present in sufficient quantities to form ozone. This provides the simplest and most direct test of acetone's mechanisms. For control purposes, similar experiments were carried out using acetaldehyde instead of acetone.

Incremental Reactivity experiments consisted of irradiations, in the presence of NO_x, of a reactive organic gas (ROG) "surrogate" mixture designed to represent ROG pollutants in ambient air, alternating (or simultaneously) with irradiations of the same mixture with varying amounts of acetone added. This provides the most direct test of a mechanism's ability to simulate acetone's incremental reactivity. For control purposes, similar experiments were carried out using acetaldehyde. In addition, relevant results of incremental reactivity experiments with ethane, carried out in a previous study, are also summarized in this report.

Experiments with varying light sources were carried out to test the mechanism for acetone under varying lighting conditions. This is important because one of the main factors affecting acetone's reactivity is the fact that it undergoes photolysis. The light sources used were blacklights, xenon arc lights, and (in outdoor chamber experiments) natural sunlight.

Direct acetone vs ethane comparison experiments consisted of irradiations of a ROG surrogate - NO_x mixture with added acetone simultaneously with irradiations of the same mixture with a comparable amount of added ethane on the other side. Although such experiments do not necessarily indicate the relative reactivity of acetone and ethane in the atmosphere (because incremental reactivities depend on conditions, and conditions in the chamber are different than in the atmosphere), they were conducted to provide a comparison with similar experiments carried out at the University of North Carolina.

Chemical Mechanism Development

As part of this work, we also re-examined the literature concerning the atmospheric reactions of acetone. The mechanism for its reaction with OH radicals was modified to be consistent with recent laboratory results. The experimental data from which acetone's photolysis quantum yields were derived were evaluated and modeled, and some corrections were made based on the results of this analysis. The resulting updated mechanism predicted a slightly lower reactivity for acetone in the atmosphere than the one used previously. This updated mechanism was then evaluated by conducting model simulations of the experiments discussed above.

Experimental and Mechanism Evaluation Results

The updated mechanism was found to simulate reasonably well the results of the experiments using the indoor chamber light source most closely resembling sunlight and the outdoor chamber runs that were conducted during the summer. However, this mechanism consistently overpredicted the rate of ozone formation in the blacklight chamber experiments and also overpredicted the ozone formation in the wintertime acetone - NO_x run in the outdoor chamber. It is unlikely that this is due to incorrect characterization of the blacklight intensity or spectra, because the model provides good simulations of the photochemical reactivity of acetaldehyde, a VOC that photolyzes in a similar wavelength region as acetone. Thus, it appears likely that the problem is that the model incorrectly represents how the acetone photolysis quantum yields depend on wavelength.

An adjusted version of the updated acetone mechanism was developed that was considerably more successful in simulating the experiments conducted in this study. The adjustment involves assuming that the quantum yields fall off with increasing wavelength much more rapidly than indicated in previous work, but that the fall off begins at a slightly longer wavelength. Although this adjustment is not theoretically unreasonable, there is no basis for it other than fitting these environmental chamber data, which are highly complex chemical systems with a number of other potential sources of error. The possibility that the problem may be due to an incorrect characterization of the effect of the mercury lines in the blacklight light source cannot be entirely ruled out. Therefore, in the assessment of the reactivities of acetone in the atmosphere, we have used both the unadjusted (or standard) and the adjusted acetone mechanism in the model calculations.

Atmospheric Reactivity Calculations

The adjusted and unadjusted updated acetone mechanisms were then used in model calculation to assess the effects of acetone on ozone formation under atmospheric conditions. The incremental reactivity of acetone, ethane, and the base ROG mixture (the mixture representing the sum of all VOCs emitted into the atmosphere) were calculated in model scenarios representing ozone episodes in 39 urban areas throughout the United States. It was found that the adjustment to the acetone quantum yields to fit our chamber data caused an approximately 13% reduction in its incremental reactivity calculated for these

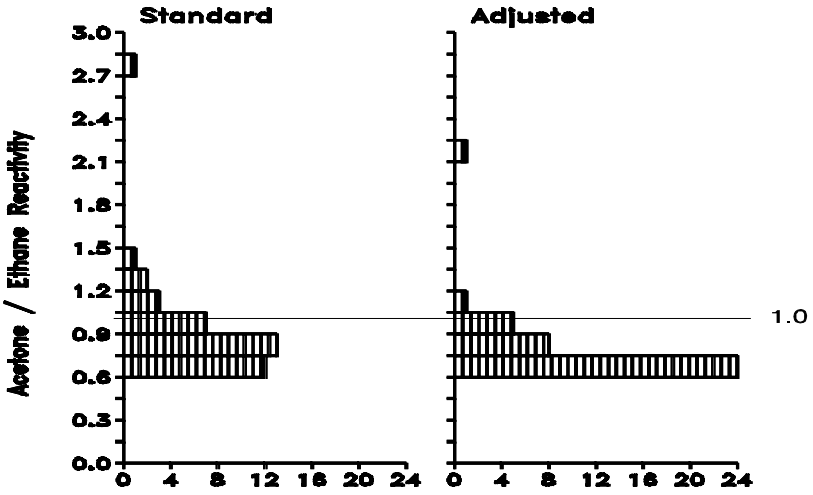

Figure EX-1. Distribution plots of incremental reactivities of acetone (standard and adjusted mechanisms) relative to ethane. Based on O_3 yields per gram VOC.

model scenarios. This is a relatively small effect compared to the extent to which the relative reactivity of acetone varied with atmospheric conditions. Thus, it is concluded that, although there are uncertainties in acetone's quantum yields, the effect of this uncertainty is not so large that it should substantively affect conclusions concerning the range of acetone's effect on ozone production under conditions represented by the model scenarios we employed.

Figure EX-1 shows distribution plots of the reactivity of acetone relative to that of ethane in the 39 scenarios, where reactivity is quantified by yield of ozone formed per gram of VOC emitted. The acetone/ethane reactivity ratio can be seen to vary among the scenarios, though in a majority of cases acetone is slightly less reactive than ethane. However, in one scenario, which represents unusually high NO_x conditions, acetone was calculated to be 2-3 times more reactive than ethane, depending on which acetone mechanism was used. As discussed below, this is due entirely to the unusually low reactivity of ethane in that scenario.

A more relevant measure of reactivity in control strategy applications is the incremental reactivity of the VOC relative to that of the sum of all ROG emissions, or the "relative reactivity". Distribution plots of the relative reactivities of acetone and ethane are shown in Figure EX-2. When looked at this way, it can be seen that the relative reactivity of ethane is far more variable than that of acetone. Thus the variability of the acetone/ethane ratio can be attributed almost entirely to the variability of the reactivity of ethane. For example, the scenario with the unusually high acetone/ethane ratio has the lowest relative reactivity for ethane but a near-average value for acetone. While the relative reactivity for ethane is as high as 0.24 under some circumstances, it is never higher than 0.18 for acetone, even

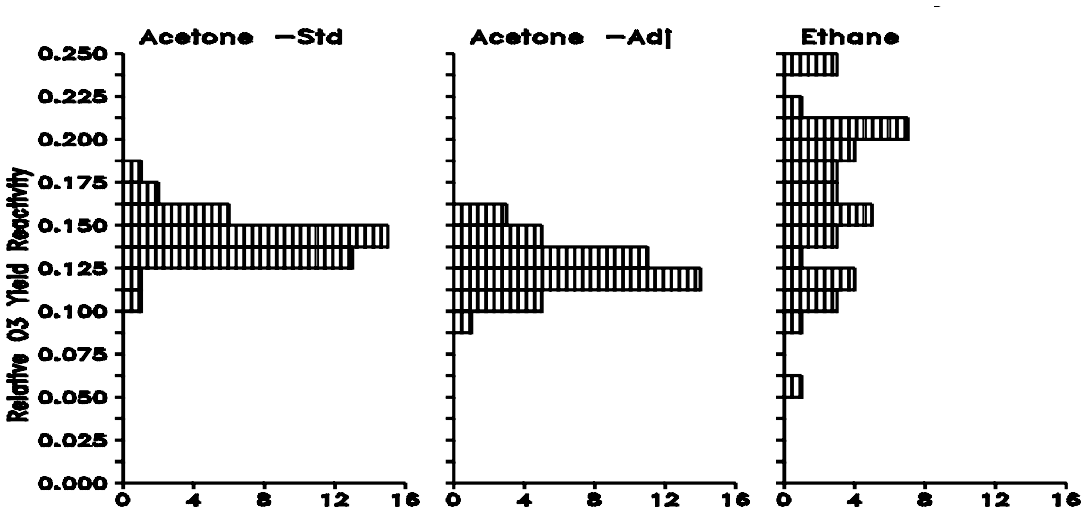

Figure EX-2. Distribution plots of relative reactivities of acetone and ethane. Based on O_3 yields per gram VOC.

using the more reactive standard mechanism for acetone. Conversely, while the relative reactivity for ethane is as low as 0.05, it is never lower than 0.11 for acetone using the standard mechanism. Thus, the relative reactivity range of acetone falls entirely within the range for ethane.

Conclusions

Although there are uncertainties in acetone's atmospheric photooxidation mechanism, the experiments and model simulations carried out in this work indicate that these uncertainties are not large enough to substantially affect conclusions concerning acetone's ozone formation potential relative to ethane or other VOCs. The standard and the adjusted acetone mechanisms can be thought of as giving respectively the upper and the lower estimates of acetone's likely reactivity in any particular scenario. The differences between these two estimates were small compared to the variability of acetone's relative reactivity from scenario to scenario.

The difference in acetone's reactivity relative to ethane was also found to be less than the variability of their relative reactivities from scenario to scenario. This variability is due more to the variability of the reactivity of ethane with scenario conditions than that for acetone. On this basis, it can be concluded the acetone and ethane can be considered to have essentially the same reactivity to within their variability with environmental conditions.

We recommend, however, that a comparison of the reactivities of acetone and ethane not be used as the sole basis for determining whether acetone should be exempt from regulation as an ozone precursor. In considering whether a compound should be exempt, it is appropriate to assess its reactivity relative to

the mixture of all VOC emissions. When EPA decided to exempt ethane, it effectively decided that it was not necessary to regulate emissions of a VOC that could be almost 25% as reactive as the average of all VOC emissions in terms of peak ozone concentrations, and almost 20% as reactive in terms of effect on integrated ozone over the ambient ozone standard. When looked at this way, exempting a compound that is calculated to be no more than 20% as reactive in terms of peak ozone, or 15% as reactive in terms of integrated ozone over the standard, does not appear to be an inconsistent policy.

TABLE OF CONTENTS

LIST OF TABLES

LIST OF FIGURES

INTRODUCTION

Background

Photochemical ozone formation is caused by the gas phase reactions of volatile organic compounds (VOCs) with oxides of nitrogen (NO_x) emitted into the atmosphere. To reduce ground level ozone and achieve air quality standards, emissions of both NO_x and VOCs are subject to controls. However, VOCs are not equal in the amount of ozone formation they cause. If a VOC can be shown to make a negligible contribution to ozone formation when it is emitted into the atmosphere, the United States Environmental Protection Agency (EPA) can exempt it from regulation as an ozone precursor. Although the EPA has no formal policy as to what constitutes "negligible" reactivity, it has the informal policy of using the reactivity of ethane as the standard because ethane is the most rapidly reacting of the compounds which has already been exempted. Thus if a compound forms comparable or less ozone on a per gram emitted basis than ethane it can be considered for exemption. The bases for the decisions to exempt ethane but not compounds more reactive than it has not been made clear, and they are probably largely subjective. However, the existing precedent provides a guideline for evaluating possible exemption of additional compounds which is relatively straightforward as long as the candidate compound is not of comparable reactivity as ethane.

Acetone is an important solvent species which reacts fairly slowly in the atmosphere, and thus might reasonably be considered as a candidate for exemption. Exempting acetone from regulation as an ozone precursor would encourage its substitution for more reactive solvent species such as toluene, and permit its use as a replacement for ozone depleters and greenhouse gases such as CFC-11, methyl chloroform and methylene chloride (Eastman Chemical and Hoechst Celanese, 1993). Acetone is also an example of a VOC which might be considered to have comparable reactivity as ethane. Meyrahn et al. (1986) estimated the average annual atmospheric half life of acetone to be 22 days, which can be compared to 25 days calculated for ethane for the same conditions. Acetone reacts with OH radicals ~15% slower than ethane (Atkinson, 1989), but unlike ethane it is also consumed by photolysis, resulting in an overall half life which is essentially the same as that for ethane to within the uncertainties of the estimates. However, acetone has a higher molecular weight than ethane, which means that fewer molecules of acetone react per unit mass emitted. This makes acetone slightly less reactive than ethane by this standard. Thus acetone would be a viable candidate for exemption by the ethane standard if the only criterion used is the rate the compounds react in the atmosphere.

However, the rate at which a VOC reacts in the atmosphere is only one of several factors which determines its effect on ozone formation (Carter and Atkinson, 1989; Carter, 1991, 1993a,b; Carter et al., 1993a,b; Jeffries and Crouse, 1991). Other factors include the amount of ozone formed once a VOC

reacts, the effect of the VOC's reactions on the reactions of other VOCs, and the effects of the reactions of the VOC's reaction products. (Carter and Atkinson, 1989; Carter et al., 1993a,b). For example, if a VOC's reactions (or those of its products) tend to promote radical levels in the atmosphere, then they would increase the rates of reactions of all the VOCs present, and the rate of ozone formation from these reactions. Because acetone photolysis is expected to form radicals (Atkinson, 1990; Meyrahn et al., 1986, and references therein), acetone may have a greater effect on ozone than expected based on its reaction rate alone.

The most direct quantitative measure of the degree to which a VOC contributes to ozone formation in a photochemical air pollution episode is its "incremental reactivity" for that episode. This is defined as the amount of additional ozone formation resulting from the addition of a small amount of the VOC to the emissions in the episode, divided by the amount of compound added. This measure of reactivity takes into account all of the factors by which a VOC affects ozone formation, including the effect of the environment where the VOC reacts. The latter is important because the amount of ozone formation caused by the reactions of a VOC depends significantly on how much NO_x is present. If NO_x is absent, no ozone is formed and all VOCs have incremental reactivities of zero. Under low NO_x conditions, ozone is NO_x-limited, and aspects of a VOCs mechanism affecting NO_x removal rates are important in affecting incremental reactivity. Under sufficiently high NO_x conditions, ozone yields are determined by how rapidly ozone is formed, and therefore aspects of the mechanism affecting overall radical levels tend to be highly important.

Methods for ranking photochemical reactivities of various VOCs have been investigated by calculating incremental reactivities of different VOCs under varying NO_x conditions in model scenarios representing 39 different urban ozone non-attainment areas in the United States (Carter, 1991; 1993a,b). Several different incremental reactivity scales were developed, based on different NO_x conditions and different methods for measuring O_3 impacts. These include the Maximum Incremental Reactivity (MIR) scale, which reflects effects of VOCs on ozone yields under relatively high NO_x conditions where VOCs have their greatest effect on ozone, and the Maximum Ozone Incremental Reactivity (MOIR) scale, which reflects effects of VOCs on ozone yields under the somewhat lower NO_x conditions which are optimum for formation of peak ozone concentrations. In addition, various "base case" reactivity scales were developed to reflect (using various averaging or weighting methods) the distribution of incremental reactivities under the varying NO_x conditions associated with the different urban areas. These tended to give similar rankings as the MIR or MOIR scales, depending on the derivation or ozone quantification method used (Carter, 1991; 1993a,b).

The incremental reactivity of acetone (in terms of ozone per gram) was previously calculated to be slightly less than that of ethane in the MOIR scale, but was 2-3 times greater than that of ethane in the MIR scale. Thus the calculations indicate that the reactivity of acetone relative to ethane depends on NO_x

conditions (Carter, 1993a,b). However, this factor of 2-3 maximum difference in reactivity is not large considering that some VOCs are calculated to have MIR reactivities greater than 40 times that of ethane, and that the calculated emissions-weighted average MIR reactivity of all VOCs is ~12 times that of ethane on a per gram basis (Carter, 1993a,b).

It is important to recognize that these reactivity calculations for acetone were based on a chemical mechanism for acetone which had not been experimentally verified. The chemical mechanism used to calculate the MIR amd MOIR scales (Carter, 1990) was tested using a variety of smog chamber experiments (Carter and Lurmann, 1991), but only one poorly-characterized outdoor chamber run was relevant for testing the mechanism for acetone, and the mechanism significantly overpredicted the amount of ozone which was formed. No reasonable adjustment of the acetone mechanism within its uncertainty range would permit that acetone experiment to be adequately simulated (unpublished results from this laboratory). Thus the predictions of this mechanism was not consistent with the limited data which was available.

To provide data needed to improve the reliability of assessments of the reactivity of acetone with respect to ozone, the Chemical Manufacturers Association (CMA) contracted us to carry out environmental chamber experiments to measure the incremental reactivity of acetone, to provide data needed to test and improve the reliability of the gas-phase atmospheric chemical mechanism for acetone. A second objective was then to use the experimentally verified mechanism to assess the incremental reactivity of acetone under atmospheric conditions, and in particular its incremental reactivity relative to that of ethane. The results of this study is documented in this report.

Approach

Three types of environmental chamber experiments with acetone were conducted for this study. These are acetone - NO_x experiments, acetone incremental reactivity experiments, and direct acetone vs ethane comparison runs. For comparison and control purposes, we also carried out acetaldehyde - NO_x experiments and incremental reactivity experiments for acetaldehyde, and include in our analysis results of incremental reactivity experiments for ethane which were carried out previously (Carter et al., 1993a). The utility of each are briefly described below.

Acetone - NO_x Experiments

Acetone - NO_x experiments consist of irradiations where acetone is the only reactive organic present in sufficient quantities to significantly affect ozone. In most experiments, low levels (less than ~10 ppb) of tracer species — usually cyclohexane or n-octane — are also present to monitor OH radical levels from their relative rates of decay. These experiments test the acetone mechanism in the absence of complications due to uncertainties in mechanisms for the other VOCs. However, it is not a realistic representation of the chemical environment when acetone reacts in typical ambient atmospheres.

Such experiments do not test the ability of the mechanism to predict the effects of acetone on ozone formation caused by the reactions of the other VOCs present in the atmosphere.

Incremental Reactivity Experiments

Incremental reactivity experiments consist of irradiations of a reactive organic gas (ROG) "surrogate" - NO_x air mixture, alternating (or simultaneously) with irradiations of the same mixture with varying amounts of a test compound such as acetone added. The ROG surrogate - NO_x mixture is designed to approximate the chemical environment in polluted ambient atmospheres, and the irradiation of this mixture without the added test compound is referred to as the "base case" experiment. The experiment where acetone or some other test VOC is added is referred to as the "test" run. The difference between ozone formation and NO oxidation in the test run relative to that in the base case run, divided by the amount of test compound added, is the experimental incremental reactivity. Note that "experimental" incremental reactivity refers to the effect of adding a finite amount of VOC, while incremental reactivity in airshed model calculations refers to the effect of the VOC at the limit as the amount added approaches zero (Carter and Atkinson, 1989). In addition, it should be emphasized that since incremental reactivities are dependent on environmental conditions, and since it is not practical to duplicate in the chamber all the environmental factors which might affect magnitudes of incremental reactivities, incremental reactivities measured in chamber experiments should not be assumed to be quantitatively the same as incremental reactivities in the atmosphere (Carter and Atkinson, 1989). The latter can only be estimated using computer airshed model calculations. The utility of incremental reactivity experiments is that they provide the most direct available means to test of the mechanism's ability to predict incremental reactivities in such calculations.

The "ROG surrogate" is the mixture of reactive organic compounds (ROGs) designed to represent the more complex mixture of ROGs which are present in polluted atmospheres. Three types of ROG surrogates were used in this study: the "mini-surrogate", the "lumped molecule" or "full" surrogate, and the "ethene surrogate". Each have their own sets of advantages and disadvantages, as discussed below.

The Mini-Surrogate is a 3-component mixture consisting of 35% (as carbon) ethene, 50% n-hexane, and 15% m-xylene. This was designed to be an experimentally simple representative of the reactive organic compounds emitted into the atmosphere. Although this mini-surrogate is a significant oversimplification of the complex mixture of ROGs present in the atmosphere (see, for example, Jeffries et al. 1989a), model calculations show that use of this simpler mixture provides a more sensitive measure of reactivities than use of more complex mixtures. In addition to having experimental simplicity while representing the three major classes of emitted hydrocarbons, this surrogate has the advantage of having a large data base of reactivity experiments for other VOCs using this surrogate (see Carter et al, 1993a).

The Full Surrogate is an 8-component mixture which is designed to represent the ROGs present in the atmosphere in as much chemical detail they are represented in the airshed model simulations of their reactions in the atmosphere. Airshed models which represent chemistry at the molecular level [i.e., models other than those using the Carbon Bond mechanisms (Gery et al. 1988)] generally use the following groupings of model species to represent ROG emissions: (1) less reactive alkanes such as n-butane; (2) more reactive alkanes such as n-octane; (3) ethene; (4) terminal alkenes such as propene; (5) internal alkenes such as the 2-butenes; (6) less reactive aromatics such as toluene; (7) more reactive aromatics such as xylenes; (8) formaldehyde; (9) higher aldehydes such as acetaldehyde; and (10) ketones such as methylethyl ketone. Except as indicated below, this surrogate uses a single "real" compound to represent each of these model species. The selected representative compound for each group is generally the one whose mechanism is used to represent that group because it dominates the group or because it is the compound for which there is the most environmental chamber data available to test its mechanism.

Based on the amounts of model species which would be used to represent ambient base ROG mixture utilized to calculate the MIR reactivity scale for the CARB (CARB, 1991; Carter, 1993a,b), the target composition for the full surrogate (as carbon fractions) is: n-butane, 28%; n-octane, 18%; ethene, 27%; propene, 3%; trans-2-butene, 4%; toluene, 9%; m-xylene, 13%; formaldehyde, 1.6%; and 20% inert carbon. (The "inert carbon" is not actually added, but is used when computing the equivalent amount of ambient mixture the surrogate represents.) A separate species is not used for ketones because of their relatively small contribution to the total reactivity of the mixture, and formaldehyde is used to represent all aldehydes in the mixture (on a molar basis) because this substitution simplified the experiments and was calculated not to have a measurable effect on the incremental reactivity results. Thus the 0.8% formaldehyde + 1.5% acetaldehyde carbon is replaced by 1.6% formaldehyde. Model calculations indicate that use of this surrogate in reactivity experiments would give indistinguishable results in reactivity experiments as using full complex ambient mixtures (Carter, 1992). Thus this surrogate has the obvious advantage of being the most realistic, while having the disadvantage of being the most complex to model.

The Ethene surrogate consists of ethene alone. It is designed to be the simplest possible "ROG surrogate" which can be used in reactivity calculations. A simple surrogate is advantageous because its use should introduce the fewest uncertainties when evaluating the ability of a chemical mechanism to predict experimental incremental reactivities. This is because errors in the model for the base ROG surrogate can introduce extraneous or compensating errors in model simulations of experimental reactivity measurements. To be suitable for this purpose, a compound or mixture (1) must have a reasonably well characterized mechanism; (2) must react to form radicals which convert NO to NO_2, (3) must provide internal radical sources which are comparable in magnitude to those from complex mixtures; and (4) should not be completely consumed before the experiment is completed. Ethene appears to be the best candidate in this regard because it has a reasonably well characterized mechanism, has sufficient (but not excessively high) internal radical sources, and because it reacts sufficiently slowly that it is not consumed

during an experiment. In addition, model calculations predict that using ethene as an ROG surrogate would yield almost the same reactivities as using the 3-component mini-surrogate, except under highly NO_x-limited conditions (Carter, 1992).

The incremental reactivity experiments were carried out under NO_x conditions similar to those used to calculate the MIR scale. Thus they are referred to as "maximum reactivity" experiments. These are NO_x conditions where the VOCs have the greatest effect on ozone formation. In addition to providing the most direct test of the ability of a model to predict maximum incremental reactivities, these experiments provide a more sensitive test of the mechanism than experiments with lower NO_x which are less sensitive to the effects of the added VOC. In this study, the NO_x levels employed were ~0.5 ppm. The levels of the base ROG surrogate depended on the surrogate, but were such that ozone formation was still occurring by the end experiments, indicating that NO_x has not been completely consumed.

Acetaldehyde Experiments

For control and comparison purposes, the various types of experiments discussed above were also carried out using acetaldehyde as the test compound. Acetaldehyde is a useful VOC for which to compare the results with acetone because, like acetone, it is photoreactive and forms PAN as the major product in both its OH radical and photolysis reactions (Atkinson, 1990, 1993). It can also be monitored reliably and with reasonably good precision in our experiments. If the model performs as poorly in simulating both acetone and acetaldehyde experiments, it may indicate that the problem is with the base case model or the model for experimental conditions. If, on the other hand, the model performs well in simulating results with one but not the other, it may indicate that problem is with the particular compound which is poorly simulated.

Acetone vs Ethane Reactivity Comparisons

Since one of the objectives of this study is to evaluate whether acetone or ethane forms more ozone in the atmosphere, an obvious type of experiment is to determine the effects of equal amounts of acetone and ethane on ozone formation under the same conditions. However, the effects of VOCs on ozone formation are known to be highly dependent on the conditions in which they react (Dodge, 1984; Carter and Atkinson, 1989; Carter, 1991, 1993a,b; Jeffries and Crouse, 1991). Because of this, if the results of such experiments are to be used to make any conclusions concerning relative reactivities in the atmosphere, the experiments need to duplicate, as closely as possible (and perhaps more closely than practical) the conditions of the atmosphere. Even then, the results would be only applicable to the specific sets of conditions being simulated.

The type of chamber experiment that would most closely duplicate atmospheric conditions would be an incremental reactivity experiment in an outdoor chamber using a fully representative ROG surrogate. Such an experiment was carried using the University of North Carolina dual outdoor chamber (Jeffries,

1993). In that experiment, a mixture consisting of a detailed surrogate + NO_x + an amount of ethane equal to the surrogate on a carbon basis was irradiated simultaneously with equal amounts (on a carbon basis) of surrogate + NO_x + acetone. The run was carried out under low ROG/NO_x conditions. The result was that there was no measurable difference in ozone formation on either side. This might be largely because the amounts of ethane and acetone added were too small to cause a very large effect on the system in the first place, so what was being measured is a difference between two small effects. This run illustrates the small effects both of these compounds have on ozone, and the inconsequential effects of any differences in their reactivities.

Because of the interest expressed by the EPA in this type of experiment (Dimitriades, 1993), we decided to carry out a limited number of such experiments for this program. The main difference is that the ethane and acetone were compared on an equal mass rather than an equal carbon basis, since VOCs are regulated on the basis of mass. The amount of added ethane was such that it had an equal amount of carbons as carbons being represented by the full surrogate (including inert carbons), and the amount of added acetone was such that it had the same mass as the added ethane. Note that because of its greater molecular weight per carbon, the amount of added acetone was 22% lower on a carbon basis than the amount of added ethane.

Experiments with Varying Light Sources

One of the main factors affecting acetone's reactivity is the fact that it undergoes photolysis. Because of this, the nature of the light source used in the environmental chamber experiments will be important. The approach used in this study was to conduct chamber experiments utilizing three different light sources, each with their own unique advantages and disadvantages as discussed below. This provides a much more comprehensive test for the atmospheric reaction mechanism for acetone, and particularly the representation for its photolysis, than would be the case had only a single type of light source been used.

The initial experiments for this study were carried out in chambers employing fluorescent blacklights as the light source. Blacklights have the advantages of being a highly reproducible and easily characterized light source which provides, at relatively low cost, the appropriate light intensity in the UV region where most atmospheric species photolyze. Because of this, it has been utilized as the light source for a large number of environmental chamber experiments which have been used for mechanism evaluation (Carter and Lurmann, 1990, 1991, and references therein), including, most recently, experimental measurements of maximum incremental reactivities of a wide variety of VOCs (Carter et al., 1993a).

Figure 1 shows the solar and blacklight spectra in the wavelength region which affects most photolysis rates in the atmosphere. The action spectra (absorption cross sections x quantum yields) for

NO_2, acetone, and several other representative species are shown for comparison. The light source spectra are all normalized to yield the same NO_2 photolysis rate. While blacklights have the appropriate short wavelength cutoff, it has higher intensity relative to sunlight in the ~330-360 nm region, and much lower intensity at wavelengths greater than ~380 nm, where NO_3 radicals and α-dicarbonyls photolyze. These differences can be corrected for in model simulations of the experiments if the absorption cross sections and quantum yields of the relevant photolyzable species are accurately known.

However, if there are uncertainties in the relevant absorption cross sections or quantum yields, these will be corresponding uncertainties in the ability of the model to appropriately correct for these differences. This is particularly important when evaluating mechanisms for photolyzable species such as acetone. For this reason, several acetone - NO_x, acetone reactivity, and acetaldehyde experiments were carried out in an outdoor chamber using natural sunlight as the light source. Although the representative-ness of the light source is obviously not a problem, the intensity and spectrum changes with time during an experiment, making such experiments more difficult to characterize for quantitative mechanism evaluation purposes. Time-varying temperature also makes such runs more difficult to characterize, especially since some chamber effects are believed to be temperature dependent (Carter and Lurmann, 1990, 1991). Therefore, the evaluation of mechanisms using outdoor chamber data is more qualitative than quantitative. However, if there are major errors in the representation of photolysis reactions in a model which make its predictions grossly inapplicable to atmospheric lighting conditions, they should become apparent when simulating such runs.

Another approach which can be used to evaluate mechanisms for photoreactive species is to conduct indoor chamber experiments using a light source which is more representative of sunlight. This could potentially provide the best features of both indoor and outdoor runs. The best commercially available artificial light source we could find to approximate sunlight is xenon arc lights (Carter and Walters, 1992). As shown on Figure 1, they provide a reasonably good (though not perfect) simulation of sunlight throughout the entire wavelength region where most atmospheric species photolyze. For this reason, we acquired, under DOE funding, a set of xenon arc lights, and constructed an environmental chamber using them. Several acetone - NO_x and acetaldehyde - NO_x runs were conducted using this light source.

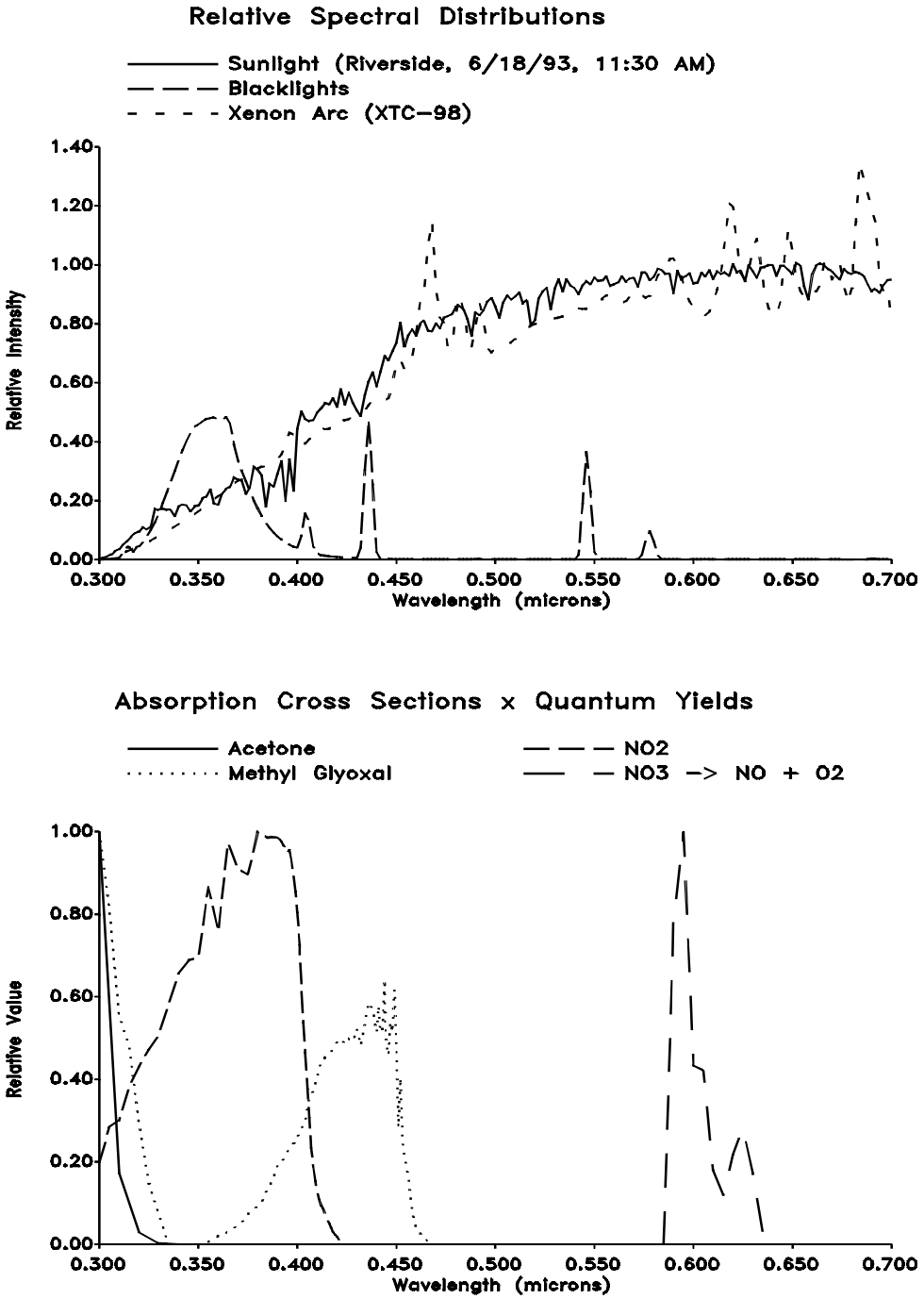

Figure 1. Top Plot shows comparison of spectra of light sources used in the environmental chamber studies. Bottom plot shows spectra of absorption cross sections x quantum yields for selected photoreactive species.

EXPERIMENTAL METHODS

Environmental Chambers

As discussed above, the experiments were carried out using four different environmental chambers using three different types of light sources. These are described in this section.

ETC Blacklight Chamber

This chamber is the same as that utilized in the study documented by Carter et al. (1993a), and is described in greater detail there. It consists of a single ~3000-liter, 2-mil thick FEP Teflon reaction bag fitted inside an aluminum frame with banks of blacklights on the top and bottom, each bank consisting of 30 Sylvania 40-W BL blacklamps. Reflective aluminum paneling is used on all sides. The temperature is controlled by the laboratory air conditioning and fans which exchange the air around the reaction bag with the air in the laboratory. Heaters are used prior to turning the lights on to minimize the temperature rise which occurs when the lights are turned on. For runs prior to ETC-323, dry pure air for the experiments was provided using the SAPRC air purification system which was described in detail previously (Doyle et al., 1977). For subsequent runs, after the chamber was moved to a different location, the dry pure air was supplied using an AADCO air purification system. This AADCO was also used to supply the pure air for the other chambers described below.

DTC Blacklight Chamber (Dividable Teflon Chamber)

This chamber, which was newly constructed during the period of this study for use in place of the ETC, is actually two adjacent chambers which can be operated simultaneously using the same light source and temperature control system. These are referred to as the two "sides" of the chamber (Side A and Side B) in the discussion of the results. The DTC consists of two 4600-liter 8’ x 6’ x 4’ 2-mil thick FEP Teflon reaction bags in an 8’ x 8’ chamber enclosure room. The bags are interconnected with two ports each with Teflon-coated fans and blowers which rapidly exchange their contents to assure that reactants which are desired to have equal concentrations in each are equalized. The fans also mix the contents within each chamber. The ports can then be closed to allow separate injections on each side, and separate monitoring of each. The chamber enclosure room has two banks of blacklights on opposing walls, with polished aluminum reflective material on the other walls and floor, and with perforated aluminum reflective material on the ceiling, through which cooling air can be forced. Specially constructed shaped aluminized plastic reflectors are used for the blacklights. The lighting system was found to provide so much intensity that only half the lights were used in these runs. A thermostatted temperature control system controlling a dedicated air conditioner for the chamber enclosure maintains the temperature to within ±1˚ C and minimizes the sudden temperature rise which would otherwise occur when the lights are turned on. The AADCO air purification system supplies pure dry air for this chamber.

This chamber would be expected to provide similar types of data as the ETC because it is constructed of the same material, utilizes the same type of lights, and has approximately the same light intensity. However, its dual chamber construction is particularly well suited for reactivity experiments, with the base case irradiation being conducted simultaneously with the added test compound experiment utilizing the same initial base case reactant concentrations and the same temperature profile and light intensity. Alternatively, two different experiments can be conducted simultaneously.

Outdoor Teflon Chamber (OTC)

The SAPRC OTC, which has been described in detail elsewhere (Carter et al., 1984, 1986), consists of a ~30,000-50,000-liter, 2-mil thick FEP Teflon, pillow-shaped reaction bag located outdoors. The reaction bag is supported by nylon ropes on a framework and held 2.5 feet off the ground to allow air circulation under the chamber. A green indoor-outdoor carpet is located under the chamber. When the chamber contents are not being irradiated, the reaction bag is covered by an opaque, grey trap attached to a dual framework of steel tubing which can be readily opened to uncover the chamber and initiate the irradiation. The AADCO air purification system supplies pure dry air for this chamber.

This chamber can be operated in a dual mode to allow two parallel experiments under the same lighting and temperature conditions. This division of the chamber into two separate reactors, which can be accomplished after reactants common to both chamber sides are injected and mixed, is accomplished by means of three 1 1/4-in diameter cast-iron pipes, which are surrounded by foam to protect the Teflon reactor. The reaction bag is divided by raising the lower pipe and placing it tightly between the upper pipes, then rotating them by 180 degrees. Previous tests have shown that this forms a tight seal, with the exchange between the chamber sides being less than 0.1% per hour (Carter et al., 1981). The chamber is oriented such that the pipes dividing the chamber run in a north-south direction, with side A, by convention, always being on the eastern half of the chamber. All OTC experiments discussed here were conducted with the chamber in the divided mode.

Xenon Teflon Chamber (XTC)

This chamber, which was completed near the end of the time period of this study, is similar in size and construction of one of the DTC chambers, but differs in the nature of the light source. The XTC consists of a ~5200-liter, 6’ x 8’ x 4’ 2-mil thick FEP Teflon reaction bag located on one end of a 8’ x 10’ chamber enclosure with reflective walls, floor and ceiling, and has a set of four Atlas RM-65A 6.5 kw Xenon arc lights mounted on the opposite wall. The design objectives for this chamber and lighting system is described elsewhere (Carter and Walters, 1992). It actually uses the same enclosure as the DTC chambers, but in a different configuration. The side walls are the molded aluminized plastic reflectors for the blacklights used for the DTC, with the blacklights removed. Sliding aluminum paneling are used to prevent the Xenon lights from irradiating the chamber when they are being turned on and stabilizing. AADCO air purification system supplies pure dry air for this chamber.

Experimental Procedures and Analytical Methods

The chambers were flushed with dry purified air for 6-9 hours on the nights before the experiments. The monitors were connected prior to reactant injection and the data system began logging data from the continuous monitoring systems. The reactants were injected as described previously (Carter et al, 1993a). For dual chamber (DTC or OTC) runs, the common reactants were injected in both sides simultaneously (using a "T" in the injection line) and were well mixed before the chamber was divided. In the case of the OTC, the reactants were mixed by manual agitation of the reaction bag, while with the DTC the contents of side A were blown into side B and vise-versa using two separate blowers. Fans were used to mix the reactants in the indoor chambers during the injection period, but these were turned off prior to the irradiation. Dividing the OTC consisted of clamping the reaction bag in two using pipes, while "dividing" the DTC consisted of closing the ports which connected the two reaction sides. After the OTC or DTC were divided, the reactants for specific sides were injected and mixed. The irradiation began by turning on the lights (for the blacklight chambers), opening the cover (for the OTC), or slighting back the panels in front of the Xenon lights (which were turned on ~30 minutes previously). The irradiation proceeded for 6 hours. After the run, the contents of the chamber(s) were emptied (by allowing the bag to collapse) and flushed with purified air.

Ozone and nitrogen oxides were continuously monitored using commercially available continuous analyzers with Teflon and borosilicate glass sample lines inserted directly into the chambers (ca 18 in.). For DTC and OTC chamber runs, the sampling lines from each half of the chamber were connected to solenoids which switched from side to side every 10 minutes, so the instruments alternately collected data from each side. Ozone was monitored using a Dasibi Model 1003AH UV photometric ozone analyzer and NO and total oxides of nitrogen (including HNO_3 and organic nitrates) were monitored using either a Columbia Model 1600 or a Teco Model 14B or 43 chemiluminescent NO/NO_x monitor. The output of these instruments, along with that from the temperature and (for OTC and XTC runs) light sensors were attached to a computer data acquisition system, which recorded the data at periodical intervals, using 30 second averaging times. For single mode (ETC or XTC) chamber runs, the O_3, NO_x, and other continuous data recorded every 15 minutes; for the divided chamber (DTC or OTC) runs, the data was collected every 10 minutes, yielding a sampling interval of 20 minutes for taking data from each side.

Organic reactants other than formaldehyde were measured by gas chromatography with FID detection as described elsewhere (Carter et al., 1993a). GC samples were taken for analysis at intervals from fifteen minutes to one hour using 100 ml gas-tight glass syringes. These samples were taken from ports directly connected to the chamber. The syringes were flushed with the chamber contents several times before taking the sample for analysis.

Formaldehyde was monitored using a diffusion scrubber system based on the design of Dasgupta and co-workers (Dasgupta et al, 1988, 1990; Dong and Dasgupta, 1987), as described elsewhere (Carter

et al., 1993a). This system alternately collected data in sample (30 minutes), zero (15 minutes), and calibrate mode (15 minutes), for a one hour cycle time. The readings at the end of the time period for each mode, averaged for 30 seconds, were recorded on the computer data acquisition system, which subsequently processed the data to apply the calibration and zero corrections. A separate sampling line from the chamber was used for the formaldehyde analysis. For the DTC or OTC, a solenoid, which was separate from the one used for O_3 and NO_x sampling, was used to select the chamber side from which the formaldehyde sample was withdrawn, which alternated every 15 minutes. This yielded formaldehyde data as frequently as every 15 minutes for single chamber (ETC and XTC) runs, and every 30 minutes for each side of DTC and OTC runs.

Characterization Methods

Temperature

For the blacklight chambers, the temperature was monitored using an unshielded thermocouple inside the chamber. Subsequent comparison of temperatures monitored with this method with simultaneous readings using the aspirated temperature probe (discussed below) gave results which were within ±0.2°C, indicating that heating of the thermocouple by the light from the blacklights is small. This is expected because of the low visible and infrared energy of those lights. The temperature in the ETC and DTC runs were typically 26-30˚C.

Prior to run XTC-090 the temperature was monitored in the XTC chamber using a thermocouple inside the chamber shielded by a piece of reflective aluminum. During that period temperature probes were also located in the formaldehyde and NO_x/O_3 sampling lines, but these data were not considered to be as reliable because the sensors were outside the chamber. Although the temperature readings in the sample lines were higher than the temperature in the laboratory, they tended to decrease with time during the run, while the probes inside the chamber indicated that the temperature was increasing slightly. Following run XTC-090, the temperature was monitored with the thermocouple inside an opaque 1/4" OD sample line inside the chamber, with air being drawn through at a rate of 2 l/min. This is referred to as the aspirated temperature probe. Provided that the flow rate past the sensor is sufficient, this method is considered to give the more accurate temperature reading. Tests showed that a flow rate of be at least 2 l/min was required for the measured temperature to be independent of the flow. Comparison of the data taken simultaneously indicated that the shielded probe in the chamber gave readings which were ~1.5˚C higher than the aspirated shielded probe.

Except for run XTC-083, the temperatures monitored during XTC runs were highly consistent, increasing rapidly from room temperature to 28-30° C immediately after the lights are turned on, to 29-31° C by the end of the runs. For some reason, the temperature probe in the chamber gave readings which were ~2 degrees higher for run XTC-083, though separate temperature probes in the sampling lines indicated no differences between the temperature in that run and the others. For that reason, and the fact

that the temperatures were consistent from run to run for the other runs, we believe that the measured readings were probably unreliable for that run.

An analogous change in temperature monitoring method was made for the outdoor chamber experiments. For the runs in 1992 (run OTC-270 and earlier), temperature was monitored using unshielded probes inside each chamber side, while for the other runs reported here (Runs OTC-271 and later) temperature was monitored by shielded probes in the sample line, located slightly outside and underneath the chamber.

Light Intensity and Spectra

The light intensity in the ETC and DTC was monitored by periodic NO_2 actinometry experiments utilizing the quartz tube method of Zafonte et al (1977), with the data analysis method modified as discussed by Carter et al. (1993a). The measurements were made either with the quartz tube in the reaction bag or with a Teflon film sleeve around the tube so the results would incorporate the effect of the light passing through the chamber walls. Based on the results of these runs, the NO_2 photolysis rate associated with the blacklight chamber runs were as follows:

- ETC-243 through ETC-247 and associated base case runs: 0.32 ± 0.02 min^{-1}.
- ETC-445: 0.336 ± 0.012 min^{-1}.
- All DTC runs: 0.38 ± 0.02 min^{-1}.

The relative spectral distributions of the blacklight light sources were measured using a LiCor LI-1800 portable spectrometer. The spectrum did not vary significantly with the chamber used or the age of the lights, and the spectra taken using the LiCor using these chambers were essentially the same as spectra of the lights in the SAPRC ITC chamber using a different spectrometer (Carter et al., 1984).

The light characterization for the XTC chamber was similar to that for the blacklight chambers, with the absolute intensity being determined by NO_2 actinometry using the quartz tube method, and the relative spectra being determined by measurements using the Li-1800 spectrometer. However, the spectra of xenon arc lights are expected to change gradually as the lights age, so spectra were taken 3-4 times during each XTC run.

The NO_2 photolysis rates measured by actinometry inside the XTC chamber was found to be 0.24-0.26 min^{-1} after the lights were first installed (run XTC-79), and declined to a constant value of 0.23 min^{-1} in subsequent determinations (runs XTC-89 and XTC-100). The relative change in NO_2 photolysis rate with time during the experiments could also be obtained from the absolute light intensities measured by the LiCor spectrometer. These data indicated that the NO_2 photolysis rates declined by ~3% between runs XTC-80 and around XTC-85, and was essentially constant after that. Based on the precision of the initial actinometry results, the NO_2 photolysis rates measured in the XTC are estimated to be uncertain by ~5%.

The sunlight intensity for the outdoor chamber runs was monitored continuously using an Eppley UV radiometer and an Eppley PSP total broadband radiometer, and the global and diffuse light spectra were measured approximately hourly during the runs using the LiCor spectrometer. The global spectrum is that obtained with the unshaded instrument, while the diffuse spectrum is that obtained by shading the sensor with a 10.0 cm disk held 90 cm from the sensor, positioned so that the shadow of the disk covers the sensor (Jeffries, personal communication; Jeffries et al., 1989b). These data were used as input to a light model, discussed later in this report, to calculate light intensity and spectra as a function of time during the runs.

Dilution

Dilution due to sampling is expected to be small because the flexible reaction bags can collapse as sample is withdrawn for analysis. However, some dilution occasionally occurs because of small leaks, and several XTC runs had larger than usual dilution due to a larger leak which was subsequently found and repaired. Information concerning dilution in an experiment can be obtained from relative rates of decay of added VOCs which react with OH radicals with differing rate constants (Carter et al., 1993a). All experiments had a more reactive compound (such as m-xylene or n-octane) present either as a reactant or added in trace amounts to monitor OH radical levels. Trace amounts (~0.1 ppm) of n-butane was added to experiments if needed to provide a less reactive compound for the purposes of monitoring dilution. In many experiments, dilution rates were zero within the uncertainties of the determinations.

Control Experiments

Several types of control experiments were conducted to characterize chamber conditions. Ozone decay rate measurements were conducted with new reactors, and the results were generally consistent with ozone decays observed in other Teflon bag reactors (Carter et. al. 1984, 1986). NO_x-air irradiations with trace amounts of propene or isobutene, or n-butane-NO_x-air experiments, were conducted to characterize the chamber radical source (Carter et al., 1982).

Reactivity Data Analysis Methods

As described above, reactivity experiments consist of one or more "base case" run(s) combined with a "test" experiment in which a VOC is added to the base case reactants. The results of these experiments can be analyzed to yield several measures of VOC reactivity (Carter et al., 1993a,b), though in this report we will focus on the effect of the VOC on the amount of NO reacted plus the amount of ozone formed at hourly intervals in the experiment. This is abbreviated as d(O_3-NO) in the subsequent discussion. As discussed elsewhere (e.g., Johnson, 1983; Carter and Atkinson, 1987; Carter and Lurmann, 1990, 1991) this gives a direct measure of the amount of conversion of NO to NO_2 by peroxy radicals formed in the photooxidation reactions, which is the process that is directly responsible for ozone

formation in the atmosphere. The incremental reactivity of the test VOC relative to $d(O_3\text{-NO})$ at time t, designated $IR[d(O_3\text{-NO})]_t^{voc}$, is given by

$$IR[d(O_3\text{-NO})]_t^{voc} = \frac{d(O_3\text{-NO})_t^{test} - d(O_3\text{-NO})_t^{base}}{[VOC]_0}$$

where $d(O_3\text{-NO})_t^{test}$ is the $d(O_3\text{-NO})$ measured at time t from the experiment where the test compound (e.g., acetone) was added, $d(O_3\text{-NO})_t^{base}$ is the corresponding value from the base case experiments where the test VOC was not present, and $[VOC]_0$ is the amount of test VOC added. The incremental reactivity with respect to $d(O_3\text{-NO})$ was calculated for each hour of the experiment.

The quantities $d(O_3\text{-NO})^{test}$ and $[VOC]_0$ are obtained from the results of each of the individual test experiments. The methods used to derive $d(O_3\text{-NO})^{base}$ depended on whether the base case experiment was being carried out at the same time under the same conditions in a divided or double chamber, as is the case with DTC or OTC runs, or whether the base case experiment was carried out separately, as was the case with the runs in the ETC. In the former case, the data from the base case side irradiated simultaneously with the test run was used. In the ETC experiments, the effects of run-to-run variability in temperature, light intensity, and initial reactant concentrations on $d(O_3\text{-NO})$ had to be taken into account. For these runs, the base case results used in the reactivity analysis of a particular test run were derived from estimates, based on a linear regression analysis of results of many base case runs, of what the result of a base case experiment would be if it were carried out with the same temperature, light intensity, and initial base case reactant concentrations as the test run. The methods and data used in the analysis of the ETC reactivity experiments are described in detail elsewhere (Carter et al., 1993a).

MODEL SIMULATION METHODS

Computer model simulations were conducted to evaluate the extent to which the results of these experiments are consistent with predictions of a current chemical mechanism for the atmospheric reactions of acetone and other VOCs. The mechanism was then used to simulate the incremental reactivities of acetone, ethane, and other VOCs under atmospheric conditions. The following sections give descriptions of the chemical mechanisms employed, of the methods used when simulating the chamber experiments, and of the model and scenarios used when simulating atmospheric reactivities. The chemical mechanism was updated for the purpose of this study. The overall mechanism used for all the atmospheric species is described first, followed by a more detailed discussion of the mechanism used for acetone.

General Atmospheric Mechanism

The chemical mechanism used as the starting point for this study is the "SAPRC-90" mechanism as documented by Carter (1990), with updates for various VOCs made in conjunction with its use to calculate the MIR scale for the California ARB (Carter, 1993a). This mechanism was then updated further before use in this study, as discussed below. These updates take into account results of several recent laboratory studies and incorporate some of the major recommendations made by Gery (1991) in his review of the SAPRC-90 mechanism. The specific changes in the mechanism, relative to the SAPRC-90 mechanism used in the MIR calculation (Carter, 1993a,b), are as follows:

(1) The formaldehyde absorption cross-sections were updated based on the recent data of Cantrell et al. (1990) and Rogers (1989). This results in a slight increase in the formaldehyde photolysis rate.

(2) The kinetics for the reactions of the acetyl peroxy radical with NO and NO_2, which are involved in the formation and decomposition of PAN, and the kinetics of the thermal decomposition of PAN, were updated based on recent experimental results of Tuazon et al. (1991) and Bridier et al. (1991). This causes the model to predict somewhat higher ozone formation rates than the SAPRC-90 mechanism.

(3) The SAPRC-90 mechanism uses model species whose photolysis rates are adjusted to fit aromatic-NO_x-air chamber experiments to represent the unknown photoreactive aromatic fragmentation products (Carter, 1990). This approach is still used in the updated mechanism, except that the change in the acetyl peroxy and PAN kinetics required reoptimization of these photolysis rates. In addition, the action spectra (absorption coefficients x quantum yields) for these products were assumed to proportional for the absorption cross section for acrolein (Gardner et al., 1987), rather than using the somewhat arbitrary action spectrum in the SAPRC-90 mechanism. These changes were found not to significantly

affect the performance of the mechanism if the reoptimization is conducted using the same set of experiments as used in the development of SAPRC-90.

(4) The mechanisms for the reactions of ozone with alkenes were modified to be consistent with the data of Atkinson and Aschmann (1993), who observed much higher yields of OH radicals than predicted by the SAPRC-90 mechanism. To account for these data, it was assumed that (1) the formation of OH radicals dominates over other radical-forming fragmentation processes, and (2) in the reactions of unsymmetrical alkenes, the more substituted Criegee biradical, which forms higher OH yields, are formed in relatively higher yields than the less substituted biradicals. The modified ozone reactions for the alkenes discussed in this paper are:

$$\text{Ethene} + O_3 \rightarrow HCHO + (HCHO2)$$
$$\text{Propene} + O_3 \rightarrow 0.6\ HCHO + 0.4\ CCHO + 0.4\ (HCHO2) + 0.6\ (CCHO2)$$
$$\underline{\text{trans}}\text{-2-Butene} + O_3 \rightarrow CCHO + (CCHO2)$$
$$\text{Isobutene} + O_3 \rightarrow 0.82\ HCHO + 0.18\ ACET + 0.18\ (HCHO2) + 0.82\ (C(C)CO2)$$

where CCHO and ACET represent acetaldehyde and acetone, and (HCHO2), etc., represent the excited Criegee biradicals, which are represented as reacting as follows:

$$(HCHO2) \xrightarrow{fast} 0.12\ CO + 0.12\ HO. + 0.12\ HO2. + 0.88\ (\text{unreactive carbon})$$

$$(CCHO2) \xrightarrow{fast} 0.3\ HCHO + 0.3\ CO + 0.6\ HO. + 0.3\ \{CCO\text{-}O2.+\ RCO3.\} + 0.3\ \{RO2\text{-}R.+\ RO2.\} + 0.9\ (\text{unreactive carbon})$$

$$(C(C)CO2) \xrightarrow{fast} HCHO + HO. + \{R2O2.+\ RO2.\} + \{CCO\text{-}O2.+\ RCO3.\}$$

[See Carter (1990) for a description of the model species and the methods used to represent peroxy radical reactions.] This is clearly an oversimplification of this complex system (e.g., see Atkinson, 1990, 1993), but is intended to account for the observed OH radical yields and represent the major features affecting these compounds' reactivities. Note that this new mechanism gives substantially higher radical yields in the ozone + alkene systems than the SAPRC-90 mechanism, particularly for internal alkenes.

(5) The reaction of NO with the peroxy radical formed in the reaction of OH radicals with isobutene was assumed to form the corresponding hydroxyalkyl nitrate 10% of the time. This assumption resulted in significant improvements to the fit of model simulations to ozone and PAN yields in isobutene - NO_x - air chamber experiments. Without this assumption, the model with the OH yields indicated by the O_3 + isobutene data of Atkinson and Aschmann (1993) significantly overpredicts O_3 formation rates. If lower radical yields in the O_3 + isobutene reaction are assumed, the model significantly underpredicts PAN (unpublished results from this laboratory).

(6) The representation of isooctane was modified to improve the model simulations of its reactivity (Carter et al., 1993a,b).

(7) Several changes were made to the mechanism for acetone. These are discussed in the following section.

A complete listing of this mechanism as used in the model simulations in this report is given in Appendix A. Further updates to this mechanism are planned and it has not been as extensively evaluated against the chamber data as the SAPRC-90 mechanism (Carter and Lurmann, 1991). However, it was evaluated in model simulations of the results of the extensive set of maximum incremental reactivity experiments recently completed in our laboratories (Carter et al, 1993a), and was found to perform somewhat better than the SAPRC-90 mechanism in simulating these data.

Acetone Mechanism

Acetone is believed to react in the atmosphere primarily by photolysis and reaction with OH radicals, and the available data concerning these reactions are discussed by Atkinson (1990, 1993). Reaction with ozone would be expected to be of negligible importance (Atkinson and Carter, 1984), and although there are no data available concerning its reaction with NO_3 radicals, the rate constant would be expected to be small (Atkinson, 1991). The mechanisms used in the model to represent the OH and photolysis reactions are discussed below.

OH Radical Reaction

The representation of the OH + acetone used in the SAPRC-90 mechanism is based on the recommendations of Atkinson (1990). The recommended rate constant expression is equivalent to $k = 1.92 \times 10^{-13} (T/300)^2 e^{0.11/RT}$ cm^3 $molec^{-1}$ sec^{-1}, which yields $k = 2.31 \times 10^{-13}$ cm^3 $molec^{-1}$ sec^{-1} at 300K. The reaction is assumed to proceed as follows:

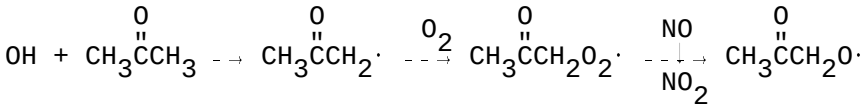

The alkoxy radical can either react with OH radicals, giving rise to methylglyoxal,

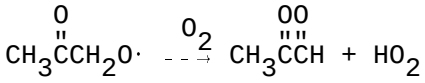

(a)

or it undergo decomposition, giving rise to methylperoxy or acetylperoxy radicals, which react further to ultimately form either formaldehyde + PAN or two formaldehyde + CO_2, depending on the $[NO]/[NO_2]$ ratio.

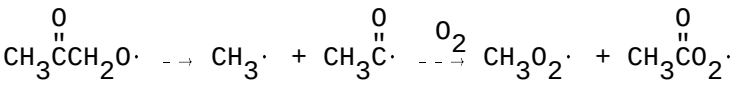

(b)

At the time the SAPRC-90 mechanism was developed, there was no experimental information available concerning the mechanism for this reaction, or the k_a/k_b branching ratio. This could be an important factor affecting acetone's reactivity because methylglyoxal is a highly photoreactive product whose formation in the mechanism would enhance acetone predicted reactivity, while PAN formation is a radical termination process whose formation would have an inhibiting effect. Based on an estimate given by Atkinson (1990), the SAPRC-90 mechanism assumes that methylglyoxal formation occurs 80% of the time, i.e., that $k_a/k_b = 4$.

However, more recent data and evaluations indicate that modifications to this OH + acetone mechanism are appropriate. In an updated evaluation, Atkinson (1993) gives a slightly different recommended rate constant expression for this reaction. The new recommendation is equivalent to $k = 4.81 \times 10^{-13} (T/300)^2 e^{-0.457/RT}$ cm^3 $molec^{-1}$ sec^{-1}, which yields $k = 2.23 \times 10^{-13}$ cm^3 $molec^{-1}$ sec^{-1} at 300 K. Although this gives essentially the same rate constants for the temperature range of these experiments, the mechanism used in this study was updated to be consistent with this new recommendation.

More significantly in terms of predictions of acetone's reactivity, recent data from Jenkin et al (1993) indicate that reaction of the $CH_3COCH_2O_2\cdot$ radical to form methylglyoxal is not important. This is consistent with predictions of a revised estimation technique developed by Atkinson and Carter (1992) based on recent data concerning decomposition and O_2 reactions of analogous reactions of alkoxy radicals formed from ethers and other compounds. Based on this, the updated OH + acetone mechanism used in this study assumes that reaction (b) is the only significant process, and that methylglyoxal formation is negligible. This results in a mechanism which predicts somewhat lower reactivity for acetone than does SAPRC-90.

Photolysis Reaction

Available data concerning the photolysis of acetone under atmospheric conditions are summarized in the latest IUPAC evaluation (Atkinson et al., 1992). The recommended absorption cross sections and quantum yields are those of Meyrahn et al. (1986), while the SAPRC-90 mechanism (Carter, 1990) uses values from Calvert and Pitts (1966). The latter agree with the recommended values at wavelengths greater than 310 nm, but are slightly lower at lower wavelengths, though the difference causes only a ~1.5% change in the calculated atmospheric photolysis rate. Nevertheless, the updated mechanism was modified to incorporate the recommended absorption cross sections.

The only energetically available photodecomposition reaction for acetone at wavelengths greater than 300 nm is scission of the C-CO bond, forming, in the presence of oxygen, methylperoxy and acetyl-peroxy radicals

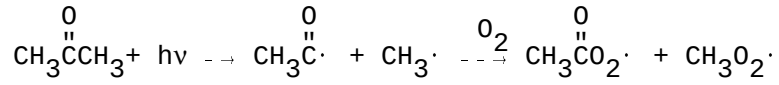

In the presence of NO_2 acetylperoxy radicals subsequently react to form PAN. There is disagreement in the literature concerning the quantum yields for this reaction under atmospheric conditions. Gardner et al. (1984) derived quantum yields of 0.07, approximately independent of wavelength over the 280-313 nm region, based on acetone loss and yields of CO_2, CO, CH_3OH, and formaldehyde products when acetone was photolyzed in air. Meyrahn et al. (1986) derived quantum yields which generally decreased wavelength from 250-330 nm based on measuring yields of PAN in photolyses of ~150 ppm of acetone and ~0.12 ppm of NO_2 in air. The IUPAC panel recommends use of the data of Meyrahn et al (1986) because they appeared to the evaluators to be more reasonable (Atkinson et al., 1992). These recommended absorption cross sections were used in the SAPRC-90 mechanism.

The validity of the quantum yields reported by Meyrahn et al (1986) is based on the assumption that under the conditions of their experiments all the acetyl peroxy radicals formed react to form PAN, and that there is no other source of these radicals. However, as discussed in the previous section, the OH reaction is also believed to form these radicals, and if sufficient OH were present in their experiments, there could be an additional source of PAN from the this reaction and the reported quantum yields may be high. To examine this, the conditions of these experiments were modeled using the updated SAPRC-90 mechanism. The model simulations predicted that the OH reaction was negligible in the experiments carried out at wavelengths of 310 nm or less, but that this reaction forms ~10% of the PAN in the experiments at 320 nm and ~50% of the PAN at 330 nm. This can be corrected for (albeit approximately) by reducing the 320 nm quantum yields by 10% (from 0.028 to 0.026) and the 330 nm quantum yields by a factor of ~2 (from 0.033 to 0.017). The corrections, particularly at 330 nm, must be considered to be highly approximate because we probably did not simulate the conditions of the experiments exactly. However, the factor of two correction of the 330 nm quantum yield gives a more reasonable decline in quantum yields with wavelength than the uncorrected data, so the updated mechanism incorporated these corrections to the Meyrahn et al. (1986) quantum yields. This correction causes a ~4% reduction of the atmospheric photolysis rate for acetone.

The model simulations of the experiments at wavelengths of 310 nm or less predict that not all the of the acetylperoxy radicals react to form PAN, since some will be lost by various peroxy + peroxy radical reactions. The model simulations we conducted suggested that the PAN yields in those experiments may underestimate the true quantum yields by ~15-20%. This would result in comparable increases of the calculated atmospheric photolysis rates for acetone, since this wavelength region accounts

for most of the photolysis reaction. These estimates are uncertain because the predicted extent of peroxy + peroxy reaction is dependent on our model for the conditions of these experiments, whose accuracy is unknown. The underprediction of quantum yields could be no more than ~20%, since otherwise the corrected quantum yields for 250 - 260 nm would be greater than unity. For this reason, no such correction to the $\lambda < 210$ nm quantum yields were applied. However, this analysis indicates that the quantum yields which are up to ~20% higher than assumed in the model may not necessarily be inconsistent with the data of Meyrahn et al (1986).

Because of the disagreement in the literature, the quantum yields for acetone photolysis must be considered the most uncertain component of acetone's atmospheric photooxidation mechanism. If the quantum yields reported by Gardner et al. (1984) are assumed, the acetone photolysis rate is calculated to be ~45% higher in the atmosphere and ~2 times higher in a blacklight chamber experiment, than calculated using the corrected data of Meyrahn et al. (1986). Given the complexity of the chemical systems utilized in both these studies, and the assumptions concerning the mechanisms that need to be made in analyzing the results, the possibility that neither of these determinations are correct cannot be ruled out.

Several adjustments were made to the assumed acetone quantum yields, and their wavelength dependencies, to improve the fits of the model simulations to the experiments carried out in this study. These are discussed in the Results section.

Model Simulations of Chamber Experiments

The testing of a chemical mechanism against environmental chamber results requires that the model include appropriate representations for chamber-dependent effects such as wall reactions and characteristics of the light source used during the experiments. The methods used to represent them in this study are based on those discussed in detail by Carter and Lurmann (1991), adapted for these specific sets of experiments as discussed by Carter et al. (1993a) or as indicated below. Where possible, the parameters were derived based on analysis of results of characterization experiments carried out in conjunction with these runs.

Light Characterization for Indoor Chamber Runs

Light characterization for indoor chamber runs consist of NO_2 actinometry experiments and measurements of the spectrum of the light source using the LI-1800 spectrometer. The former give the absolute light intensities in terms of the NO_2 photolysis rates, while the latter give information needed to calculate the ratios of rates of all other photolysis reactions to that for NO_2, given the absorption cross sections and quantum yields for the NO_2 and other photolysis reactions. In particular, the relative spectral measurements are converted to absolute actinic fluxes by multiplying them by a factor which, when used with the currently accepted NO_2 absorption cross sections and quantum yields (Atkinson, 1990; Carter,

1990), result in the calculated NO_2 photolysis rate being equal to the value derived from the actinometry experiments. The absolute actinic fluxes are then used to calculate the rates of all the other photolysis reactions in the model simulations.

This procedure uses the data from the actinometry experiments to give the absolute light intensities, with the LI-1800 spectrometer only being used to obtain relative spectra. However, the LI-1800 spectrometer is calibrated at the factory to give absolute light intensity readings, and thus, in theory at least, it could be used to as a means to assess the accuracy of the actinometry experiments. Unfortunately, the spectrometer measures light intensity on a plane, while photolysis rates are determined by spherically integrated light intensities. To determine the latter from the former, and thus provide an independent check of the accuracy of our actinometry measurements, we developed a model for the special distribution of the light in the chamber, making measurements to estimate reflectances within the chamber (unpublished results from this laboratory). The NO_2 photolysis rate derived from this procedure was found to be ~10% lower than that measured using the quartz tube actinometer. This is considered to be agreement to within the uncertainties of the model and the measurements, and thus a validation of our NO_2 actinometry method.

The spectra for the blacklight chambers were found to be essentially independent of chamber and lamp age, at least in the wavelength region which affects photolysis rates. Thus the same spectrum was used in the model simulations of these runs. However, the spectrum of the xenon arc light source used in the XTC runs was found to change slowly with time, becoming somewhat weaker in the shortest wavelengths as the lamps aged. The affected wavelengths were shorter than those which significantly influence NO_2 photolysis rates, and the intensity of the spectra indicated that NO_2 photolysis rates decreased by only ~3% during the course of this study. On the other hand, the photolysis of other species, including acetone, are more affected by this change. For example, between runs XTC-80 and XTC-98 the photolysis rate of acetone, relative to that for NO_2 was calculated to decline by ~14%. Because of this, photolysis rates were calculated separately for each XTC run. Based on the results of the actinometry experiments, combined with the monitoring of the light intensity with the spectrometer, we assign an NO_2 photolysis rate of 0.24 min^{-1} for run XTC-80, 0.23 for run XTC-85 and those following, and intermediate values for runs between XTC-80 and XTC-85. The photolysis rates for the other reactions were calculated using the relative spectra measured during each individual run.

Light Characterization for Outdoor Chamber Runs

The light characterization data for the outdoor chamber runs consist of continuous UV and broadband radiometer data, and approximately hourly global and diffuse solar spectra taken using the LI-1800 spectrometer. The global and diffuse spectra, along with the JSPECTRA solar light model developed by Jeffries (1988, 1989b, 1991), were used as the primary means for light characterization for modeling purposes. The procedure employed is only applicable to clear sky conditions, so no runs on

cloudy or overcast days were used for mechanism evaluation. The radiometer data was used as a cross-check to assure that the light conditions were not changing abruptly between the times spectral measurements were made. The outdoor chamber light characterization procedures will be documented in a subsequent report, and will only be summarized here.

The JSPECTRA solar light model is designed to calculate ground-level solar spectra given relevant parameters such as time of day, day of year, total ozone column, atmospheric aerosol parameters, and extraterrestrial solar fluxes. It can be used either to calculate spherically integrated actinic fluxes for calculation of photolysis rates or to predict global or diffuse spectra as measured by the LiCor spectrometer. Some of the inputs to the program, such as the time of day or day of year, are known, others, such as the extraterrestrial fluxes, are assumed not to be variable and are provided with the program, while other inputs, such as the ozone column and the aerosol parameters, are uncertain or variable. The most sensitive of the uncertain inputs were adjusted, using a non-linear optimization algorithm, to fit the global and diffuse LiCor spectra taken during the run, while for the less sensitive parameters the defaults used by Jeffries (1988) for "summer conditions" were used in all calculations. Although moderately good fits of adjusted model calculation to LiCor spectra could obtained by adjusting only the parameters in the JSPECTRA model, for best fits to the data three separate parameters were added to scale the overall intensity as a function of wavelength. These consisted of scaling factors for the intensities at 300, 500, and 800 nm; the scaling factors for other wavelengths were obtained by linear interpolation of these. With the set of parameters we used, these scaling factors were consistently 0.7, 1, and 1.1 at these three wavelengths, respectively. An example showing the comparison obtained between the adjusted model calculation and the global and diffuse LiCor spectra is shown on Figure 2

The results of the optimization of the JSPECTRA input parameters could then be used to calculate spherically integrated actinic fluxes for the times the LiCor spectra were taken. The calculated spherically integrated fluxes were not sensitive to the specific set of JSPECTRA parameters optimized, as long as the model could closely simulate the direct and diffuse LiCor data. If the run was carried out on a clear day, the parameters affecting light fluxes might reasonably be assumed not to change abruptly with time. In this case, the values of the adjusted parameters for times between those where LiCor data were taken could be estimated by linear interpolation of the optimized values. Based on this assumption, parameters were estimated at each 20 minute interval during the run, from which actinic fluxes for those times were calculated. The fact that this assumption is not valid for cloudy days is not a significant limitation because the JSPECTRA model was not designed to calculate solar fluxes for those conditions in any case. For this reason, only data from clear day runs were characterized for modeling purposes. The few runs carried out on days with unfavorable weather are not discussed.

The JSPECTRA program, with its time-varying inputs derived as discussed above, could also be used to calculate how the data from the UV and broadband radiometers should vary with time. Thus,

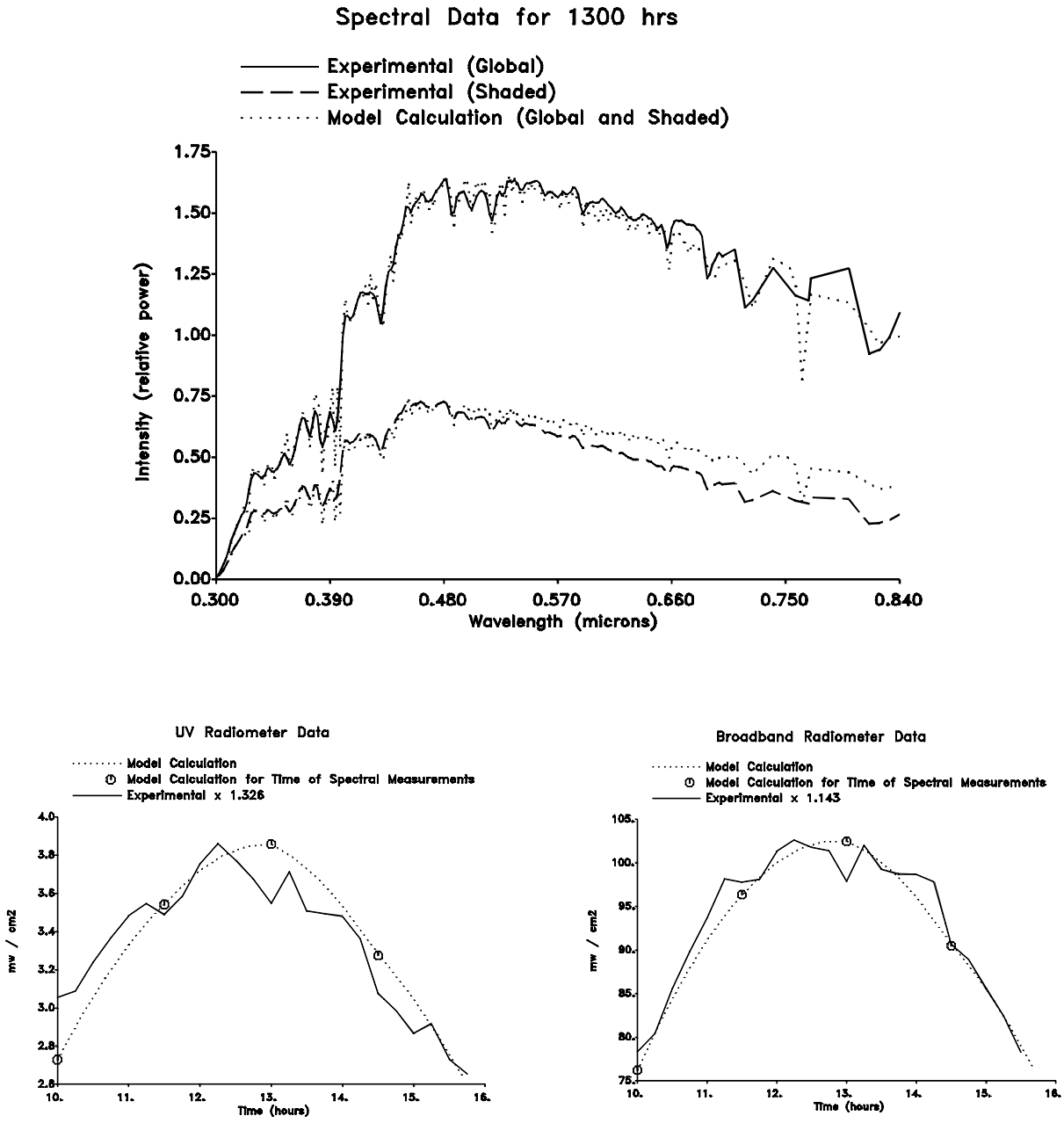

Figure 2. Examples of fits of adjusted solar light model to light characterization data for two outdoor chamber runs. Top plots: fits to direct and diffuse spectral data. Bottom plots: fits to changes with time in the data from the UV and broadband radiometers.

while this method does not directly utilize these data in the photolysis rate calculations, they can be used as a check on the appropriateness of the model's interpolations. Typical results are included on Figure 2, which shows plots of observed and calculated radiometer data vs. time for run OTC-274. In general, the model gave somewhat better predictions of the time profiles of the broadband data than the UV data. This can be attributed to the fact that the spectral response of UV radiometers such as those employed in this study are not particularly well characterized, and the JSPECTRA model uses a highly idealized representation in this regard.

The above procedure predicts light spectra outside the chamber, but the relevant quantities are the light spectra inside the Teflon reaction bag. Jeffries et al. (1989b) measured light reflection and transmission through 2 mil and 5 mil FEP teflon film as a function of wavelength and the incidence angle of the light beam, and developed a parameterized model to fit these data. Although this model includes a term for absorption, the fraction of light absorbed is small (less than 1% for 2-mil film) and can be neglected. Thus only loss due to reflection on the outer chamber walls, or enhancement due to reflection on the inner walls, need be considered. The OTC can be thought of as a transparent bag suspended in space, with light entering it from all directions. If the effect of the presence of the bag on the light coming in from the bottom is neglected, it can be shown that the light enhancement by the reflections from inside the bag just makes up for the light lost due to the reflection when it enters the bag, with the result being that the intensity (and spectrum) inside the bag should be exactly the same as outside. The principle behind this is exactly the same as the principle behind the arguments given by Zafonte et al. (1977) when they concluded that reflections off quartz tubes do not affect results of actinometry measurements using such tubes. Consistent with this is the fact that no significant differences were observed when NO_2 actinometry measurements were made inside and outside the OTC on the same days.

The assumption that the presence of the OTC does not affect light coming from the bottom is not totally valid because the reaction bag is sufficiently close to the ground that all the light coming from the bottom has first passed through the bag, and was thus attenuated by the first reflection from the top. An approximate correction for this was made based on assuming the top and the bottom of the chamber are flat planes of film parallel to the surface, and that the albedo of the carpet under the chamber is the same as the general albedo which is the default in the JSPECTRA model. Parameterized fits to 2-mil FEP Teflon transmission data provided by Jeffries (private communication) were used to calculate the transmissions and reflectance through the chamber walls. This is a fairly small correction, causing the predicted in-chamber photolysis rates to be ~4% than those calculated for outside.

The in-chamber actinic fluxes calculated for every 20 minutes during the run were used as input into model when simulating the run. The model then calculated the photolysis rates for these periods using the absorption cross sections and quantum yields for the various reactions. The photolysis rates

were updated at each time step in the simulation, with the model deriving the photolysis rates for intermediate times between these 20 minute intervals by linear interpolation.

Temperature Characterization

The temperature was observed to varied with time in both the indoor and the outdoor chamber runs, though the variation was much greater in the latter case. The measured temperature data (with any applicable corrections, discussed below), were fit to various straight line segments, and these lines were then used to describe how the temperature varied with time in the model simulations. Subjective judgement was used in determining how many different line segments were required to fit the time variation of the temperature data, but a least squares error optimization program was used to determine the best fit lines once the end points of the line segments have been specified. A single line was sufficient to describe variation in most of the indoor runs, but usually 3-4 lines were required for outdoor runs. For divided chamber runs (OTC and DTC), separate temperature profiles were derived from the data for each side.

The ETC and DTC temperature measurements made with the unshielded probes inside the chamber were used without correction. The XTC temperature measurements made with the aspirated temperature probe were assumed to be accurate and were used without correction. For runs where such data are not available, data taken with the shielded thermocouple inside the chamber were used after being corrected by subtracting 1.5 degrees, as indicated by comparison tests. As discussed above, the in-chamber temperature data for run XTC-083 appear to be anomalous, and the temperature profiles derived for modeling run XTC-086 were also used for modeling this run because the temperature readings in the sampling line were very close for these two runs.

The OTC temperature measurements made with the thermocouple in the sampling line immediately outside the chamber were assumed to be accurate and used without correction. This is applicable to all runs discussed in this report except OTC-270, where unshielded probes inside the chamber were used. There are no data concerning the temperature corrections appropriate for this run. There was also some inconsistency between temperature measurements from the two sides of the chamber. Because of this, this run was modeled with the temperature input varied within its probable uncertainty.

Chamber Radical Source

As discussed elsewhere (Carter et. al, 1982; Carter and Lurmann, 1990, 1991), model simulations of chamber runs must include a representation for a chamber radical source. Although certain runs, especially alkane - NO_x - air runs, are highly sensitive to this parameter, it is less important in affecting results of runs containing complex mixtures designed as atmospheric surrogates, or runs containing species, such as acetone, which are radical initiators. Because of the high sensitivity of alkane - NO_x runs to the chamber radical source (Carter et al., 1979), we carried out n-butane - NO_x - air

irradiations for determining this parameter. The radical source is then adjusted in model simulations to fit the NO oxidation observed in these runs. We found that modeling n-butane runs is a more sensitive method for determining the chamber radical source than analysis of radical tracer - NO_x runs as we have employed previously (Carter et al., 1982).

For the DTC and XTC runs, the chamber radical source parameters were adjusted to fit results of n-butane - NO_x irradiations carried out in those chambers. Based on these results, an OH radical input rate used for both these chambers was 0.06 ppb x the NO_2 photolysis rate. This is lower than the range of values used for the SAPRC ITC (Carter and Lurmann, 1990, 1991), but within the range used for the ETC runs (Carter et al., 1993a).

Since the chamber radical source is expected to be dependent on temperature (Carter et al., 1982), and since temperature varies widely in outdoor runs, use of a temperature-dependent radical source parameter would be appropriate when modeling such runs. Better results in modeling alkane - NO_x runs carried out in the UNC outdoor chamber was obtained when a temperature-dependent radical source was assumed (Carter and Lurmann, 1990, 1991). The three n-butane - NO_x runs carried out in the OTC for this study had average temperatures of 309, 312, AND 317° K, and, if the radical source input parameter (OH input rate / NO_2 photolysis rate — given in units of ppb) is assumed to be independent of temperature, the values which resulted in model simulations best fitting these runs were 0.2, 0.3, and 0.3-0.4 ppb, respectively. All three runs could be fit by assuming the following temperature dependence for the ratio of the OH input flux to the NO_2 photolysis rate: 290°K: 0.02 ppb; 300°K: 0.05 ppb; 310°K: 0.3 ppb; and 320°K: 0.4 ppb. Values for intermediate temperatures were obtained by interpolation. The value for 300° K is based on typical values for indoor runs, and the value for 290° K is an estimate.

Other Chamber-Dependent Parameters

The various other chamber dependent effects which are included in the model simulations of these chamber runs include humidity, dilution, ozone decay rate, initial nitrous acid, NO_x offgasing rates, N_2O_5 hydrolysis, and NO conversion due to background VOCs (Carter and Lurmann, 1990, 1991; Carter et al., 1993a). In the case of the indoor Teflon chambers (the ETC, DTC, and XTC), these were represented in a similar manner as discussed by Carter et al. (1993a) for the ETC, except as follows. The dilution rates were based on decay rates of slowly reacting species in the individual runs, when such data were available. If not, the default dilutions used were those derived from the ETC data (Carter et al., 1993a). No initial nitrous acid was assumed to be present because the NO_x injection procedures employed were designed to eliminate its formation (Carter et al., 1993a).

The chamber-dependent parameters for the OTC runs were the same as used in our previous mechanism evaluation studies using data from this chamber (Carter and Lurmann, 1990, 1991), except that

dilution rates were based on decay rates of slowly reacting observed in individual runs were used when such data were available.

Modeling Incremental Reactivity Measurements

Modeling of incremental reactivity measurements consisted of conducting model simulations of both the base case and the added test VOC experiment, and then analyzing the results using the same procedures as employed experimental data. In the case of the ETC runs, where there is no single base case run associated with any particular test run, the base case simulation associated with a particular test run consisted of modeling the conditions of the that test run, but without the test compound added.

As discussed by Carter et al. (1993a,b), the SAPRC-90 mechanism was found to underpredict the rate of ozone formation in the base case mini-surrogate - NO_x experiments used in conjunction with the ETC acetone reactivity runs. The updates to the mechanism discussed above did not significantly change this. If the model cannot adequately simulate the base case experiments, it cannot be used as a reliable test of mechanisms for test compounds to predict their incremental reactivities in those experiments. Therefore, in the model simulations of the mini-surrogate experiments only, the model for m-xylene in the mini-surrogate was adjusted slightly so the model could better simulate the base case experiment (Carter et al, 1993a,b). The modified m-xylene mechanism is included in the reaction listing in Appendix A. Note that this adjustment was not used in the simulation of the full surrogate runs in the same chamber, since those runs were fit better using the standard m-xylene model (see Results).

EXPERIMENTAL AND MECHANISM EVALUATION RESULTS

The experiments carried out in this program, which were carried out in either the ETC, DTC, XTC, or OTC chamber, consisted of acetone - NO_x, acetone incremental reactivity, acetaldehyde - NO_x, acetaldehyde incremental reactivity, and direct acetone vs ethane comparison runs. In addition, results of selected ethane incremental reactivity experiments are also presented. The conditions and selected results of the single compound experiments are given in Table 1, and the conditions and selected results of the incremental reactivity experiments and their associated base case runs are given in Table 2. Table 2 also gives the conditions and results of the direct acetone vs ethane comparison experiments and the associated side equivalency test run. Plots of selected experimental results, and of results of model simulations of these experiments, are presented in the following sections, where the various types of experiments are discussed in more detail.

Blacklight Chambers

Acetone - NO_x Experiments

Three acetone - NO_x experiments were carried out for this program, one in the ETC and two in the DTC. The runs in the DTC were carried out simultaneously with acetaldehyde - NO_x runs whose results are discussed below. The conditions and results of these experiments are summarized on Table 1, and Figure 3 shows concentration-time profiles of selected species in these experiments. Results of model simulations are also shown. Also shown are results of model simulations with the acetone photolysis quantum yields adjusted as discussed later. It can be seen that the standard model (i.e., the model where the acetone quantum yields are not adjusted) overpredicts the rate of ozone formation in all three of these experiments.

Acetone Reactivity Experiments

A total of seven incremental reactivity experiments with added acetone were carried out in the blacklight chambers, three using the mini-surrogate, two using the full surrogate, and two using the ethene surrogate. Table 2 summarizes the conditions and major results of these experiments, along with the results of the corresponding base case runs. Note that in the case of the ETC experiments only the base case runs carried out immediately before or after the acetone runs are shown on the table, though a much larger number of base case runs were used in establishing the base case conditions (Carter et al., 1993a).

Concentration time profiles for selected species in the base case experiments are shown on Figures 4-6. In all cases the base case experiment were carried out under sufficiently high NO_x (or low ROG/NO_x) conditions that ozone formation is still occurring at the end of the run. This type of

Table 1. Summary of conditions and selected results of the single compound - NO_x - air experiments

VOC	Run	Initial NO_x (ppm)	Initial VOC (ppm)	Average T (°K)	Average k_1 [a] (min^{-1})	Final O_3 (ppm)
Acetone	ETC-445	0.131	7.50	300.9	0.336	0.232
	DTC-54B	0.288	11.15	302.1	0.379	0.205
	DTC-55A	0.147	15.27	301.4	0.379	0.410
	XTC-84	0.237	9.24	302.4	0.233	0.374
	XTC-90	0.194	9.67	305.0	0.233	0.345
	OTC-270B	0.305	5.07	308.5	0.282	0.029
	OTC-273A	0.304	12.11	312.7	0.352	0.928
	OTC-274B	0.272	9.78	307.0	0.349	0.682
Acetaldehyde	DTC-55B	0.146	1.24	301.8	0.379	0.336
	XTC-83	0.251	0.997	302.9	0.233	0.279
	XTC-92	0.257	1.11	302.3	0.233	0.222
	OTC-273B	0.302	1.15	314.3	0.352	0.873
	OTC-274A	0.279	1.08	306.6	0.349	0.725
	OTC-305A	0.272	1.50	315.0	0.309	0.858

[a] NO_2 photolysis rate used in model simulation of run. For indoor runs, value is assigned based on results of NO_2 actinometry experiments. For outdoor (OTC) runs, value shown is average of values calculated as described in the text.

experiment was used for the base case because it represents "maximum reactivity" conditions where VOCs have the greatest effect on ozone formation (Carter, 1991, 1993a,b). It is also particularly useful for mechanism evaluation because it is the most sensitive type of experiment to the effect of the added VOC.

Results of model simulations of the base case experiments are also shown on figures 4-6. It can be seen that the mechanism simulates these experiments fairly well. However, as indicated above, the m-xylene mechanism had to be adjusted to obtain the fits shown for the mini-surrogate runs (Carter et al., 1993a,b). The simulation of the mini-surrogate base case experiment using the unadjusted mechanism is shown on Figure 4 to indicate the effect of this m-xylene adjustment. On the other hand, the available data base of m-xylene - NO_x chamber experiments (Carter and Lurmann, 1990. 1991), and the full surrogate runs carried out in the same chamber (see Figure 4) are better fit by the standard updated SAPRC-90 m-xylene mechanism. This indicates problems with the mechanisms for either m-xylene or the other components of the mini-surrogate, but a discussion of this is beyond the scope of this report.

Table 2. Summary of conditions and results of the incremental reactivity and direct reactivity comparison experiments.

Run	Initial NO_x (ppm)	Initial ROG^{base} (ppmC)	Initial VOC^{test} (ppm)	Avg. T (°K)	Avg. k_1 [a] (min^{-1})	Final $d(O_3-NO)$ (ppm)	Base [b] $d(O_3-NO)$ (ppm)	IR $d(O_3-NO)$ [c]
Mini-Surrogate - NO_x with Added Acetone								
ETC-243	0.463	4.37	0.85	301.8	0.336	0.770	0.748	[d]
ETC-245	0.504	4.65	2.19	302.3	0.336	0.886	0.757	0.059
ETC-247	0.497	4.32	4.15	301.9	0.336	0.942	0.757	0.045
Mini-Surrogate - NO_x with Added Ethane								
ETC-092	0.518	3.73	17.1	301.4	0.343	0.581	0.463	0.007
ETC-099	0.509	3.67	16.6	300.8	0.338	0.562	0.443	0.007
ETC-235	0.494	4.56	43.7	302.0	0.336	1.006	0.754	0.006
Mini-Surrogate - NO_x Base Case [e]								
ETC-091	0.513	3.66	-	301.3	0.344	0.433		
ETC-093	0.520	3.68	-	301.6	0.342	0.473		
ETC-098	0.517	3.58	-	301.4	0.338	0.445		
ETC-100	0.516	3.58	-	301.1	0.337	0.449		
ETC-234	0.504	4.43	-	302.1	0.336	0.727		
ETC-236	0.502	4.39	-	302.0	0.336	0.705		
ETC-242	0.452	4.49	-	301.8	0.336	0.724		
ETC-244	0.484	4.31	-	302.2	0.336	0.707		
ETC-246	0.496	4.44	-	302.2	0.336	0.737		
ETC-250	0.499	4.69	-	299.9	0.336	0.746		
Ethene - NO_x with Added Acetone								
ETC-480	0.419	3.35	3.13	301.4	0.336	1.202	1.146	0.02
ETC-481	0.414	3.05	5.11	301.4	0.336	1.188	1.133	0.01
ETC-490	0.419	3.24	7.97	302.0	0.336	1.259	1.209	0.006
OTC-278A	0.496	1.22	2.85	311.5	0.335	1.170	0.613	0.20
OTC-279B	0.526	2.00	1.27	312.6	0.345	1.317	1.271	0.04
OTC-280A	0.550	2.09	1.99	310.7	0.347	1.397	1.238	0.08
Ethene - NO_x with Added Ethane								
ETC-506	0.407	3.01	50.1	300.6	0.336	1.211	1.033	0.0036

Table 2 (continued)

Run	Initial NO_x (ppm)	Initial ROG^{base} (ppmC)	Initial VOC^{test} (ppm)	Avg. T (°K)	Avg. k_1 [a] (min^{-1})	Final $d(O_3\text{-}NO)$ (ppm)	Base [b] $d(O_3\text{-}NO)$ (ppm)	IR $d(O_3\text{-}NO)$ [c]
Ethene - NO_x Base Case [f]								
ETC-479	0.409	3.36	-	301.4	0.336	1.146		
ETC-482	0.427	3.01	-	301.3	0.336	1.160		
ETC-486	0.440	3.36	-	301.4	0.336	1.082		
ETC-497	0.450	3.68	-	301.9	0.336	1.198		
ETC-505	0.401	3.15	-	301.0	0.336	1.079		
OTC-278B	0.498	1.23	-	312.0	0.335	0.613		
OTC-279A	0.534	1.98	-	312.0	0.345	1.271		
OTC-280B	0.545	2.15	-	311.1	0.347	1.238		
Full Surrogate - NO_x with Added Acetone								
DTC-28A	0.489	4.12	9.37	301.7	0.379	1.056	0.819	0.03
DTC-64B	0.495	4.07	17.08	302.7	0.379	1.120	0.757	0.02
OTC-275A	0.561	4.58	10.48	317.5	0.363	1.565	1.518	0.013
OTC-276B	0.571	4.46	5.81	313.7	0.355	1.498	1.405	[d]
OTC-312A	0.578	4.42	2.16	315.0	0.272	1.285		
OTC-313B	0.494	4.14	1.86	303.4	0.247	0.900		
Full Surrogate - NO_x with Added Ethane								
OTC-312B	0.578	4.65	3.35	315.8	0.272	1.279		
OTC-313A	0.496	4.11	3.26	302.7	0.247	0.853		
Full Surrogate - NO_x Base Case [g]								
DTC-28B	0.492	4.14	-	301.9	0.379	0.819		
DTC-64A	0.494	4.25	-	302.0	0.379	0.757		
OTC-275B	0.625	4.58	-	317.8	0.363	1.518		
OTC-276A	0.580	4.47	-	313.4	0.355	1.409		
OTC-314A	0.577	4.67	-	300.7	0.238	0.749		
OTC-314B	0.576	4.61	-	301.6	0.238	0.755		

[a] NO_2 photolysis rate used in model simulation of run. For indoor runs, value is assigned based on results of NO_2 actinometry experiments. For outdoor (OTC) runs, value shown is average of values calculated as described in the text.

[b] $d(O_3\text{-}NO)$ from base case run. For divided chamber runs with a simultaneous irradiation of a "base case" mixture, this the $d(O_3\text{-}NO)$ from the "base case" side. For single chamber runs, this was derived by estimating the results of a base case run for the conditions of this experiments using linear regressions derived from the results of the base case runs, as discussed by Carter et al. (1993).

Table 2 (concluded)

[c] Incremental reactivity in units of mol O_3 per mol test VOC added
[d] Effect of added VOC too small for meaningful incremental reactivity measure.
[e] Representative runs carried out around the time of the added acetone or ethane experiments. For full listing of runs used in data analysis, see Carter et al. (1993).
[f] The ETC runs are representative runs carried out around the time of the added acetone experiments in that chamber. Results of other runs were very similar. The OTC runs are the base cases for the added acetone carried out at the same time (i.e., with the same OTC run number) but on the other chamber side.
[g] Base cases for the added acetone carried out at the same time (i.e., with the same DTC or OTC run number) but on the other chamber side.

Figures 4-6 also give plots of concentration-time profiles for selected species in the added acetone experiments, along with results of model simulations of these experiments. In addition, Figures 7 and 8 show plots, as a function of irradiation time, of the d(O_3-NO) incremental reactivities which were derived from these experiments. The error bars give the uncertainties in the measured incremental reactivities based on estimated run to run variability and precisions of initial acetone measurements (Carter et al, 1993a). Model simulations of the incremental reactivities are also shown. It can be seen that the model consistently and significantly overpredicts the ozone formation in the added acetone experiments, and thus the incremental reactivity of acetone, regardless of what is being used as the base case ROG surrogate.

Acetaldehyde Experiments

As discussed above, acetaldehyde is a useful VOC for which to compare the results with acetone because, like acetone, it is photoreactive and forms similar products in its reactions. The conditions and selected results of the acetaldehyde - NO_x and the acetaldehyde reactivity experiments are given on Tables 1 and 2, respectively. Note that the acetaldehyde - NO_x run in the DTC was carried out at the same time as an acetone - NO_x run. Much less acetaldehyde is added compared to acetone because of its much greater reactivity.

Figure 9 shows selected results of the acetaldehyde runs carried out in the blacklight chambers. This includes concentration-time plots for selected species in the acetaldehyde - NO_x run and plots of incremental reactivities in the acetaldehyde reactivity experiment. Results of model calculations are also shown. It can be seen that the model gives reasonably good simulations of these data. There may be a slight tendency for the model to overpredict acetaldehyde's reactivity, but the discrepancy is far less than is the case for the acetone experiments.

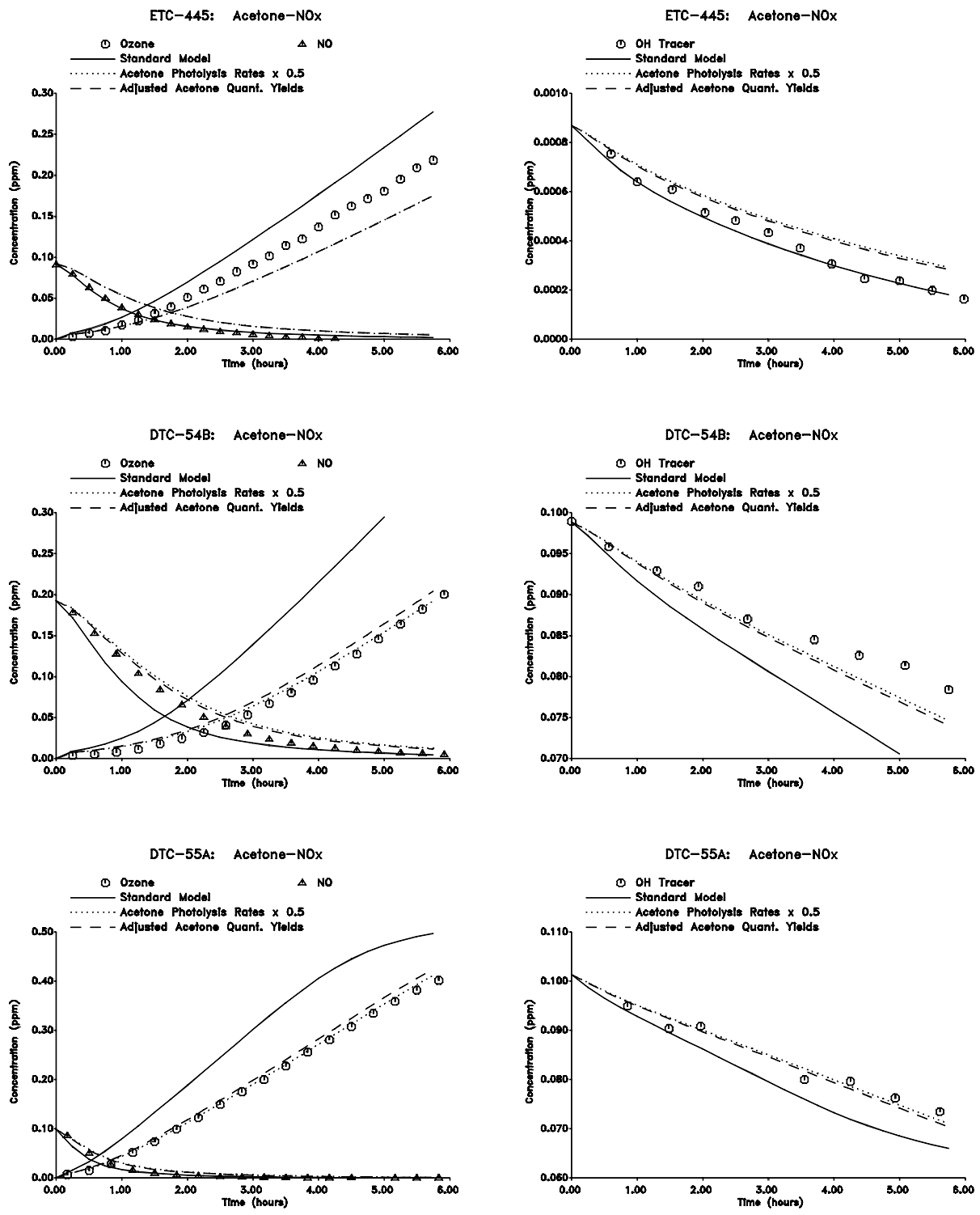

Figure 3. Experimental and calculated concentration-time profiles for selected species in the acetone - NO_x runs carried out in the blacklight chambers.

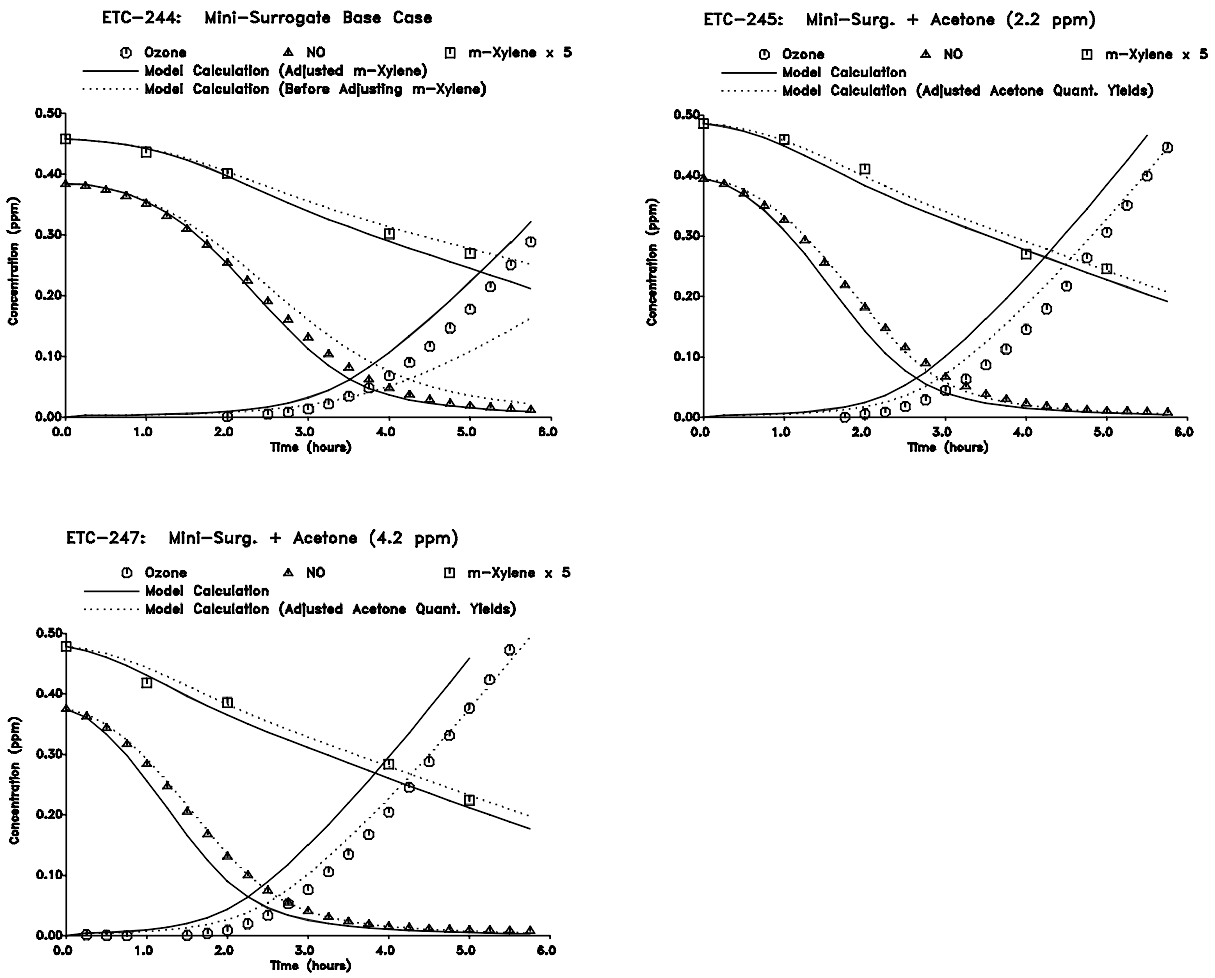

Figure 4. Experimental and calculated concentration-time profiles for selected species in a selected base case run and in the added acetone reactivity experiments using the mini-surrogate in the ETC blacklight chamber.

Ethane Experiments

Since one objective of this study is to assess the reactivities of acetone relative to those of ethane, it is useful to also include available data for ethane. A number of incremental reactivity experiments for ethane were carried out in the ETC using the mini-surrogate, and the results have been presented elsewhere (Carter et al., 1993a). In addition, an ethane reactivity experiment using the ethene surrogate has also been carried out. Table 2 gives a summary of conditions and results of the most reliable ethane reactivity experiments carried out using the mini-surrogate and of the ethane reactivity run using the ethene surrogate, and Figure 10 gives plots of the experimental and calculated incremental reactivities for of these runs. (Runs carried out before the NO_x injection system was modified to remove

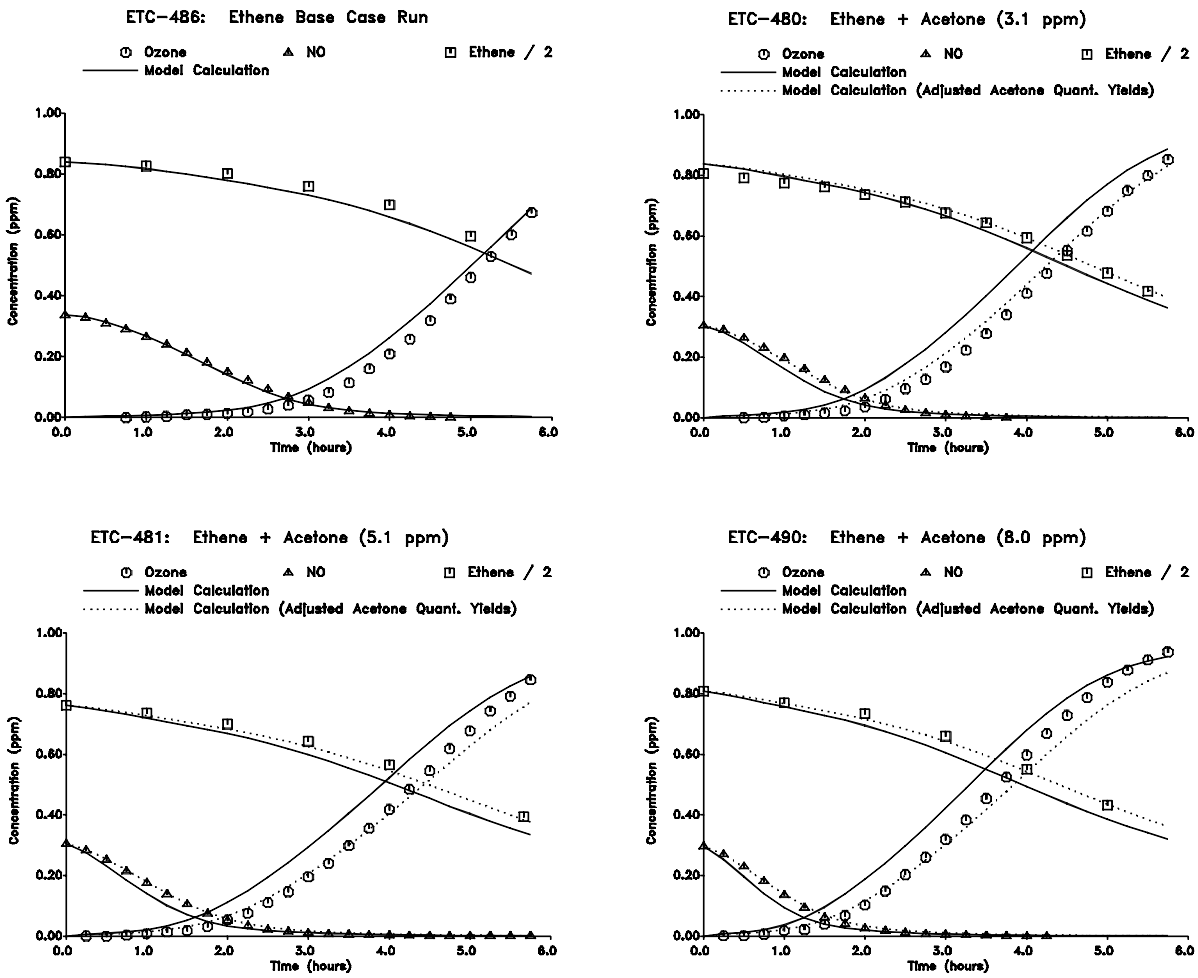

Figure 5. Experimental and calculated concentration-time profiles for selected species in a selected base case run and in the added acetone reactivity experiments using the ethene surrogate in the ETC blacklight chamber.

nitrous acid contamination, and runs which had anomalously high reactivities which can be attributed to an impure ethane sample, are not shown. See Carter et al., 1993.)

It can be seen that the model simulates the ethane reactivity measurements quite well. This is expected given that ethane's reaction mechanism is not considered uncertain, and the fact that ethane's major oxidation product is acetaldehyde, whose reactions the model apparently simulates quite well.

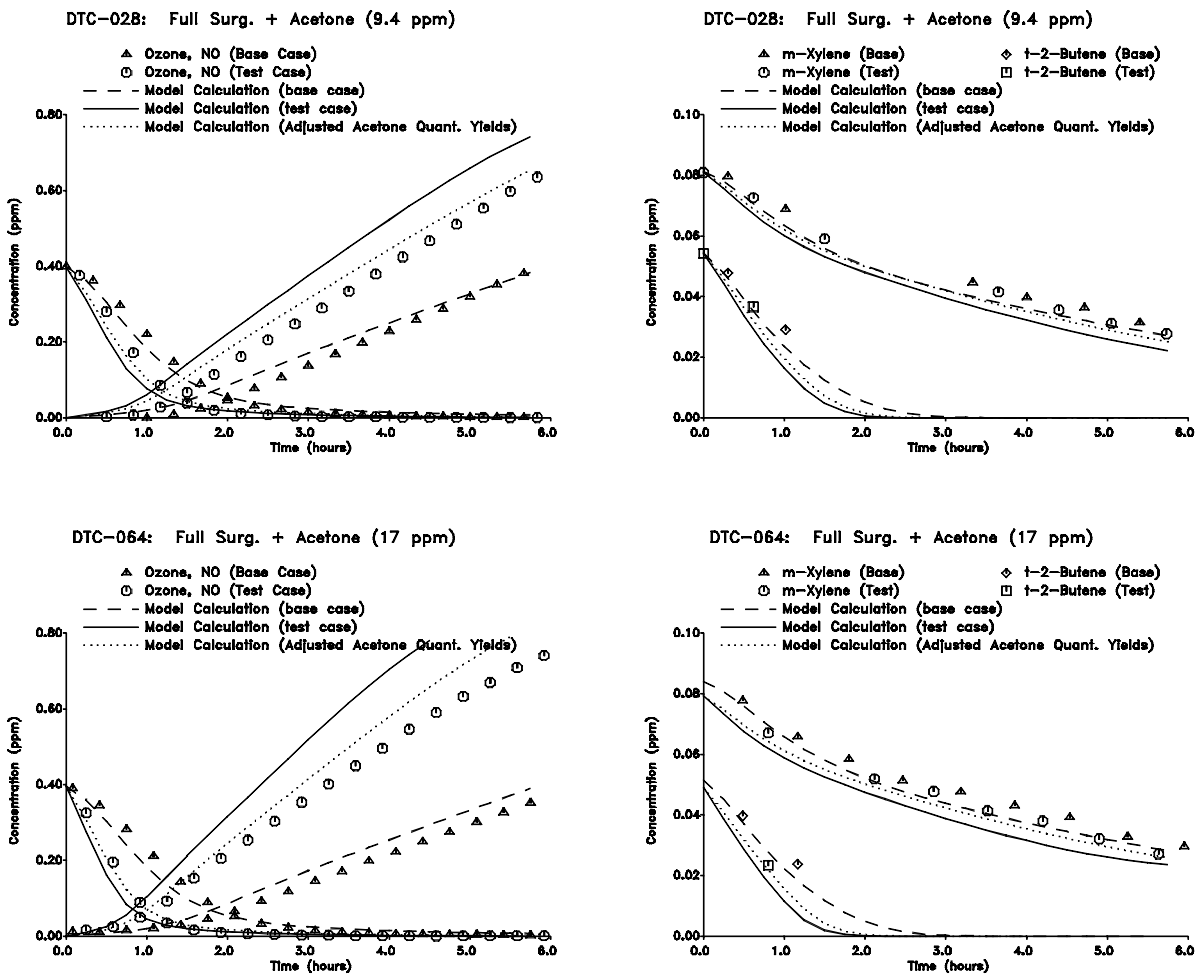

Figure 6. Experimental and calculated concentration-time profiles for selected species in a in the added acetone reactivity experiments using the full surrogate in the DTC blacklight chamber.

Xenon Chamber

Acetone - NO_x Experiments

Two acetone - NO_x experiments were carried out using the XTC chamber with the xenon arc light source. The conditions and selected results of the acetone - NO_x experiments are summarized on Table 2, and concentration-time plots of selected species are shown on Figure 11. Results of model calculations are also shown. It can be seen that, in contrast with the results with the blacklight chambers, the standard model may be biased towards underestimating the reactivity of acetone. The model fits the data well in one run, but underpredicts ozone somewhat in the other. The model with the photolysis rates

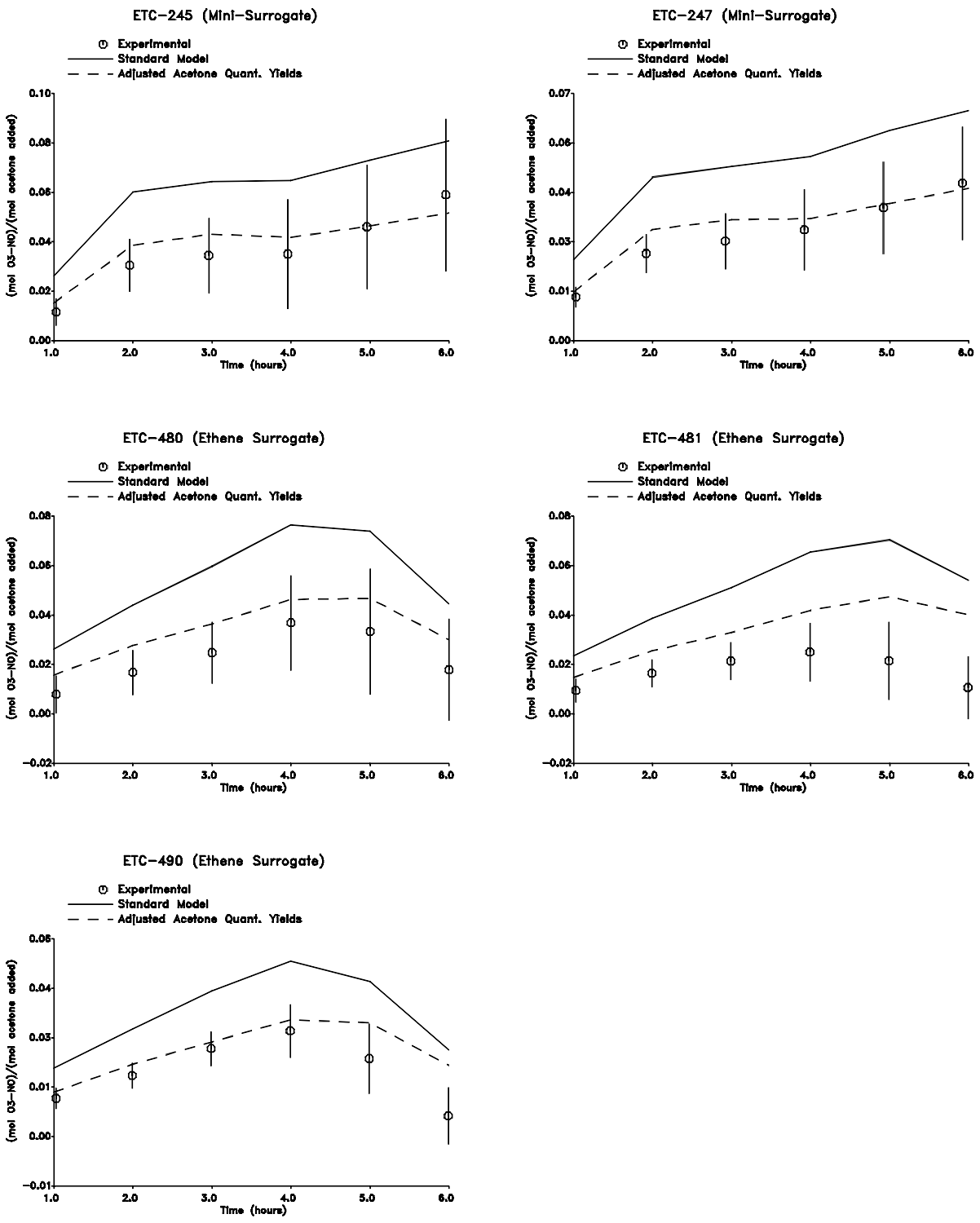

Figure 7. Experimental and calculated incremental reactivities, as a function of reaction time, in the added acetone reactivity experiments using the mini-surrogate and the ethene surrogate in the ETC blacklight chamber.

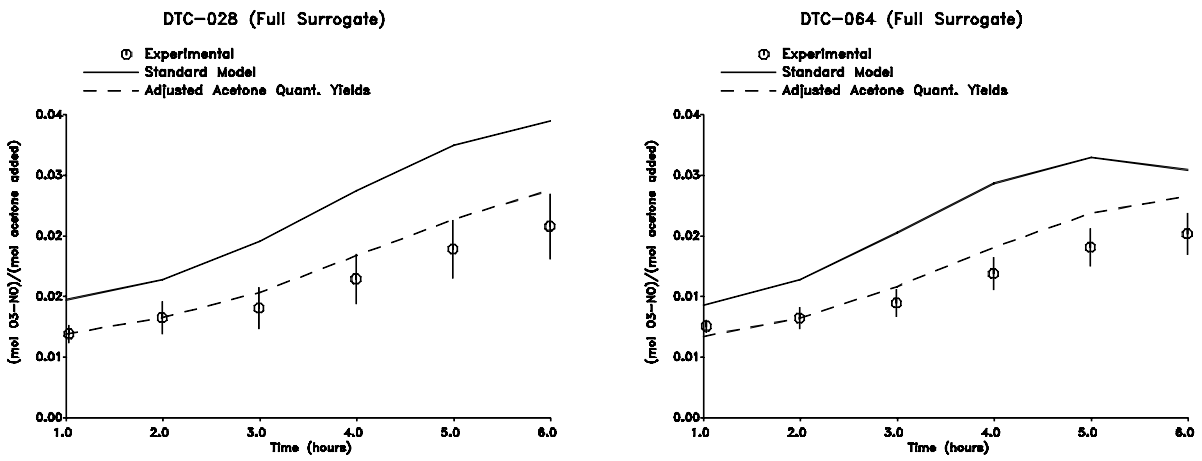

Figure 8. Experimental and calculated incremental reactivities, as a function of reaction time, in the added acetone reactivity experiments using the full surrogate in the DTC blacklight chamber.

reduced by a factor of two significantly underpredicts the ozone formation and radical levels in both these experiments.

Acetaldehyde - NO_x Experiments.

For comparison and control purposes, we also carried out acetaldehyde - NO_x experiments in this chamber. The conditions and selected results of the acetaldehyde - NO_x experiments are summarized on Table 2, and concentration-time plots of selected species are shown on Figure 12. Results of model calculations are also shown. It can be seen that, as with the blacklight chamber runs, the model fits the data very well.

Outdoor Chamber

Acetone - NO_x Experiments

A total of six acetone - NO_x experiments were conducted in the outdoor chamber for this program, of which three are used for mechanism evaluation. The conditions and selected results of these runs are summarized on Table 2. Three of these runs were carried out on overcast days, and since our procedures for light characterization for outdoor runs is not applicable for such conditions they were not modeled. Concentration-time plots for selected species for the other three runs are shown on Figure 13, where they can be compared with the model predictions. Note that run OTC-270 was carried out in November of 1992, while the other two runs were carried out in June of 1993.

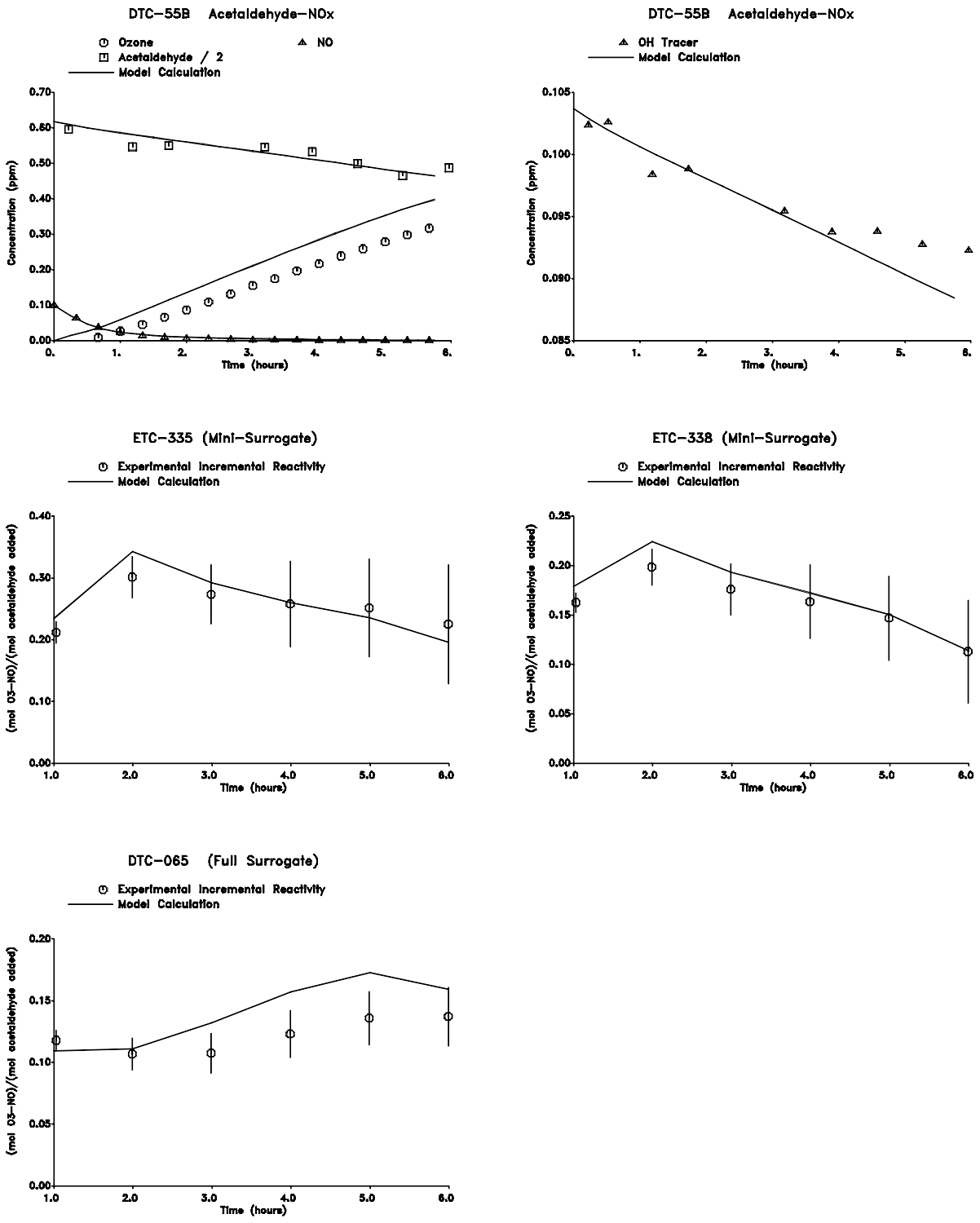

Figure 9. Selected experimental and calculated results for the acetaldehyde - NO_x experiments and the added acetaldehyde reactivity experiments carried out using the blacklight chambers.

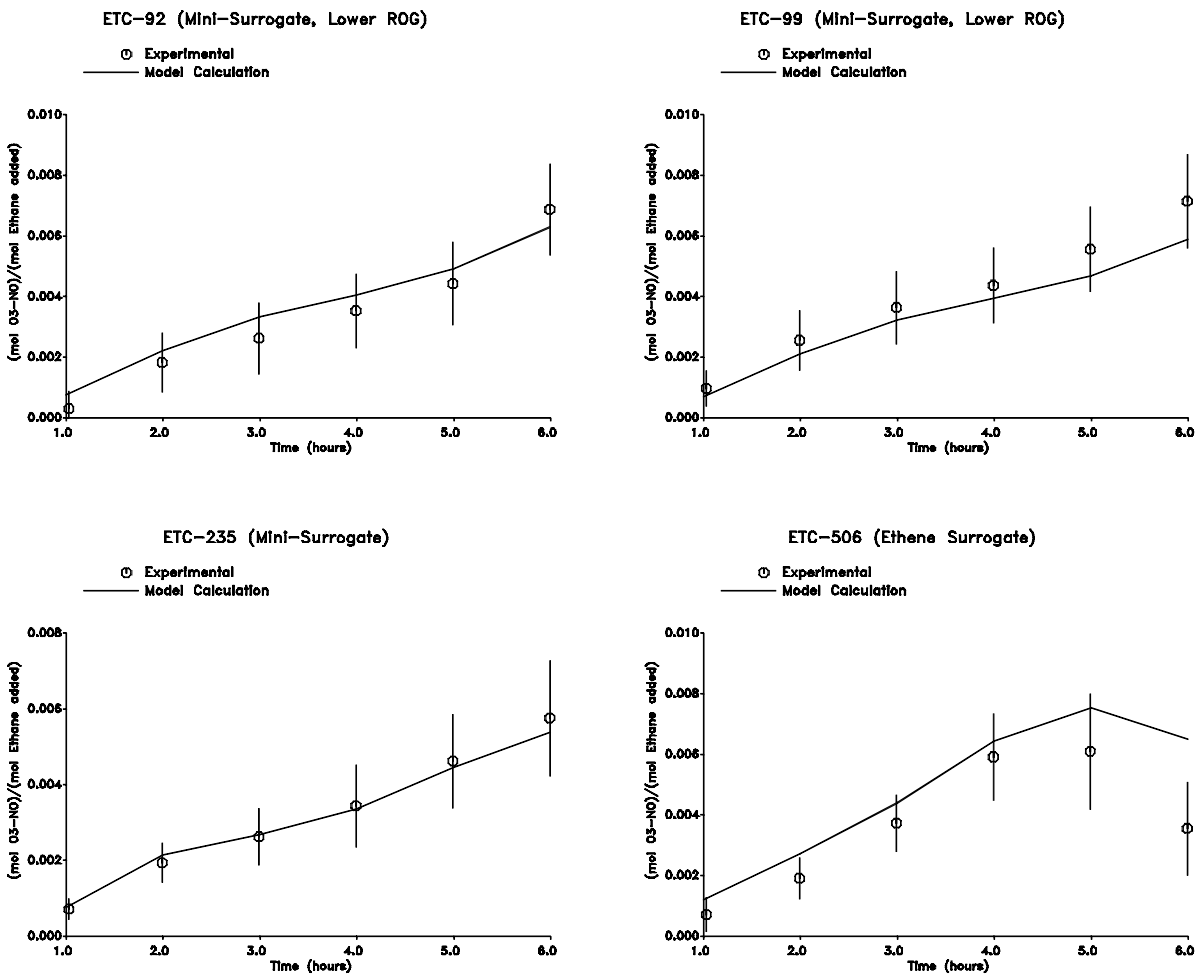

Figure 10. Experimental and calculated incremental reactivities, as a function of reaction time, in the added ethane reactivity experiments. All experiments were carried out in the ETC blacklight chamber.

It can be seen that the model simulation overpredicts the ozone formation and NO oxidation rates in the winter run (OTC-270), but fits data in the summer runs reasonably well. Although the temperatureis somewhat uncertain in run OTC-270, adjusting the temperature within its estimated uncertainty does not significantly improve the model simulation.

Acetaldehyde - NO_x Experiments.

As with the XTC, acetaldehyde - NO_x experiments were carried out in the outdoor chamber for control and comparison purposes. The conditions and selected results of the acetone - NO_x experiments are summarized on Table 2, and concentration-time plots of selected species are shown on Figure 14. Results of model calculations are also shown. It can be seen that, as with the runs in the

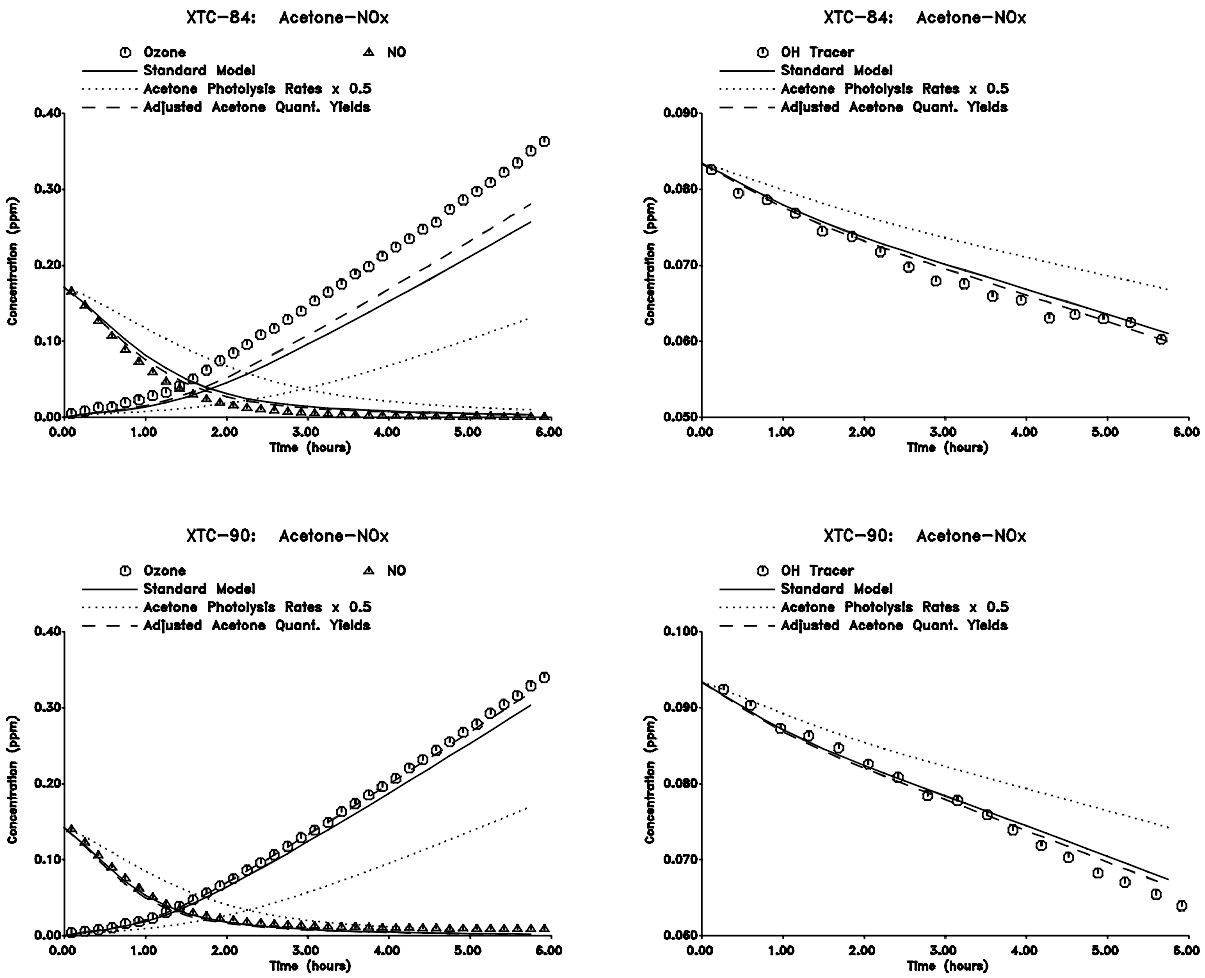

Figure 11. Experimental and calculated concentration-time profiles for selected species in the acetone - NO_x runs carried out in the xenon arc chamber.

other chamber, the model fits the data very well. This is particularly gratifying in this case, given the greater uncertainties and difficulties in characterizing light conditions for outdoor runs. However, all the acetaldehyde runs were carried out in the summer, and thus these data give no indication of the ability of the model to simulate conditions in winter runs.

Acetone Reactivity Experiments

Two acetone reactivity experiments were carried out using the full surrogate and three using the ethene surrogate. The conditions and selected results of these runs are summarized in Table 1, concentration-time plots for selected species are given on Figure 15 for runs using the full surrogate

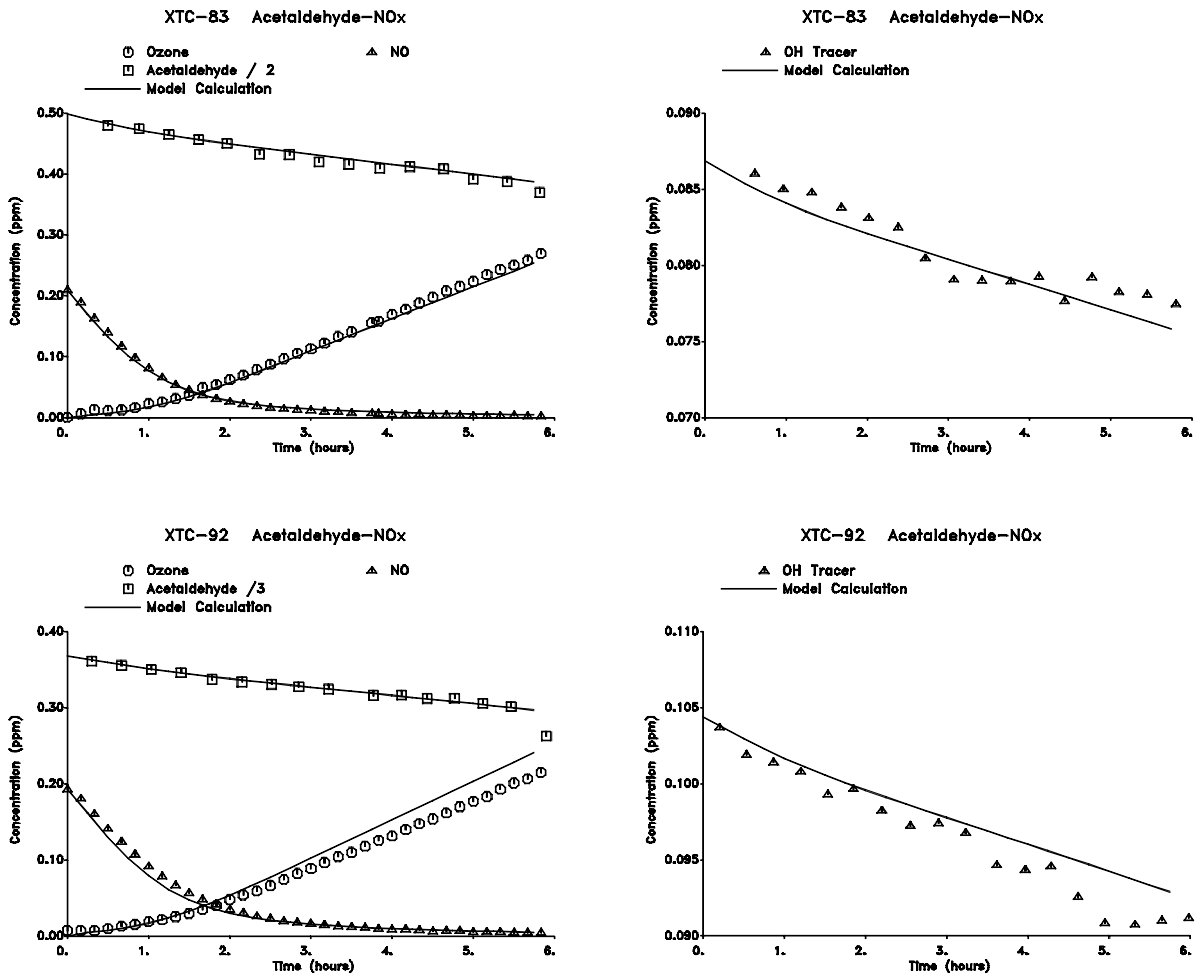

Figure 12. Experimental and calculated concentration-time profiles for selected species in the acetaldehyde - NO_x runs carried out in the xenon arc chamber.

and on Figure 16 for those using the ethane surrogate. Incremental reactivity plots are given on Figure 17. Results of model simulations are also shown. Note that all of these are summer runs carried out under clear sky conditions.

Figures 15 and 16 shows that the model consistently underpredicts the ozone formation rates in the base case experiments. This underprediction may be due to the relatively high temperatures for these runs, and the fact that the mechanisms for most species have not been evaluated at these higher temperatures. The relatively good performance in the case of the acetaldehyde runs may be due to the fact that the temperature dependencies for its main temperature-dependent reaction — the decomposition of PAN — are now reasonably well characterized. One might have expected better performance in the case of

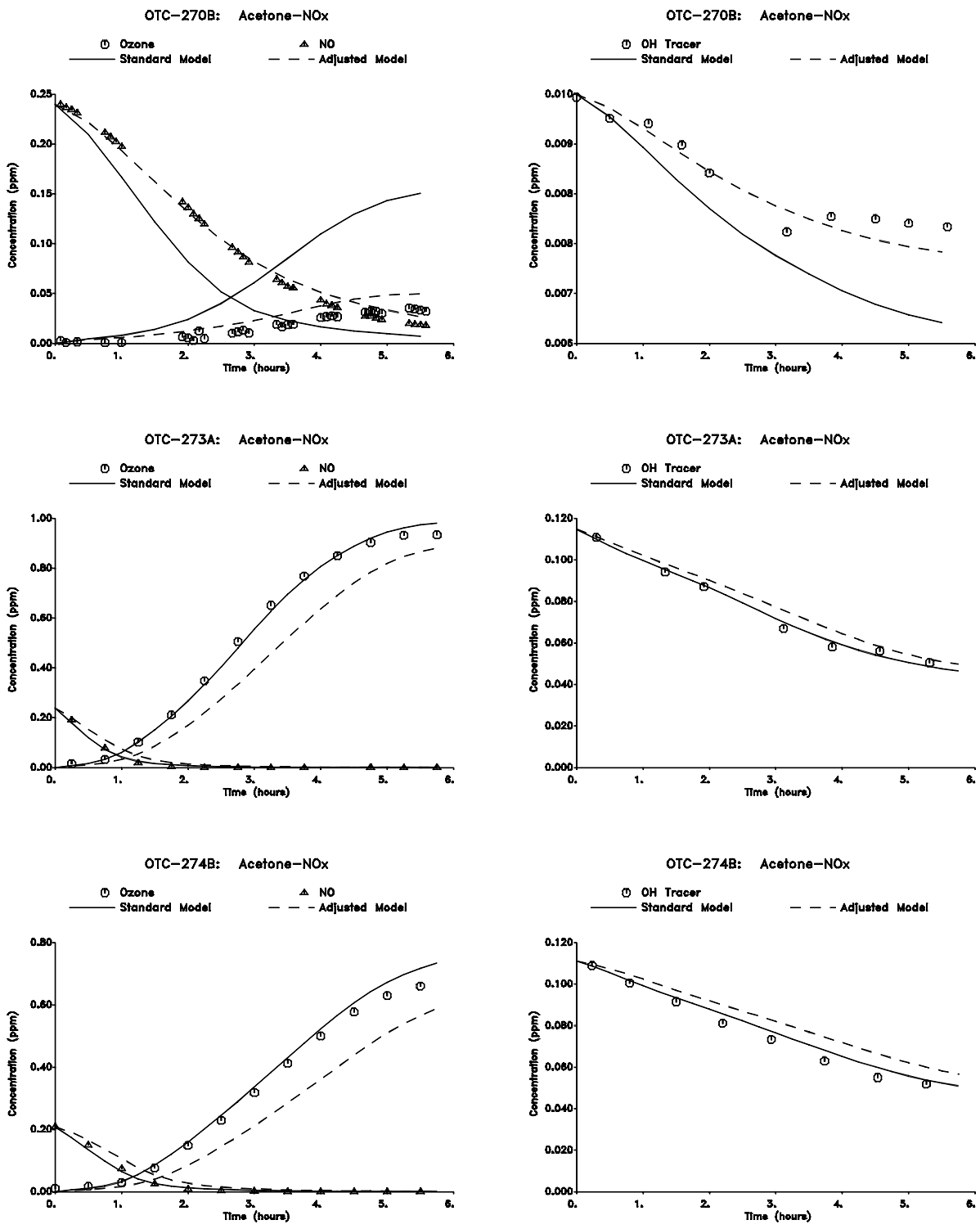

Figure 13. Experimental and calculated concentration-time profiles for selected species in the acetone - NO_x runs carried out in the outdoor chamber.

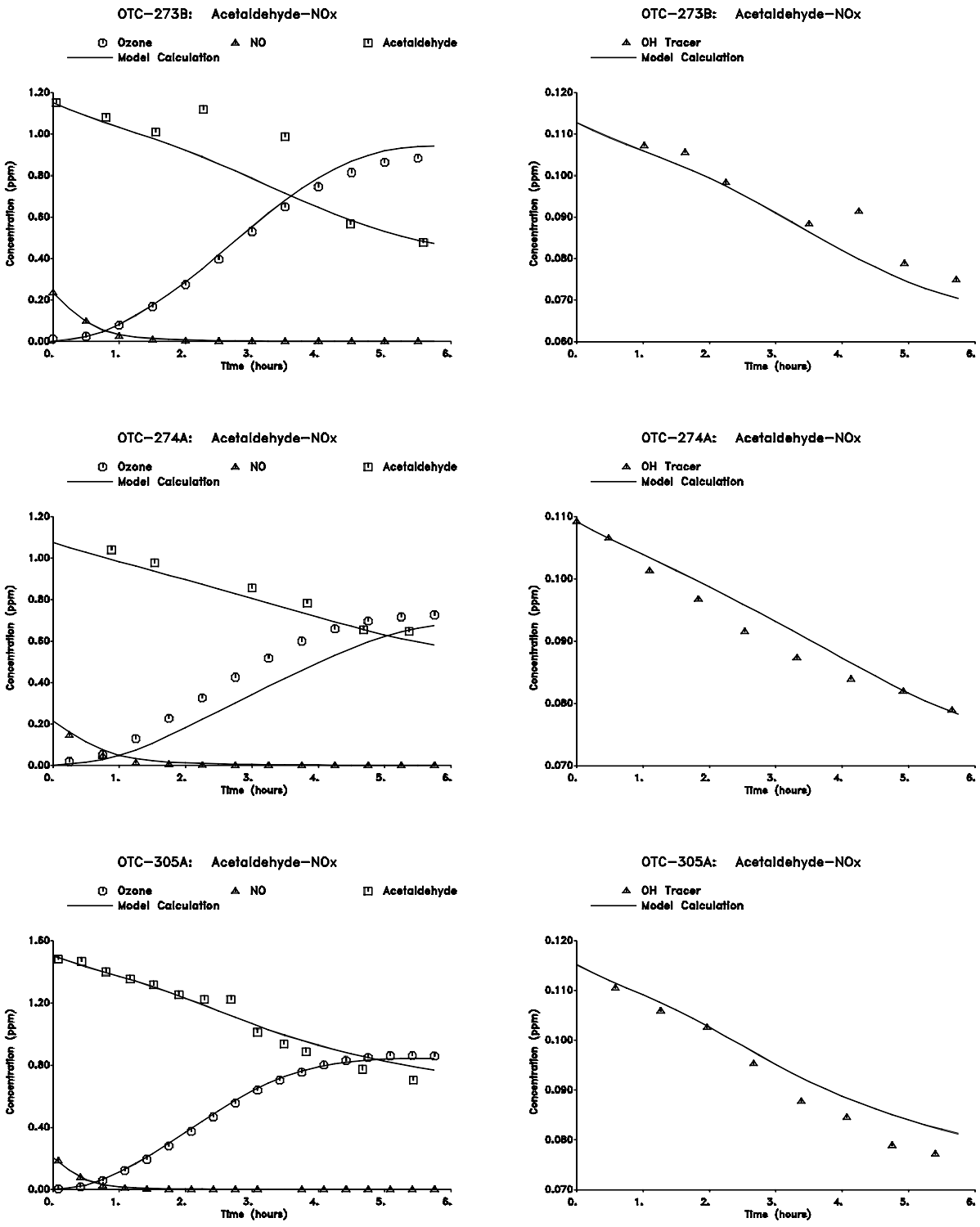

Figure 14. Experimental and calculated concentration-time profiles for selected species in the acetaldehyde - NO_x runs carried out in the outdoor chamber.

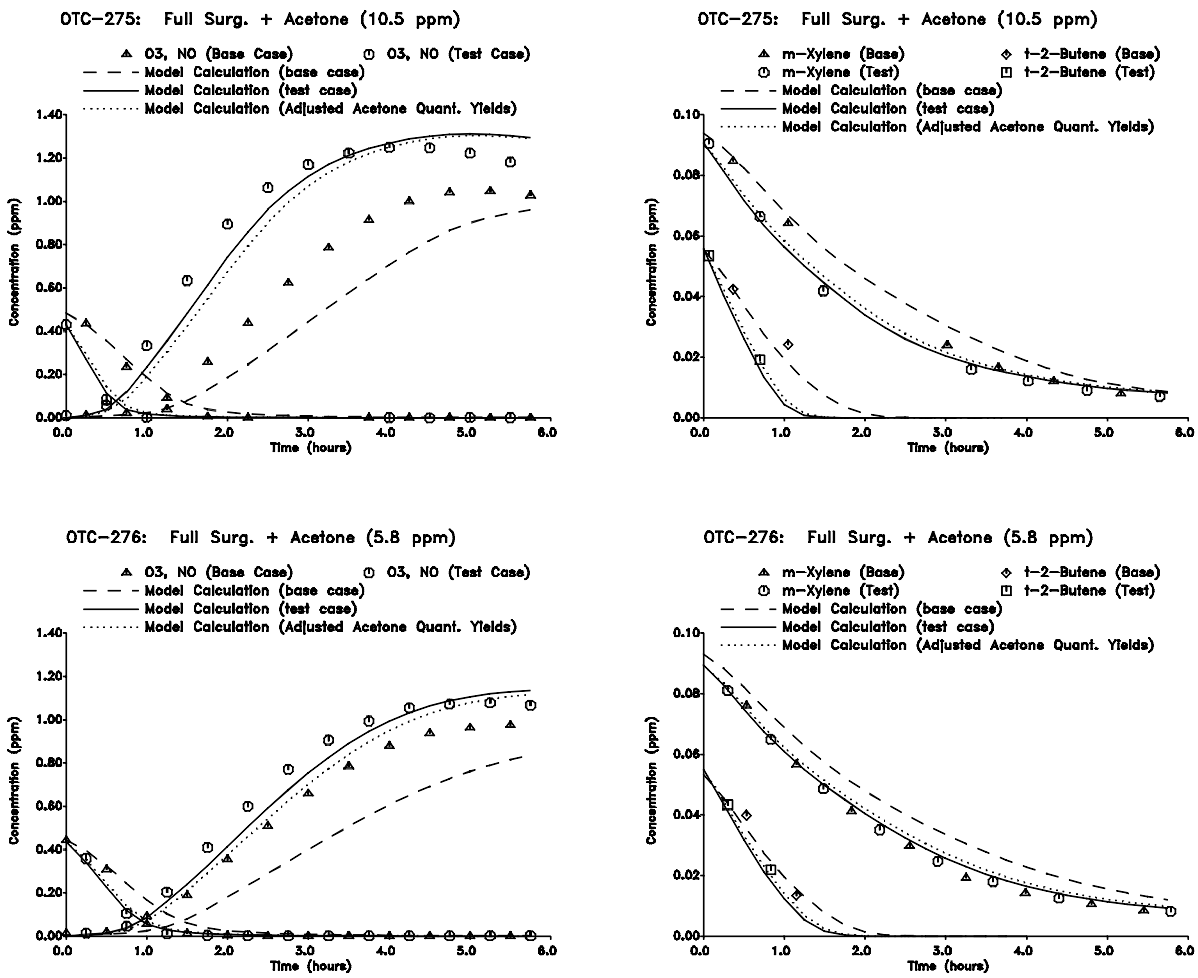

Figure 15. Experimental and calculated concentration-time profiles for selected species in a in the added acetone reactivity experiments using the full surrogate in the outdoor chamber.

the ethene runs, but the temperature dependence of the radical yields in the O_3 + ethene reaction have not been characterized, and adjustment of this radical yield can significantly improve the results of the model simulations of these runs. However, an investigation of the reasons for the discrepancies in the model simulations of the ethene and full surrogate runs is beyond the scope of this program.

Figure 17 shows that the model does not simulate the reactivity results very well, especially in the later periods of the runs. The biases of the model predictions later in the runs are also not consistent from run to run — in some cases the reactivities are reactivities are overpredicted, and in some cases they are underpredicted. This can be attributed, at least in part, to the poor performance of the model in simulating the base case experiments. The model gives somewhat better predictions of the incremental

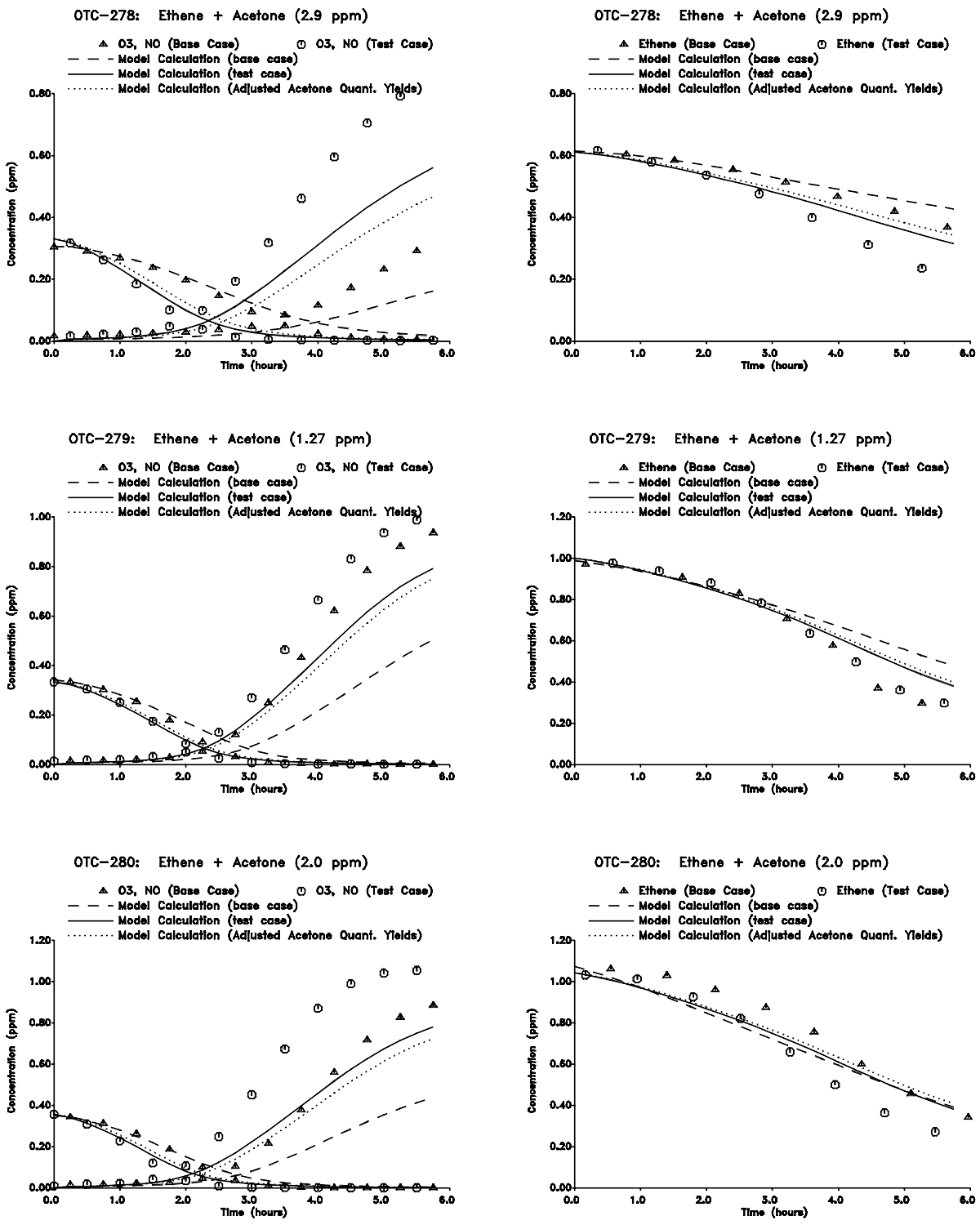

Figure 16. Experimental and calculated concentration-time profiles for selected species in a in the added acetone reactivity experiments using the ethene surrogate in the outdoor chamber.

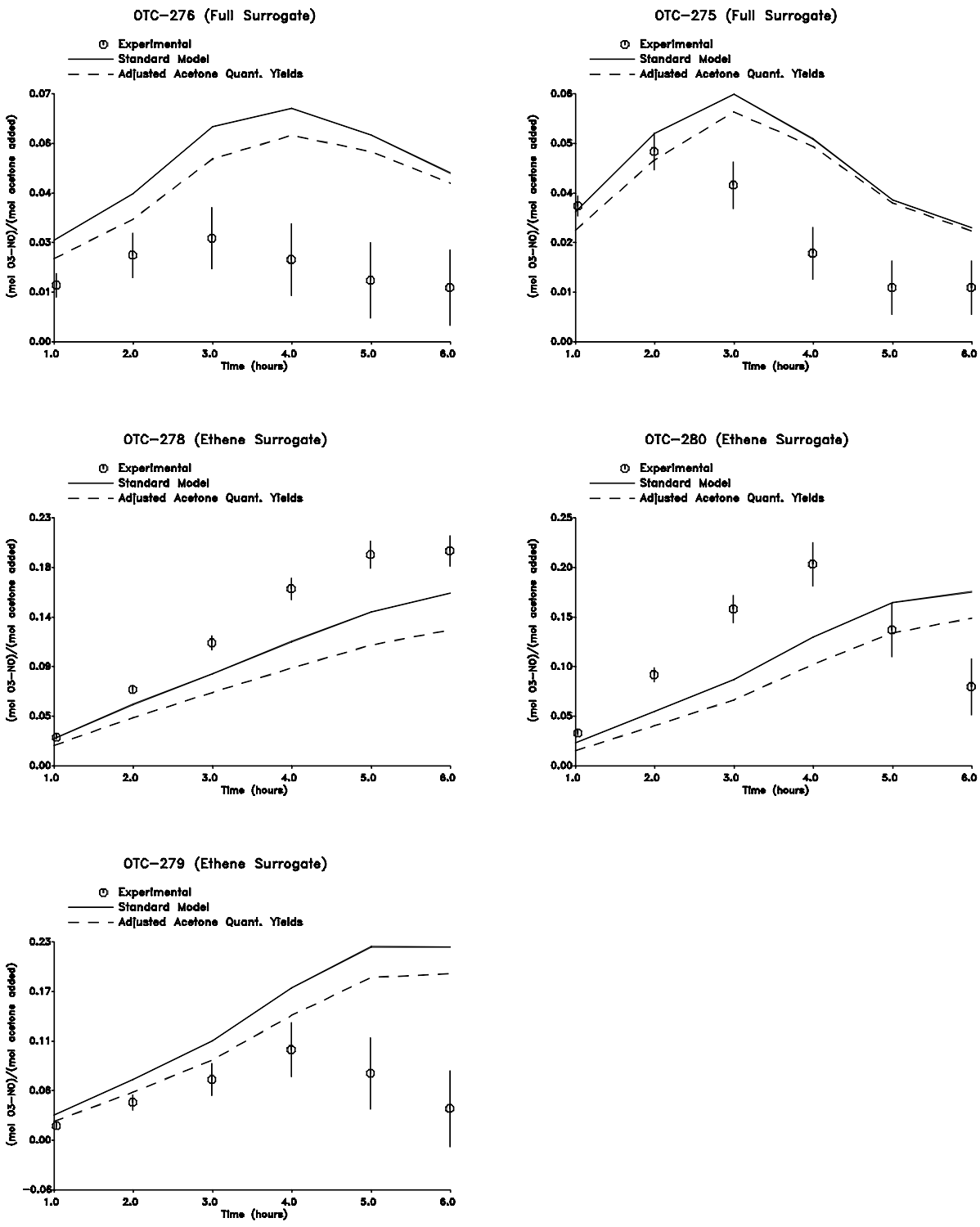

Figure 17. Experimental and calculated incremental reactivities, as a function of reaction time, in the added acetone reactivity experiments carried out in the outdoor chamber.

reactivities at earlier periods in the runs, before the predictions of the model for the base case experiment began to deviate significantly from the data. However, until the problems which caused the poor performance of the model in simulating the base case runs are addressed, we consider the outdoor chamber acetone reactivity experiments to be inconclusive and not useful for mechanism evaluation.

Ethane vs Acetone Comparison Experiments

Two outdoor chamber experiments were conducted on the outdoor chamber where the effects of adding approximately equal masses of acetone or ethane to a full surrogate - NO_x mixture were determined. In the first experiment (run OTC-312), the acetone was added to Side A (on the eastern side) while ethane was added to side B, while in the second experiment (OTC-313) the sides were reversed. For control purposes, a side equivalency test, where equal amounts of the surrogate - NO_x mixture were irradiated on both sides without any other additions, was also carried out. The same amount of surrogate and NO_x was used in all three runs. The conditions and selected results of these experiments are shown on Table 2, and selected results are shown on Figure 18. Note that the temperature was much higher in run OTC-312 than in the other two runs, and as a result much more ozone was formed than in run OTC-313, despite the fact that essentially the same reactant concentrations were employed.

The results of both acetone vs ethane experiments suggest that acetone has a slightly greater ozone reactivity than ethane under the conditions of these experiments. However, the differences are not the same in the two runs. In the higher temperature run (OTC-312), the NO oxidation and ozone formation rates were somewhat faster on the acetone side compared to the ethane side, though the final ozone yields were essentially the same. On the other hand, in the lower temperature run (OTC-313), the ozone formation and NO oxidation rates were essentially equal on both sides until the last hour, when slightly more ozone was formed on the side with acetone. The side equivalency test showed that the NO oxidation and ozone formation rate is slightly faster on the eastern side (Side A), presumably due to the fact the sun is to the east in the mornings. However, the effect of the side differences is small compared to the differences observed in run OTC-312. Since acetone is on the less reactive side in run OTC-313, where the acetone and ethane sides had equal NO and ozone results for most of the run, this suggests that the NO oxidation and ozone formation rates might have been slightly higher on the acetone side had this inequivalency not existed. On the other hand, the apparent greater reactivity of acetone relative to ethane would have been reduced in run OTC-312, where acetone is on the more reactive side.

The results of model simulations of these experiments are also shown on Figure 18. As with the other OTC runs employing the full surrogate, the model consistently underpredicts the rate of ozone formation and NO oxidation. It also significantly overpredicts the differences in reactivity between acetone and ethane in the lower temperature run, and the differences in final ozone yields in the higher temperature run.

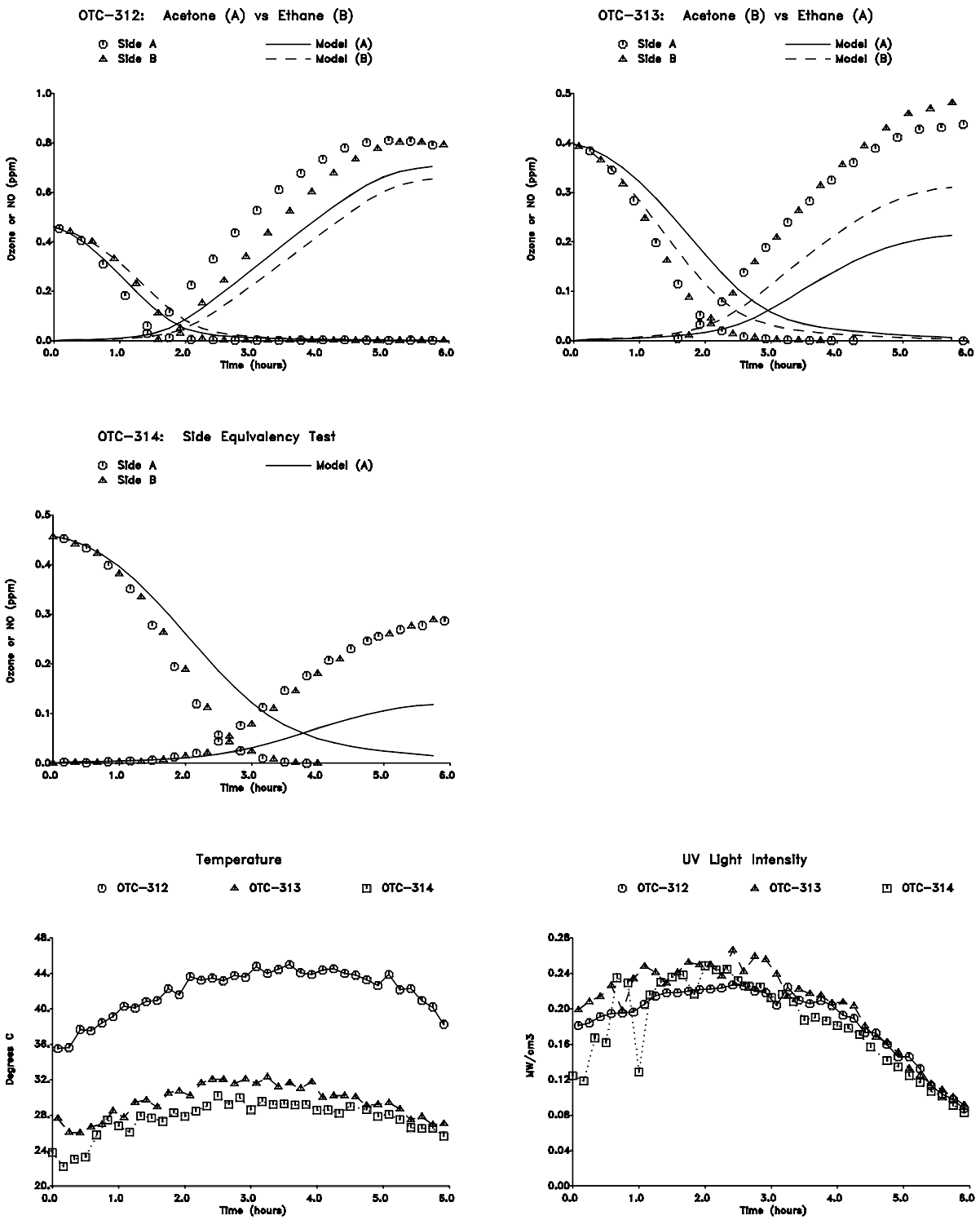

Figure 18. Experimental and calculated concentration-time profiles for ozone and NO, and experimental temperature and UV light intensity data, in the acetone vs ethane comparison experiments and the associated side equivalency test.

These results can be compared with the results of a very similar experiment reported by Jeffries (1993), where equal amounts of ethane and acetone (on a per carbon basis) were added to an ROG surrogate - NO_x mix on the two sides of the University of North Carolina (UNC) outdoor chamber, and simultaneously irriadiated. As with our OTC experiments, an equal amount of ethane was added on a per carbon basis as the ROG surrogate, but unlike our experiments the amount of acetone added had the same number of carbons, rather than the same mass, as the added ethane. This meant that the amount of acetone added was 28% higher, compared to added ethane, in the UNC experiment compared to our runs. Despite the relatively higher amount of added acetone, in the UNC experiment there was no measurable difference in the amount of ozone formed in the added acetone side compared to the added ethane side. Thus, either the reactivity difference was too small to be measured under the conditions of the UNC experiment, or acetone is slightly less reactive than ethane under the conditions of that run. This is in contrast with our results, where acetone was found to be very slightly more reactive in both experiments.

Although the runs (both ours and UNC's) need to be reproduced before definitive conclusions can be reached, the two OTC experiments suggest that the differences in reactivity of acetone and ethane may be temperature dependent, with the reactivities being nearly equal at the lower temperature (which is more representative of most ambient conditions), but with acetone becoming relatively more reactive as the temperature increases to above 40°C (104°F). A temperature effect in the differences of reactivity might be attributed to the relative importance of PAN formation in the photooxidation of acetone, since the decomposition of PAN to form radicals is highly temperature dependent. However, the average temperature in the UNC experiment was approximately 305°K, which is closer to (but slightly higher than) the lower temperature run in this study. Thus, a temperature effect cannot be the reason for the lower apparent reactivity of acetone relative to ethane in the UNC experiment compared to these runs. More research concerning effects of temperature on the base case system is needed before any conclusions can be made concerning the ability of the model to predict temperature effects on relative reactivities.

Model Simulations Using the Adjusted Acetone Mechanism

The model simulations of the acetone experiments in the chambers with the blacklight and xenon arc light sources, taken together, indicate that there is a problem with how the mechanism predicts the acetone photolysis rate is affected by the spectrum of the light source. Although the possibility of compensating errors can never be ruled out in model simulations of environmental chamber experiments (Jeffries et al., 1992), the fact that the model gives reasonably good fits to the results of the acetaldehyde experiments using the various light sources suggests that the discrepancies observed for acetone in these chambers are not likely to be due to errors in our characterization of experimental conditions. If the absorption cross sections are assumed to be correct (they are fairly straightforward to measure and there is no significant inconsistency in the literature concerning them) this discrepancy can only be explained by the model having an incorrect dependence of the quantum yields on wavelength. As discussed above, there are inconsistencies in the literature concerning the acetone quantum yields, and the accepted values

are based on analyses of chemical systems which are almost as complex as these chamber experiments.

The data in the literature do not provide any guidance for reducing the discrepancy, since the quantum yields we use in the model already are lower than any of the published values (see above). If we had not corrected the quantum yields of Meyrahn et al. (1986), or used the higher quantum yields of Gardner et al. (1984), the discrepancy between the model and our data from the blacklight chambers would be even worse. Therefore, the only option we have is to make arbitrary adjustments to the quantum yields to see if it is possible to make the model simulations more consistent with our experimental data.

We found that a factor of two downward adjustment of the photolysis rates resulted in a model which gave excellent predictions to the experimental incremental reactivities in the blacklight chamber, and somewhat better predictions of the results of the acetone - NO_x runs using that light source. This is shown on Figures 3-8, where the "adjusted acetone quantum yields" model uses acetone photolysis rates which are 54% of the value used in the standard model. However, if this adjustment is made by reducing the quantum yields by the same factor at all wavelengths, the result would be that the photolysis rate is also reduced by a factor of ~2 in the XTC runs, which would cause a significant underprediction of ozone formation in the acetone - NO_x runs in that chamber. This is shown in Figure 11, where the dotted lines show the model prediction where the acetone photolysis rate is reduced by approximately the same factor that gives the best fits to the blacklight chamber runs. Since the XTC light source has a spectrum which more closely resembles sunlight than do blacklights, this would clearly not be an acceptable adjustment for a model to be used in ambient simulations.

To fit both the blacklight and xenon arc chamber data, it is necessary to adjust the quantum yields such that the photolysis rates for the blacklight light source is reduced by ~2, while the rates with the xenon arc are relatively unchanged. A possible approach for doing this is suggested by examining the spectra of the light sources in the wavelength regions which affect acetone photolysis. Figure 1 shows the spectra of these light sources over the full wavelength region affecting most photolysis reactions, but shows that only a relatively narrow wavelength region, from ~290 - 320 nm, affects the photolysis of acetone. Figure 19 shows more clearly the spectra of the light sources, and the action spectrum for acetone, in the 300 - 320 nm wavelength region. It can be seen that the blacklights have a much lower intensity in this wavelength region than do the xenon lights or sunlight, which means that it would have a lower photolysis rate relative to that for NO_2. This should already be taken into account in the model simulations, since the spectra shown are used to calculate the photolysis rates. However, it also significant to note that the ratios of intensities of the xenon light to the blacklights increase significantly with increasing wavelength in this region. Therefore, the wavelength region affecting the acetone photolysis rates for blacklights is higher than that affecting the photolysis rate for the xenon arc light

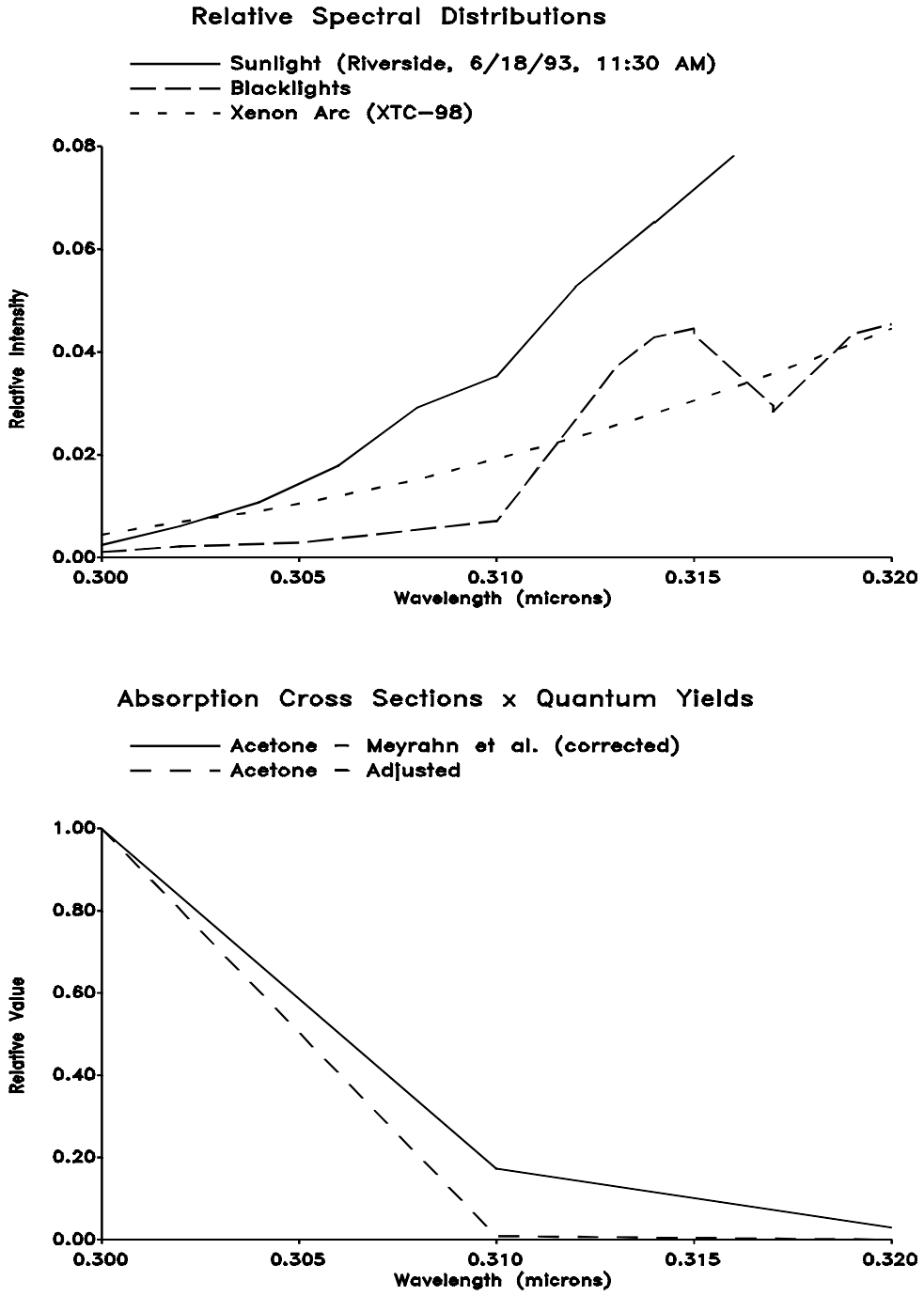

Figure 19. Top Plot shows comparison of spectra of light sources used in the environmental chamber studies, for the wavelength range 300 - 320 nm. Bottom plot shows spectra of absorption cross sections x quantum yields for the standard and the adjusted acetone mechanisms.

source. This means that decreasing the quantum yields at the higher wavelengths which are more important in affecting the rate in the blacklight chamber while increasing them at the lower wavelengths which are more important for the rate in the XTC might yield the desired photolysis rates under both conditions.

An adjusted acetone action spectrum which causes the desired reduction in the acetone photolysis rate with blacklights without significantly changing the photolysis rate in the XTC is shown on Figure 19. This spectrum results assuming that the quantum yield is essentially constant at ~0.6 at wavelengths below 290 nm, decreases to 0.005 at 310 nm, and to essentially 0 at 320 nm, in contrast with the corrected quantum yields of Meyrahn et al. (1986), where the quantum yields decrease more gradually with wavelength from ~0.6 at 290 nm to 0.01 at 320 nm and 0 at 330 nm. Thus the adjusted quantum yields are essentially the same as to those of Meyrahn et al (1986) at wavelengths ≤ 280 nm, are respectively ~2 and ~1.5 times higher at 290 and 300 nm, and are significantly lower at wavelengths ≥ 310 nm. (The specific quantum yields are given with the mechanism listing in Appendix A.) The model using this set of quantum yields is referred to as the "adjusted acetone" model. Although the set of quantum yields used in this adjusted model is not theoretically unreasonable, we have no justification for it other than its use results in significantly better fits to our chamber data.

The model simulations of our chamber experiments using the adjusted acetone model are shown on Figures 3-8 for blacklight chamber runs, on Figure 11 for the XTC runs, and on Figures 13 and 15-17 for the outdoor chamber runs. As discussed above, the improvement for the blacklight chamber runs is significant, though the adjusted model somewhat underpredicts the NO oxidation and ozone formation rates in run ETC-445 (Figure 3). On the other hand, the adjustment does not degrade the simulation of the acetone runs in the XTC (Figure 11); instead it slightly improves it. The adjusted model also gives a significantly better simulation of the wintertime outdoor acetone - NO_x run (OTC-270B), though the simulation of the summertime runs (OTC-273A and OTC-274B) are not quite as good as the unadjusted model (Figure 13). The changes in the predictions of the incremental reactivities in the outdoor runs (Figure 17) caused by the adjustment are relatively small compared to the discrepancy between the model calculation and the experimental data. Thus, the simulations of the outdoor runs are not sufficiently consistent to make any conclusions concerning which mechanism performs better. However, simulations of the better characterized indoor runs provide a much less ambiguous test of the mechanism, and the results indicate that the adjusted model performs significantly better in simulating acetone's reactivity and in predicting the effects of changing the spectrum of the light source.

ATMOSPHERIC REACTIVITY CALCULATIONS

Since incremmental reactivities of VOCs have been shown to be highly dependent on environmental conditions, incremental reactivities measured in environmental chamber experiments cannot necessarily be assumed to be applicable to atmospheric conditions (Carter and Atkinson, 1989). The only method available to obtain quantitative estimates of incremental reactivities of VOCs in ambient air pollution episodes is to conduct airshed model simulations of the episodes. Since these simulations cannot be any more reliable than the chemical mechanisms used, a major objective of this program was to assess the reliability of the acetone mechanism for use in such simulations. This was discussed in the previous sections. In this section, we discuss the results of model simulations of acetone's incremental reactivity in a variety of model scenarios representing ozone exceedence episodes in various areas in the United States (Bauges, 1990), and compare the results to incremental reactivities calculated for ethane and for the base ROG, i.e., the mixture representing total ROG emissions from all sources. Both the adjusted and the unadjusted acetone mechanism are used.

Scenarios Used for Reactivity Assessment

The set of airshed scenarios employed to assess acetone's reactivity for this study is the same as those used for calculating the MIR and other reactivity scales, as discussed previously (Carter, 1993a). The objective is to use a set of scenarios which represents, as much as possible, a comprehensive distribution of the environmental conditions where unacceptable levels of ozone is formed. Although a set of scenarios has not been developed for the specific purpose of VOC reactivity assessment, the EPA developed an extensive set of scenarios for conducting analyses of effects of ROG and NO_x controls on ozone formation using the EKMA modeling approach (Gipson et al., 1981; Gipson and Freas, 1983; EPA, 1984; Gery et al., 1987; Bauges, 1990). The EKMA approach involves use of single-cell box models to simulate how ozone formation in one day episodes is affected by changes in ROG and NO_x inputs. Although single-cell models cannot represent realistic pollution episodes in great detail, they can represent dynamic injection of pollutants, time-varying changes of inversion heights with entrainment of pollutants from aloft as the inversion height increases throughout the day, and time-varying photolysis rates, temperatures, and humidities (Gipson and Freas, 1981; EPA, 1984; Gipson, 1984; Hogo et al., 1988). Thus, they can be used to simulate a wide range of the chemical conditions which affect ozone formation from ROG and NO_x. These are the same as those affecting VOC reactivity. Therefore, at least to the extent they are suitable for their intended purpose, an appropriate set of EKMA scenarios should also be suitable for assessing methods to develop reactivity scales encompassing a wide range of conditions.

Base Case Scenarios

The set of EKMA scenarios used in this study were developed by the United States EPA for assessing how various ROG and NO_x control strategies would affect ozone nonattainment in various areas of the country (Bauges, 1990). The characteristics of these scenarios and the methods used to derive their input data are described in more detail elsewhere (Bauges, 1990; Carter, 1993a). Briefly, 39 urban areas in the United States were selected based on geographical representativeness of ozone nonattainment areas and data availability, and a representative high ozone episode was selected for each. The initial NMOC and NO_x concentrations, the aloft O_3 concentrations, and the mixing height inputs were based on measurement data for the various areas, the hourly emissions in the scenarios were obtained from the National Acid Precipitation Assessment Program emissions inventory (Bauges, 1990), and biogenic emissions were also included. Table 3 gives a summary of the urban areas represented and other selected characteristics of the scenarios.

Several changes to the scenario inputs were made based on discussions with the California ARB staff and others (Carter, 1993a). Two percent of the initial NO_x and 0.1% of the emitted NO_x in all the scenarios was assumed to be in the form of HONO. The photolysis rates were calculated using solar light intensities and spectra calculated by Jeffries (1991b) for 640 meters, the approximate mid-point of the mixed layer during daylight hours. The composition of the NMOCs entrained from aloft was based on the analysis of Jeffries et al (1989a). The composition of the initial and emitted reactive organics was derived as discussed below. Complete listings of the input data for the scenarios are given elsewhere (Carter, 1993a).

This set of 39 EKMA scenarios are referred to as "base case" to distinguish them from the scenarios derived from them by adjusting NO_x inputs to yield standard conditions of NO_x availability as discussed below. No claim is made as to the accuracy of these scenarios in representing any real episode, but they are a result of an effort to represent, as accurately as possible given the available data and the limitations of the formulation of the EKMA model, the range of conditions occurring in urban areas throughout the United States. When developing general reactivity scales it is more important that the scenarios employed represent a realistic distribution of chemical conditions than any accurately representing the details of any one particular episode.

The Base ROG mixture is the mixture of reactive organic gases used to represent the chemical composition of the initial and emitted anthropogenic reactive organic gases from all sources in the scenarios. Consistent with the approach used in the original EPA scenarios, the same mixture was used for all scenarios. The speciation for this mixture was derived by Croes (1991) based on an analysis of the EPA database (Jeffries et al. 1989a) for the hydrocarbons and the 1987 Southern California Air Quality Study (SCAQS) database for the oxygenates (Croes et al., 1993; Lurmann et al., 1992). This mixture consists of 52% (by carbon) alkanes, 15% alkenes, 27% aromatics, 1% formaldehyde, 2% higher

Table 3. Summary of conditions of base case scenarios used for atmospheric reactivity assessment.

City, State	Calc. Max O_3 (ppb)	ROG /NO_x	NO_x /NO_x^{MOR}	Final Height (km)	Init.+Emit Base ROG (mmol m^{-2})	Aloft O_3 (ppb)
Atlanta, GA	174	7.3	0.7	2.1	12	63
Austin, TX	171	9.3	0.5	2.1	11	85
Baltimore, MD	304	5.2	1.1	1.2	17	84
Baton Rouge, LA	235	6.8	1.0	1.0	11	62
Birmingham, AL	233	6.9	0.6	1.8	13	81
Boston, MA	191	6.5	0.6	2.6	14	105
Charlotte, NC	142	7.8	0.3	3.0	7	92
Chicago, IL	273	11.6	0.5	1.4	25	40
Cincinnati, OH	192	6.4	0.8	2.8	17	70
Cleveland, OH	239	6.6	1.0	1.7	16	89
Dallas, TX	192	4.7	1.3	2.3	18	75
Denver, CO	195	6.3	1.2	3.4	29	57
Detroit, MI	229	6.8	0.8	1.8	17	68
El Paso, TX	177	6.6	1.1	2.0	12	65
Hartford, CT	166	8.4	0.5	2.3	11	78
Houston, TX	291	6.1	1.0	1.7	25	65
Indianapolis, IN	201	6.6	0.9	1.7	12	52
Jacksonville, FL	152	7.6	0.7	1.5	8	40
Kansas City, MO	151	7.1	0.6	2.2	9	65
Lake Charles, LA	282	7.4	0.7	0.5	7	40
Los Angeles, CA	546	7.6	1.0	0.5	23	100
Louisville, KY	203	5.5	0.9	2.5	14	75
Memphis, TN	218	6.8	0.7	1.8	15	58
Miami, FL	131	9.6	0.4	2.7	9	57
Nashville, TN	163	8.1	0.5	1.6	7	50
New York, NY	350	8.1	0.8	1.5	39	103
Philadelphia, PA	230	6.2	1.0	1.8	19	53
Phoenix, AZ	258	7.6	1.0	3.3	40	60
Portland, OR	161	6.5	0.7	1.6	6	66
Richmond, VA	225	6.2	0.8	1.9	16	64
Sacramento, CA	194	6.6	0.9	1.1	7	60
St Louis, MO	301	6.1	1.1	1.6	26	82
Salt Lake City, UT	179	8.5	0.6	2.2	11	85
San Antonio, TX	126	3.9	1.1	2.3	6	60
San Diego, CA	186	7.1	1.0	0.9	8	90
San Francisco, CA	222	4.8	1.8	0.7	25	70
Tampa, FL	217	4.4	1.1	1.0	8	68
Tulsa, OK	216	5.3	0.9	1.8	15	70
Washington, DC	268	5.3	0.9	1.4	13	99

aldehydes, 1% ketones, and 2% acetylene. The detailed composition of this mixture is given elsewhere (Carter, 1993a).

Maximum Incremental Reactivity (MIR) and Maximum Ozone Reactivity (MOR) Scenarios

Incremental reactivities in the base case scenarios would be expected to vary widely, since incremental reactivities depend on the ROG/NO_x ratio, and that ratio varies widely among the base case scenarios. To obtain reactivity scales for specified NO_x conditions, a separate set of scenarios, designated MIR (for maximum incremental reactivity) and MOR (for maximum ozone reactivity) were developed (Carter, 1991, 1993a,b). In the MIR scenarios, the NO_x inputs were adjusted so the base ROG mixture (and most other VOCs) have their highest incremental reactivity. In the MOR scenarios, the NO_x inputs were adjusted to yield the highest ozone concentration. The changes in the base case ROG/NO_x ratios which yielded the MOR scenarios are given in Table 3. As discussed by Carter (1993a,b) the MIR ROG/NO_x ratios are ~1.4 times higher than MOR ratios in all cases.

NO_x Conditions in the Base Case Scenarios

As indicated above, the variability of ROG/NO_x ratios in the base case scenarios suggest a variability of reactivity characteristics in the base case scenarios. However, as discussed previously (Carter, 1993a,b), the ROG/NO_x ratio is also variable in the MIR or MOR scenarios, despite the fact that the NO_x inputs in these scenarios are adjusted to yield a specified reactivity characteristic. Thus, the ROG/NO_x ratio, by itself, is not necessarily a good predictor of reactivity characteristics of a particular scenario. The NO_x/NO_x^{MOR} ratio is a much better predictor of this, with values greater than 1 indicating relatively high NO_x conditions where ozone formation is more sensitive to VOCs, and values less than 1 indicating NO_x-limited conditions. NO_x/NO_x^{MOR} ratios less than 0.7 represent conditions where NO_x control is a more effective ozone control strategy than ROG control (Carter, 1993a,b). Note that more than half of the base case scenarios represent NO_x-limited conditions, and ~25% of them represent conditions where NO_x control is more beneficial than VOC control. A relatively small number of scenarios represent MIR or near MIR conditions. However, as discussed elsewhere (Carter, 1993a,b), this set of scenarios is based on near-worst-case conditions for ozone formation in each of the airsheds. Had scenarios representing less-than-worst-case conditions been included, one might expect a larger number of MIR or near MIR scenarios. This is because NO_x is consumed more slowly on days with lower light intensity or temperature, and thus the scenario is less likely to become NO_x-limited.

Incremental and Relative Reactivities

The incremental reactivity of a VOC in an airshed scenario is the change in ozone caused by adding the VOC to the emissions, divided by the amount of VOC added, calculated for sufficiently small amounts of added VOC that the incremental reactivity is independent of the amount added. The procedure used to calculate incremental reactivities in a scenario was as discussed in detail elsewhere (Carter, 1993a). The incremental reactivities depend on how the amount of VOC added are quantified. In this work, the

added VOC was quantified on a mass basis, since this is how VOCs are regulated. In addition, the incremental reactivities also depend on how ozone impacts are quantified (Carter, 1993a,b). In this work, two different ozone quantifications were used, resulting in two different incremental reactivities being calculated for a VOC in a scenario. These are discussed below.

The "Ozone Yield" incremental reactivities measure the effect of the VOC on the total amount of ozone formed in the scenario at the time of its maximum concentration. In this work, this is quantified as grams O_3 formed per gram VOC added. This gives the same ratios of incremental reactivities as reactivities calculated from peak ozone concentrations, but is preferred because it permits magnitudes of reactivities in scenarios with differing dilutions to be compared on the same basis. Most previous recent studies of incremental reactivity (Dodge, 1984; Carter and Atkinson, 1987, 1989, Chang and Rudy, 1990; Jeffries and Crouse, 1991) have all been based on ozone yield or peak ozone concentration reactivities.

The ozone yield incremental reactivities do not necessarily measure the effect of the VOC on exposure of unacceptable levels of ozone because it does not measure how long high levels of ozone is present. A quantification which reflects this is integrated ozone over the standard, which is defined as the sum of the hourly ozone concentrations for the hours when ozone exceeds the standard in the base case scenarios (Carter 1993a,b). In the previous work (Carter, 1993a,b), we used the California ozone standard of 90 ppb, but in this work we will use the national standard of 0.12 ppm. Reactivities relative to this quantification of ozone are referred to by the abbreviation "IntO_3>0.12" reactivities.

Relative reactivities are ratios of incremental reactivities to incremental reactivities of some standard VOC or mixture. Since these are the quantities which usually are the most relevant to control strategy applications, the results in this work will be given in terms of relative reactivities. In our previous work (Carter 1991, 1993a,b), we used the incremental reactivity of the base ROG mixture, i.e., the mixture representing ROG pollutants from all sources, as the standard to define relative reactivities. To be consistent with the terminology in the previous work, if the term "relative reactivity" is used without qualifier it refers to incremental reactivities relative to the base ROG mixture. However, because of the tendency within the EPA to consider ethane as the standard to define exempt vs controlled VOCs, we will also give reactivity ratios where ethane is used as the standard.

Reactivity Scales

A reactivity scale is a set of incremental or relative reactivities for a particular scenario or group of scenarios. Two types of reactivity scales will be discussed here, "base case" scales and adjusted NO_x scales. Base case scales are simply the set of incremental or relative reactivities in the 39 base case scenarios. Two sets of base case scales are derived — those based ozone yield reactivities and those based on IntO_3>0.12 reactivities. In the previous work (Carter, 1991, 1993a,b) we derived various multi-scenario scales from the individual base case scales by averaging or other procedures, to evaluate alternative

approaches for developing single reactivity scales for applications requiring single scales. However, the decision of whether to exempt a VOC should not be made based on relative reactivities of a single scale, but on a knowledge of the range of relative reactivities for a variety of conditions. Thus in this work we present the distribution of base case relative reactivities for the 39 individual scenarios rather than developing aggregated or optimum scales which represent the distribution by single numbers.

The adjusted NO_x incremental reactivity scales refer to the MIR (maximum incremental reactivity) or the MOIR (maximum ozone incremental reactivity) scales. These consist of averages of incremental reactivities MIR or MOIR scenarios, respectively. Relative reactivities in these scales are ratios of incremental reactivities in these scales. Reactivities in the MIR scale are of interest because the California Air Resources Board utilized an MIR scale to calculate reactivity adjustment factors in its clean fuels/low emissions vehicle regulations (CARB, 1991). The justification for using this scale in applications requiring a single scale (such as the CARB vehicle regulations) is that it reflects conditions where ozone is most sensitive to changes in VOC emissions, and complements NO_x control, which is most effective for reducing ozone under conditions where the MIR scale is least applicable (Carter, 1993a,b). The MOIR scale is preferred by many as an alternative for such applications because it reflects conditions which are most favorable for ozone, and is more representative of the distribution of conditions in the base case scenarios (Carter 1993a,b). Most other alternative reactivity scales which might be appropriate for assessing VOC control strategies (i.e., excluding scales representing highly NO_x-limited conditions where ozone is more sensitive to NO_x than VOCs) tend to fall in the range defined by the MIR and MOIR scales.

Note that the MIR, MOIR and base case scales derived in this work are somewhat different from those calculated previously (Carter, 1993a,b) because an updated chemical mechanism was used. Table 4 gives the MIR and MOIR incremental reactivities using the mechanism employed in this work and compares them with those calculated previously (Carter, 1993a,b), which were derived using the SAPRC-90 mechanism. The updates to the mechanism result in higher incremental reactivities for all species except for formaldehyde, acetone, and benzaldehyde, higher relative reactivities for internal alkenes, alkanes other than methane and benzene, lower relative reactivities for formaldehyde, acetone, and benzaldehyde, and slightly lower relative reactivities for most other species. The decrease in relative reactivity for formaldehyde and acetone, and increase for internal alkenes, are directly attributable to changes in their mechanisms as discussed above.

Calculated Relative Reactivities of Acetone and Ethane

Table 5 gives a tabulation of the relative reactivities of acetone and ethane in the various base case and MIR and MOIR reactivity scales calculated using the updated mechanism. Distribution plots of the relative reactivities of acetone and ethane in the base case scenarios are shown on Figure 20, Figures 21 gives distribution plots of the acetone/ethane incremental reactivity ratio for the base case scenarios, and

Table 4. Comparison of incremental and relative reactivities in the MIR and MOIR scales calculated using the updated and the SAPRC-90 mechanisms.

Compound	MIR Scale [a]				MOIR Scale [a]			
	SAPRC-90 IR	Updated IR	Change (%) IR	RR	SAPRC-90 IR	Updated IR	Change (%) IR	RR
CO	0.054	0.061	13%	-3%	0.038	0.040	4%	-10%
Methane	0.0150	0.016	10%	-6%	0.0093	0.0099	6%	-8%
Ethane	0.25	0.30	21%	4%	0.17	0.20	24%	6%
n-Butane	1.02	1.26	23%	5%	0.66	0.83	26%	9%
n-Octane	0.60	0.83	37%	17%	0.41	0.57	38%	19%
iso-Octane	0.93	1.16	25%	7%	0.54	0.72	33%	15%
n-Decane	0.46	0.68	46%	25%	0.31	0.47	51%	30%
Ethene	7.4	8.3	12%	-4%	3.2	3.4	6%	-9%
Propene	9.4	11.2	18%	1%	3.8	4.3	13%	-3%
trans-2-Butene	10.0	13.5	35%	16%	3.8	4.7	25%	7%
Isobutene	5.3	6.0	13%	-3%	1.9	2.0	4%	-10%
1-Hexene	4.4	5.7	30%	11%	1.7	2.3	31%	13%
Benzene	0.42	0.60	42%	22%	0.138	0.20	48%	27%
Toluene	2.7	3.2	16%	-1%	0.63	0.69	10%	-5%
m-Xylene	8.2	8.8	8%	-8%	2.5	2.5	2%	-12%
135-TM-Benzene	10.1	11.3	11%	-5%	3.1	3.2	4%	-11%
Methanol	0.56	0.63	11%	-5%	0.28	0.29	4%	-11%
Ethanol	1.34	1.6	21%	4%	0.72	0.90	24%	7%
Formaldehyde	7.2	7.0	-2%	-16%	2.1	1.9	-11%	-23%
Acetaldehyde	5.5	6.3	15%	-2%	2.2	2.4	12%	-3%
Acetone [b]	0.56	0.49	-13%	-25%	0.20	0.19	-7%	-20%
Benzaldehyde	-0.57	-0.24	58%	64%	-1.24	-1.41	-14%	2%
Cresols	2.3	2.6	13%	-3%	-0.58	-0.59	3%	-12%
Base ROG Mix	3.1	3.7	17%	0%	1.17	1.36	16%	0%

[a] IR = incremental reactivities in units of grams O_3 per gram VOC; RR = reactivity relative to base ROG mixture.
[b] Standard acetone mechanism.

Table 5. Relative ozone yield and $IntO_3$>0.12 reactivities and reactivity ratios for acetone and ethane in the base case scenarios and the MIR and MOIR scales.

Scenario or Scale	Base ROG IR [a]	Reactivities Relative to Base ROG — Ozone Yield Reactivities — Ethane	Acetone (Standard)	Acetone (Adjusted)	— IntO3 > 0.12 Reactivities — Ethane	Acetone (Standard)	Acetone (Adjusted)
Base Case Scenarios							
ATL GA	0.93	0.17	0.144	0.128	0.130	0.123	0.107
AUS TX	0.74	0.20	0.147	0.133	0.149	0.117	0.103
BAL MD	1.7	0.132	0.142	0.123	0.086	0.126	0.104
BAT LA	1.00	0.142	0.136	0.117	0.103	0.117	0.098
BIR AL	0.80	0.24	0.17	0.16	0.129	0.120	0.103
BOS MA	0.79	0.21	0.147	0.136	0.143	0.120	0.106
CHA NC	0.60	0.22	0.16	0.145	0.18	0.138	0.125
CHI IL	0.38	0.24	0.18	0.16	0.135	0.115	0.096
CIN OH	1.14	0.19	0.141	0.129	0.120	0.112	0.096
CLE OH	1.25	0.139	0.135	0.118	0.092	0.115	0.096
DAL TX	2.5	0.103	0.125	0.104	0.085	0.114	0.094
DEN CO	1.7	0.097	0.132	0.111	0.074	0.122	0.100
DET MI	1.02	0.20	0.144	0.130	0.121	0.114	0.098
ELP TX	1.5	0.104	0.130	0.107	0.081	0.118	0.095
HAR CT	0.86	0.21	0.15	0.140	0.16	0.130	0.116
HOU TX	1.21	0.17	0.140	0.125	0.104	0.111	0.094
IND IN	1.37	0.15	0.131	0.115	0.110	0.116	0.098
JAC FL	0.82	0.16	0.137	0.120	0.143	0.126	0.109
KAN MO	1.10	0.20	0.143	0.131	0.16	0.124	0.111
LAK LA	0.60	0.21	0.15	0.138	0.135	0.118	0.099
LOS CA	0.77	0.121	0.128	0.110	0.075	0.106	0.084
LOU KY	1.36	0.18	0.144	0.129	0.128	0.119	0.103
MEM TN	0.89	0.20	0.15	0.138	0.126	0.119	0.102
MIA FL	0.61	0.19	0.148	0.133	0.18	0.141	0.127
NAS TN	0.81	0.24	0.17	0.16	0.19	0.149	0.135
NEW NY	0.45	0.16	0.130	0.114	0.084	0.100	0.080
PHI PA	1.20	0.16	0.135	0.121	0.105	0.116	0.099
PHO AZ	1.41	0.144	0.139	0.121	0.093	0.115	0.095
POR OR	1.08	0.18	0.139	0.125	0.142	0.124	0.108
RIC VA	1.11	0.18	0.144	0.132	0.110	0.120	0.103
SAC CA	1.29	0.16	0.15	0.132	0.125	0.133	0.115
SAI MO	1.42	0.124	0.137	0.119	0.081	0.120	0.101
SAL UT	0.94	0.19	0.16	0.140	0.128	0.125	0.108
SAN TX	1.8	0.124	0.126	0.107	0.120	0.124	0.105
SDO CA	0.98	0.110	0.109	0.090	0.085	0.099	0.078
SFO CA	1.9	0.053	0.146	0.116	0.050	0.142	0.114
TAM FL	1.8	0.123	0.132	0.113	0.094	0.119	0.099
TUL OK	1.27	0.17	0.137	0.124	0.120	0.118	0.103
WAS DC	1.07	0.19	0.146	0.132	0.110	0.112	0.096
Average	1.13	0.166	0.142	0.126	0.118	0.120	0.103
Adjusted NO_x Scales							
MIR Scale	3.7	0.082	0.133	0.110			
MOIR Scale	1.36	0.150	0.139	0.121			

[a] Incremental reactivity in units of gm O3/gm VOC.

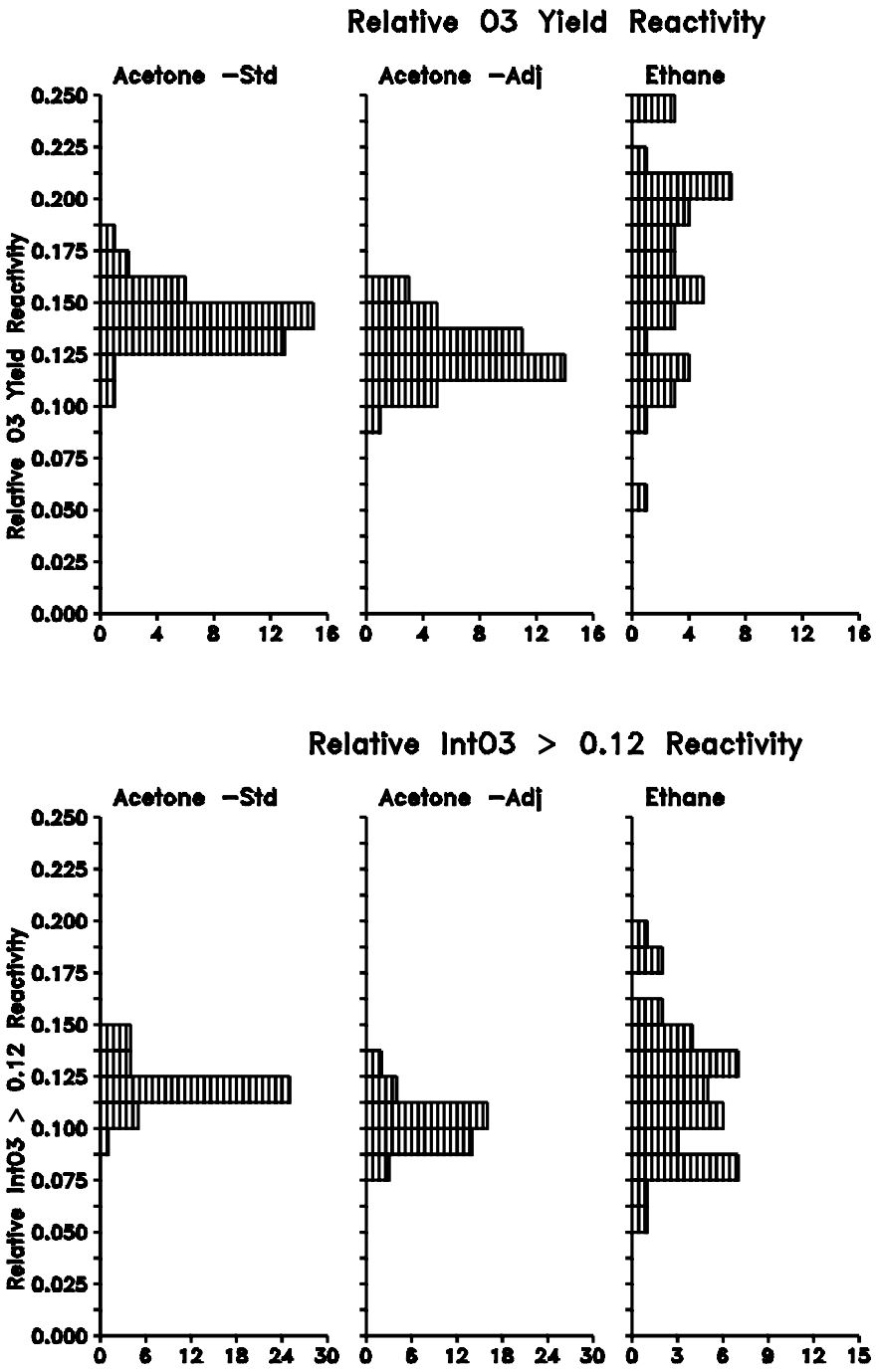

Figure 20. Distribution plots of ozone yield and $IntO_3$>0.12 reactivities, relative to the base ROG mixture, for acetone and ethane in the base case scenarios.

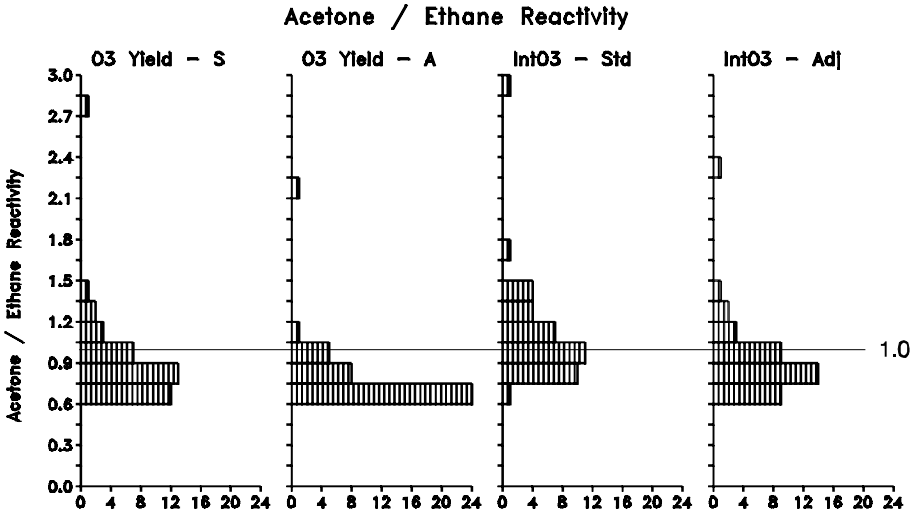

Figure 21. Distribution plots of ratios of ozone yield and $IntO_3$>0.12 reactivities of acetone relative to ethane for the base case scenarios.

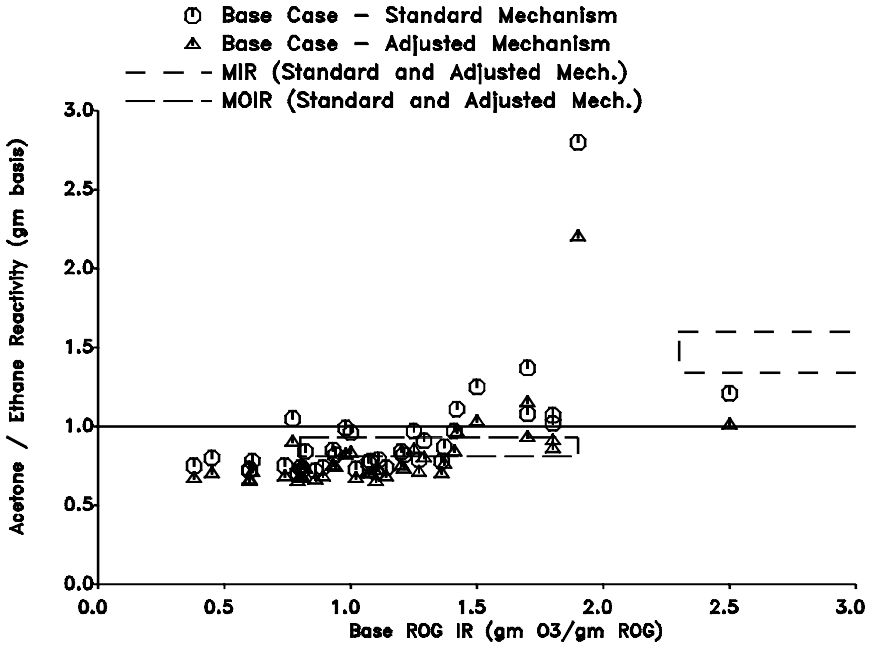

Figure 22. Plots of ratios of ozone yield reactivities of acetone relative to ethane against the incremental reactivity of the base ROG for the base case scenarios. Reactivity ratios and ranges of base ROG reactivities for the MIR and MOIR scales are also shown.

figure 22 plots the acetone/ethane reactivity ratios against the incremental reactivity of the base ROG. Reactivities of acetone were calculated both using the standard updated mechanism and using the mechanism with the acetone quantum yields adjusted to fit the blacklight and xenon arc chamber data as discussed above.

It can be seen that the adjustment to the acetone mechanism to fit the chamber data causes a slight (~13%) reduction in the incremental and relative reactivity of acetone. This is a fairly small difference compared to the variability of its relative reactivity or reactivity relative to ethane. The differences between these two calculations can be thought of as an indication of the lower limit to the chemical uncertainty in calculations of acetone's reactivity.

Figures 21 and 22 show that acetone is less reactive than ethane in a majority of the base case scenarios, though there are a few scenarios where acetone is slightly more reactive, and one where the unusually low relative reactivity of ethane results in an unusually high acetone/ethane reactivity ratio. The reactivity ratio in this case does not appear to be significantly affected by how O_3 is quantified — though it should be noted that this is not the case for all VOCs (Carter 1993a,b). Figure 22 shows that the reactivity ratio tends to increase as the reactivity ratio increases above the range which is characteristic of maximum ozone conditions. Thus, although acetone is of equal or lesser reactivity to ethane in most scenarios, its reactivity relative to ethane tends to increase as the scenario becomes more sensitive to VOC emissions. Because of this, incremental reactivity of acetone in the MIR scale is calculated to be 1.3 or 1.6 times higher than that of ethane, depending on whether the quantum yields are adjusted to fit the chamber data. However, all but one of the base case scenarios have lower reactivity ratios than in the MIR scale. The distribution of reactivity ratios in the base case scenarios is better represented by the reactivity ratio in the MOIR scale, where acetone is calculated to be slightly less reactive than ethane.

An alternative — and we believe more relevant — standard for assessing whether to regulate emissions of a compound is its reactivity relative to the mix of all other emitted VOCs, or the base ROG mixture. Figure 20 shows that the relative reactivities of acetone varies over a much narrower range than those for ethane, though the variation is somewhat less when ozone is quantified by integrated O_3 over the standard. The range of ozone yield relative reactivities are 0.05 - 0.24 for ethane and 0.11 - 0.18 for acetone with the more reactive standard mechanism. Thus acetone with the standard mechanism is between 5.6 - 9 times less reactive in terms of ozone yields than the base ROG, while ethane is between 4 - 20 times less reactive. For ozone yield reactivities, the ranges of relative reactivities are 0.074 - 0.19 for ethane and 0.10 - 0.15 for the standard acetone mechanism. Thus acetone with the standard mechanism is between 7 - 10 times less reactive in terms of integrated ozone over the standard than the base ROG, while ethane is 5 - 13 times less reactive. The MIR and MOIR relative reactivities are within these ranges.

It is interesting to note that the scenarios where acetone looks the most reactive compared to ethane are not necessarily the same as those where acetone has the highest reactivity relative to the base ROG mixture. From Figure 21 it can be seen that there is one scenario where the acetone/ethane reactivity ratio is unusually high, being 3 for the unadjusted mechanism. However, Table 5 shows that the corresponding ozone yield relative reactivity for the unadjusted acetone mechanism in that scenario is only 0.146, which is very close to the average for all scenarios. Thus the high acetone/ethane reactivity ratio in that case is due entirely to an unusually low relative reactivity for ethane. Furthermore, the scenario with the highest relative reactivity for acetone has an acetone/ethane reactivity ratio of ~0.75 for the standard mechanism, which is lower than average. In general, because the relative reactivity of ethane is so much more variable than that of acetone (as shown on Figure 20), it is the reactivity of ethane which is the primary factor which determines the reactivity of acetone relative to ethane.

CONCLUSIONS

The decision whether it is appropriate to regulate a compound as an ozone precursor requires a qualitative assessment of its reactivity relative to ozone formation under a variety of environmental conditions. This requires developing and experimentally validating a chemical mechanism for the compounds relevant atmospheric reactions, which can then be used in airshed models to predict its atmospheric reactivity. Although mechanisms for the atmospheric reactions of acetone have been available for some time, until this study there have been no reliable data available to evaluate their accuracy when used in such models. The major objective of this study was to provide the data needed for this purpose.

The data base which was developed to evaluate the mechanism of acetone is now more extensive than that for a vast majority of the other VOCs emitted into the atmosphere, including many which are far more important in contributing to the ozone problem. Acetone has been studied in NO_x-air environmental chamber irradiations by itself and in the presence of other reactive VOCs, and experiments utilizing a variety of light sources, including natural sunlight and artificial lights closely resembling natural sunlight. Although the incremental reactivity experiments in the outdoor chamber are inconclusive because of the inability of the model to simulate the base case conditions, the outdoor chamber experiments with acetone in the absence of other added VOCs, and the wide variety of indoor chamber experiments, provide a useful data base for evaluating acetone's mechanism. The indoor runs using the blacklights provide information concerning the effects of acetone on ozone formation under a wide variety of conditions, and the runs using the xenon arc light source provide information concerning acetone which more closely resembles sunlight. The difference in spectral distribution of the blacklight and xenon arc light sources provide a valuable means to test the model for how the photolysis of acetone depends on light spectrum. This is important because the spectrum of ambient sunlight is not constant, it varies significantly depending on the time of day, day of year, and the extent of atmospheric haze and the tropospheric ozone column.

An examination of the recent literature and reviews concerning the atmospheric reactions of acetone indicate that the mechanism we have previously used for acetone (Carter, 1990) needed to be updated in some respects. The greatest uncertainty in the acetone photooxidation mechanism is the quantum yields for its photolysis, concerning which the data in the literature are not in agreement. The evaluations (e.g., Atkinson et al., 1992) recommend the models use the data of Meyrahn et al. (1986), but our model simulations of their experiments indicate that the quantum yields in longest wavelengths (where sunlight and blacklights are more intense) are unreliable and need correction. The acetone mechanism used in our model was updated to be consistent with the latest evaluations in the literature, and to incorporate the estimated correction to the quantum yield data of Meyrahn et al (1986). These corrections

had a tendency to make acetone somewhat less reactive than was previously predicted, but still of comparable reactivity to ethane.

The updated mechanism was found to simulate reasonably well the results of the experiments using the indoor chamber light source most closely resembling sunlight and the outdoor chamber runs which were conducted during the summer. However, this mechanism consistently overpredicted the rate of ozone formation in the blacklight chamber experiments and also overpredicted the ozone formation in the wintertime acetone - NO_x run in the outdoor chamber. It is considered unlikely that this is due to incorrect characterization of the blacklight intensity or spectra, because the model could give good simulations of the photochemical reactivity of acetaldehyde, a VOC which photolyzes in a similar wavelength region as acetone. Thus it appears likely that the problem is that the model incorrectly represents how the acetone photolysis quantum yields depend on wavelength.

An adjusted version of the updated acetone mechanism was developed which was considerably more successful in simulating the data base developed in this study. The adjustment involves assuming that the quantum yields fall off with increasing wavelength much more rapidly than indicated by the data of Meyrahn et al. (1986), but that the fall off begins at a slightly longer wavelength. Although this adjustment is not theoretically unreasonable, there is no basis for it other than fitting these environmental chamber data, which are highly complex chemical systems with a number of other potential sources of error. The possibility that the problem may be due to an incorrect characterization of the effect of the mercury lines in the blacklight light source cannot be entirely ruled out. Therefore, in the assessment of the reactivities of acetone in the atmosphere, both the unadjusted (or standard) mechanism and the adjusted acetone mechanism were used in the model calculations. A comparison of the predictions of the two mechanisms give an indication of the approximate minimum magnitude of the effects of chemical mechanistic uncertainties associated with calculations of acetone's atmospheric reactivity.

It was found that the adjustment to the acetone quantum yields to fit our chamber data caused an approximately 13% reduction in the calculated incremental reactivity of acetone under atmospheric conditions. This is a relatively small effect compared to the extent to which the relative reactivity of acetone varied with atmospheric conditions. Thus it is concluded that although there are uncertainties in acetone's quantum yields, the effect of this uncertainty is not large enough to substantively affect conclusions concerning the range of acetone's effect on ozone production under conditions represented by the model scenarios we employed. However, the effect may be larger in model simulations of wintertime conditions, since the adjustment has the greatest effect under lighting conditions which have relatively low intensity in the UV. Since all the scenarios used in this study were based on worst case or near-worst case conditions, conditions of low UV intensity are not well represented.

The model simulations indicate that acetone is slightly less reactive than ethane in a majority of the scenarios representing worst-case or near-worst-case conditions. However, there was one scenario where the ethane was calculated to have an unusually low relative reactivity, resulting in acetone being calculated to be more reactive than ethane by factors of 2-3, depending on whether or not the adjusted quantum yields are used. In general, acetone becomes increasingly more reactive relative to ethane as NO_x conditions approach those yielding the highest incremental reactivities, with the result being that acetone has a slightly higher (by a factor of 1.3 to 1.6, depending on the quantum yields) MIR incremental reactivity than ethane. On the other hand, in the MOIR scale, which represents NO_x conditions most favorable for ozone formation, acetone is calculated to be slightly less reactive than ethane, regardless of which set of quantum yields are used. In general, the MIR and MOIR scales represent the range of conditions which are appropriate to consider when evaluating relative reactivities of VOC for control strategy purposes (Carter, 1991; 1993a,b).

However, other than considerations of precedence, the reactivity of acetone relative to ethane is of essentially no practical relevance. The two chemicals have vastly different physical properties and come from quite different types of sources, and to our knowledge no substitutions of acetone for ethane (or vise-versa) are being contemplated. If a reactive VOC is exempted, and if it is not used primarily as a substitute for more reactive VOCs, the net effect would be that there would have to be a slightly greater controls on all other (non-exempt) VOCs to achieve the same air quality gains. Thus, in effect, the proposal to exempt a VOC is equivalent to proposing to substitute it for the base ROG mixture. Therefore, the more relevant consideration when considering whether to exempt acetone is its reactivity compared to the base ROG mixture.

When compared on the basis of reactivities relative to the base ROG mixture, a somewhat different picture is obtained concerning the relative impacts of acetone and ethane on ozone formation. In particular, the relative reactivity (i.e., incremental reactivity relative to the base ROG) of acetone is found to vary over a considerably narrower range than is the case for ethane. Indeed, it is the variability of the relative reactivity of ethane, not acetone, which causes the variability of the acetone/ethane reactivity ratios among the scenarios. For example, the scenario with the most extreme acetone/ethane reactivity ratios (of 2-3) had relative reactivities for acetone very close to the average. The minimum, maximum, and average relative reactivities we obtained are summarized on Table 6, where they are compared with relative reactivities in the MIR and MOIR scales. It should be noted that the base case scenarios were designed to represent near-worst-case conditions only, and the results may be more variable if a greater variety of scenarios were included. However, these scenarios are representative of a wide variety of conditions which need to be considered when assessing effects of VOC controls.

Table 6. Summary of reactivities of acetone and ethane relative to the base ROG mixture.

	Based on effect on O_3 Yield			Based on Integrated O_3 > 0.12 ppm		
	Acetone (standard)	**Acetone (adjusted)**	**Ethane**	**Acetone (standard)**	**Acetone (adjusted)**	**Ethane**
Base case						
Minimum	0.11	0.09	0.05	0.10	0.07	0.05
Maximum	0.18	0.16	0.24	0.15	0.14	0.19
Average Base	0.14±0.01	0.13±0.02	0.17±0.04	0.12±0.01	0.10±0.01	0.12±0.03
MIR Scale	0.13	0.11	0.08			
MOIR Scale	0.14	0.12	0.15			

We believe the type of data on Table 6 provides a more appropriate basis for deciding whether it is appropriate to exempt acetone or ethane. Note that when the EPA decided to exempt ethane, in effect it decided it was not necessary to regulate emissions of a VOC which could be almost 25% asreactive as the average of all emissions in terms of peak ozone concentrations, and almost 20% as reactive in terms of effect on integrated ozone over the standard. When looked at this way, exempting a compound which is calculated to be no more than 20% as reactive in terms of peak ozone, or 15% as reactive in terms of integrated ozone over the standard, does not appear to be an inconsistent policy.

To conclude, when considering whether a VOC should be exempted from regulation as an ozone precursor, the most appropriate factor to consider is its relative reactivity, i.e., its reactivity relative to the mixture of all other VOC emissions. The results of this study indicate that the difference in relative reactivities between ethane and acetone is less than the variability of their relative reactivities from scenario to scenario. On this basis, it can be concluded the acetone and ethane can be considered to have essentially the same reactivity to within their variability with environmental conditions. However, it should be emphasized that the scenarios we employed were designed to represent near-worst-case conditions only, and the variability may be greater when considering a wider range of scenarios.

REFERENCES

Atkinson, R. and W. P. L. Carter (1984): "Kinetics and Mechanisms of the Gas-Phase Reactions of Ozone with Organic Compounds under Atmospheric Conditions," Chem. Rev. 1984, 437-470.

Atkinson, R. (1989): "Kinetics and Mechanisms of the Gas-Phase Reactions of the Hydroxyl Radical with Organic Compounds," J. Phys. Chem. Ref. Data, Monograph no 1.

Atkinson, R. (1990): "Gas-Phase Tropospheric Chemistry of Organic Compounds: A Review," Atmos. Environ., 24A, 1-24.

Atkinson, R. (1991): "Kinetics and Mechanisms of the Gas-Phase Reactions of the NO_3 Radical with Organic Compounds," J. Phys. Chem. Ref. Data, 20, 459-507.

Atkinson, R. and W. P. L. Carter (1992): "Reactions of Alkoxy Radicals under Atmospheric Conditions: The Relative Importance of Decomposition versus Reaction with O_2," J. Atm. Chem., 13, 195-210.

Atkinson, R., D. L. Baulch, R. A. Cox, R. F. Hampson, Jr., J. A. Kerr, and J. Troe (1992): "Evaluated Kinetic and Photochemical Data for Atmospheric Chemistry. Supplement IV. IUPAC Subcommittee on Gas Kinetic Data Evaluation for Atmospheric Chemistry," J. Phys. Chem. Ref. Data 21, 1125-1568.

Atkinson, R. (1993): "Gas-Phase Tropospheric Chemistry of Organic Compounds," J. Phys. Chem. Ref. Data, Monograph No. 2, in press.

Atkinson, R., S. M. Aschmann, J. Arey and B. Shorees (1992): "Formation of OH Radicals in the Gas-Phase Reactions of Ozone with a Series of Terpenes," J. Geophys. Res. 97, 6065-6073.

Atkinson, R. and S. M. Aschmann (1993): "OH Radical Production from the Gas-Phase Reactions of O_3 with a Series of Alkenes under Atmospheric Conditions," Environ. Sci. Technol, 27, 1357-1363.

Bauges, K (1990): "Preliminary Planning Information for Updating the Ozone Regulatory Impact Analysis Version of EKMA," Draft Document, Source Receptor Analysis Branch, Technical Support Division, U. S. Environmental Protection Agency, Research Triangle Park, NC, January.

Bridier, I., H. Caralp, R. Loirat, B. Lesclaux and B. Veyret (1991): "Kinetic and Theoretical Studies of the Reactions of $CH_3C(O)O_2 + NO_2 + M <=> CH_3C(O)O_2NO_2 + M$ between 248 and 393 K and between 30 and 760 Torr," J. Phys. Chem. 95, 3594-3600.

Calvert, J. G., and J. N. Pitts, Jr. (1966): Photochemistry, John Wiley and Sons, New York.

Cantrell, C. A., J. A. Davidson, A. H. McDaniel, R. E. Shetter and J. G. Calvert (1990): "Temperature-Dependent Formaldehyde Cross Sections in the Near Ultraviolet Spectral Region," J. Phys. Chem. 94, 3902-3908.

CARB (1991): "Proposed Reactivity Adjustment Factors for Transitional Low-Emissions Vehicles: Technical Support Document," California Air Resources Board, Sacramento, CA., September 27.

Carter, W. P. L., A. C. Lloyd, J. L. Sprung, and J. N. Pitts, Jr. (1979): "Computer Modeling of Smog Chamber Data: Progress in Validation of a Detailed Mechanism for the Photooxidation of Propene and n-Butane in Photochemical Smog", Int. J. Chem. Kinet, 11, 45.

Carter, W. P. L., R. Atkinson, A. M. Winer, and J. N. Pitts, Jr. (1982): "Experimental Investigation of Chamber-Dependent Radical Sources," Int. J. Chem. Kinet., 14, 1071.

Carter, W. P. L., P. S. Ripley, C. G. Smith, and J. N. Pitts, Jr. (1981): "Atmospheric Chemistry of Hydrocarbon Fuels: Vol I, Experiments, Results and Discussion," Final report to the U. S. Air Force, ESL-TR-81-53, November.

Carter, W. P. L., Dodd, M. C., Long, W. D. and Atkinson, R. (1984): Outdoor Chamber Study to Test Multi-Day Effects. Volume I: Results and Discussion. Final report, EPA-600/3-84-115, November

Carter, W. P. L., W. D. Long, L. N. Parker, and M. C. Dodd (1986): "Effects of Methanol Fuel Substitution on Multi-Day Air Pollution Episodes," Final Report on California Air Resources Board Contract No. A3-125-32, April.

Carter, W. P. L. and R. Atkinson (1987): "An Experimental Study of Incremental Hydrocarbon Reactivity," Environ. Sci. Technol., 21, 670-679

Carter, W. P. L. and R. Atkinson (1989): "A Computer Modeling Study of Incremental Hydrocarbon Reactivity", Environ. Sci. and Technol., 23, 864.

Carter, W. P. L. (1990): "A Detailed Mechanism for the Gas-Phase Atmospheric Reactions of Organic Compounds," Atm. Environ., 24A, 481-518.

Carter, W. P. L., and F. W. Lurmann (1990): "Evaluation of the RADM Gas-Phase Chemical Mechanism," Final Report, EPA-600/3-90-001.

Carter, W. P. L. (1991): "Development of Ozone Reactivity Scales for Volatile Organic Compounds", EPA-600/3-91/050, August.

Carter, W. P. L. and F. W. Lurmann (1991): "Evaluation of a Detailed Gas-Phase Atmospheric Reaction Mechanism using Environmental Chamber Data," Atm. Environ. 25A, 2771-2806.

Carter, W. P. L. (1992): "Analysis of ROG Surrogates for Environmental Chamber Studies of VOC Reactivity," interim report for CRC contract ME-9, October 15.

Carter, W. P. L. and R. Walters (1992): "Design and Specification of a Light Source for Experimental Studies of Atmospheric Reactivities of Volatile Organic Compounds," report to the National Renewable Energy Laboratory Contract No. XZ 2120751, August 15.

Carter, W. P. L. (1993a): "Development and Application of an Up-To-Date Photochemical Mechanism for Airshed Modeling and Reactivity Assessment," Draft final report for California Air Resources Board Contract No. A934-094, April 26.

Carter, W. P. L. (1993b): "Development of Ozone Reactivity Scales for Volatile Organic Compounds," Submitted to J. A&WMA, September 22.

Carter, W. P. L., J. A. Pierce, I. L. Malkina, D. Luo and W. D. Long (1993a): "Environmental Chamber Studies of Maximum Incremental Reactivities of Volatile Organic Compounds," Report to Coordinating Research Council, Project No. ME-9, California Air Resources Board Contract No. A032-0692; South Coast Air Quality Management District Contract No. C91323, United States Environmental Protection Agency Cooperative Agreement No. CR-814396-01-0, University Corporation for Atmospheric Research Contract No. 59166, and Dow Corning Corporation. April 1.

Carter, W. P. L., J. A. Pierce, D. Luo and I. L. Malkina (1993b): "Environmental Chamber Studies of Maximum Incremental Reactivities of Volatile Organic Compounds," To be submitted to Atmospheric Environment, October 4.

Croes, B. E. (1991): Technical Support Division, California Air Resources Board, personal communication.

Croes, B. E. et al. (1993): "Southern California Air Quality Study Data Archive," Research Division, California Air Resources Board.

Dasgupta, P. K, Dong, S. and Hwang, H. (1988): "Continuous Liquid Phase Fluorometry Coupled to a Diffusion Scrubber for the Determination of Atmospheric Formaldehyde, Hydrogen Peroxide, and Sulfur Dioxide," Atmos. Environ. 22, 949-963.

Dasgupta, P.K, Dong, S. and Hwang, H. (1990): Aerosol Science and Technology 12, 98-104

Dimitriades, B. (1993): U. S. Environmental Protection Agency, Atmospheric Research and Exposure Assessment Laboratory, Research Triangle Park, NC: Letter to Dr. David Morgott of Eastman Kodak Co., dated September 25.

Dodge, M. C. (1984): "Combined Effects of Organic Reactivity and NMHC/NO_x Ratio on Photochemical Oxidant Formation -- A Modeling Study," Atmos. Environ., 18, 1657.

Dong, S. and Dasgupta, P. K. (1987): "Fast Fluorometric Flow Analysis of Formaldehyde," Environ. Sci. and Technol. 21, 581-588.

Doyle, G. J., P. J. Bekowies, A. M. Winer, and J. N. Pitts, Jr. (1977): Environ. Sci. Technol. 11, 45.

Eastman Chemical Company and Hoechst Celanese Corporation (1993): "Petition for the Exemption of Acetone from Regulation under the Clean Air Act as a Precursor to Tropospheric Ozone," Petition before the U. S. Environmental Protection Agency, Latham & Watkins, Counsel, Washington DC.

EPA (1984): "Guideline for Using the Carbon Bond Mechanism in City-Specific EKMA," EPA-450/4-84-005, February.

Gardner, E. P., R. D. Wijayaratne, and J. G. Calvert (1984): "Primary Quantum Yields of Photodecomposition of Acetone in Air under Tropospheric Conditions," J. Phys. Chem. 88, 5069-5076.

Gardner, E. P., P. D. Sperry, and J. G. Calvert (1987): "Photodecomposition of Acrolein in O_2-N_2 Mixtures," J. Phys. Chem. 91, 1922.

Gery, M. W., R. D. Edmond and G. Z. Whitten (1987): "Tropospheric Ultraviolet Radiation. Assessment of Existing Data and Effects on Ozone Formation," Final Report, EPA-600/3-87-047, October.

Gery, M. W., G. Z. Whitten, and J. P. Killus (1988): "Development and Testing of the CBM-IV For Urban and Regional Modeling,", EPA-600/ 3-88-012, January.

Gery, M. W. (1991): "Review of the SAPRC-90 Chemical Mechanism," Report to the California Air Resources Board, Contract No. A132-055, Sacramento, CA.

Gipson, G. L., W. P. Freas, R. A. Kelly and E. L. Meyer (1981): "Guideline for Use of City-Specific EKMA in Preparing Ozone SIPs, EPA-450/4-80-027, March.

Gipson, G. L. and W. P. Freas (1983): "Use of City-Specific EKMA in the Ozone RIA," U. S. Environmental Protection Agency, July.

Gipson, G. L. (1984): "Users Manual for OZIPM-2: Ozone Isopleth Plotting Package With Optional Mechanism/Version 2," EPA-450/4-84-024, August.

Hogo, H. and M. W. Gery (1988): "Guidelines for Using OZIPM-4 with CBM-IV or Optional Mechanisms. Volume 1. Description of the Ozone Isopleth Plotting Package Version 4", Final Report for EPA Contract No. 68-02-4136, Atmospheric Sciences Research Laboratory, Research Triangle Park, NC. January 1988.

Jeffries, H. E. (1988): Department of Environmental Science and Engineering, University of North Carolina, Chapel Hill, NC, diskette containing JSPECTRA code and input files. Main JSPECTRA source file dated June 22. Example input files dated November 10.

Jeffries H. E., K. G. Sexton, J. R. Arnold, and T. L. Kale (1989a): "Validation Testing of New Mechanisms with Outdoor Chamber Data. Volume 2: Analysis of VOC Data for the CB4 and CAL Photochemical Mechanisms," Final Report, EPA-600/3-89-010b.

Jeffries H. E., K. G. Sexton, J. R. Arnold, and T. L. Kale (1989b): "Validation Testing of New Mechanisms with Outdoor Chamber Data. Volume 3: Calculation of Photochemical Reaction Photolysis Rates in the UNC Outdoor Chamber," Final Report, EPA-600/3-89-010c.

Jeffries, H. E. and R. Crouse (1991): "Scientific and Technical Issues Related to the Application of Incremental Reactivity. Part II: Explaining Mechanism Differences," Report prepared for Western States Petroleum Association, Glendale, CA, October.

Jeffries, H. E. (1991a): "UNC Solar Radiation Models," unpublished draft report for EPA Cooperative Agreements CR813107, CR813964 and CR815779". Undated.

Jeffries, H. E. (1991b): Department of Environmental Science and Engineering, University of North Carolina, Chapel Hill, NC, personal communication.

Jeffries, H. (1992): "Comments on CARB's Request for Waiver of Federal Preemption in CAAA," Presented at the EPA Public Hearing for California ARB's Request for Waiver of Waiver of Federal Preemption.

Jeffries, H. E., M. W. Gery and W. P. L. Carter (1992): "Protocol for Evaluating Oxidant Mechanisms for Urban and Regional Models," Report for U. S. Environmental Protection Agency Cooperative Agreement No. 815779, Atmospheric Research and Exposure Assessment Laboratory, Research Triangle Park, NC.

Jeffries, H. E. (1993): Department of Environmental Science and Engineering, University of North Carolina, Chapel Hill, NC, communication to J. J. Bufalini, U. S. Environmental Protection Agency, Atmospheric Research and Exposure Assessment Laboratory, Research Triangle Park, NC.

Jenkin, M. E., R. A. Cox, M. Emrich and G. K. Moortgat (1993): "Mechanisms for the Cl-atom-initiated Oxidation of Acetone and Hydroxyacetone in Air," J. Chem. Soc. Faraday Trans. 89, 2983-2991.

Johnson, G. M. (1983): "Factors Affecting Oxidant Formation in Sydney Air," in "The Urban Atmosphere -- Sydney, a Case Study." Eds. J. N. Carras and G. M. Johnson (CSIRO, Melbourne), pp. 393-408.

Lurmann, F. W., H. H. Main, K. T. Knapp, L. Stockburrger, R. A. Rasmussen and K. Fung (1992): "Analysis of Ambient VOC Data Collected in the Southern California Air Quality Study," Final Report to California Air Resources Board Contract No. A382-130; Research Division, Sacramento, CA, February.

Meyrahn, H., J. Pauly, W. Schneider, and P. Warneck (1986): "Quantum Yields for the Photodissociation of Acetone in Air and an Estimate for the Life Time of Acetone in the Lower Troposphere," J. Atmos. Chem. 4, 277-291.

Rogers, J. D. (1990): "Ultraviolet Absorption Cross Sections and Atmospheric Photodissociation Rate Constants of Formaldehyde," J. Phys. Chem., 90, 4011-4015.

Tuazon, E. C., W. P. L. Carter and R. Atkinson (1991): "Thermal Decomposition of Peroxyacetyl Nitrate and Reactions of Acetyl Peroxy Radicals with NO and NO_2 Over the Temperature Range 283-313 K," J. Phys. Chem., in 95, 2434.

Zafonte, L., P. L. Rieger, and J. R. Holmes (1977): "Nitrogen Dioxide Photolysis in the Los Angeles Atmosphere," Environ. Sci. Technol. 11, 483-487.

APPENDIX A.
LISTING OF THE UPDATED SAPRC MECHANISM

A complete listing of the updated SAPRC used in this study is given in Tables A-1 through A-3. Table A-1 gives a list of the model species, Table A-2 gives the reactions, and Table A-3 gives the absorption cross sections and quantum yields used to calculate the photolysis rates.

Table A-1. List of model species used in the SAPRC-93 mechanism for the base case simulations.

name	description
Constant Species.	
O2	Oxygen
M	Air
H2O	Water
Active Inorganic Species.	
O3	Ozone
NO	Nitric Oxide
NO2	Nitrogen Dioxide
NO3	Nitrate Radical
N2O5	Nitrogen Pentoxide
HONO	Nitrous Acid
HNO3	Nitric Acid
HNO4	Peroxynitric Acid
HO2H	Hydrogen Peroxide
Active Radical Species and Operators.	
HO2.	Hydroperoxide Radicals
RO2.	Operator to Calculate Total Organic Peroxy Radicals
RCO3.	Operator to Calculate Total Acetyl Peroxy Radicals
Active Reactive Organic Product Species.	
CO	Carbon Monoxide
HCHO	Formaldehyde
CCHO	Acetaldehyde
RCHO	Lumped C3+ Aldehydes
ACET	Acetone
MEK	Lumped Ketones
PHEN	Phenol
CRES	Cresols

Table A-1, (continued)

Name	Description
BALD	Aromatic aldehydes (e.g., benzaldehyde)
GLY	Glyoxal
MGLY	Methyl Glyoxal
AFG1	Reactive Aromatic Fragmentation Products from benzene and naphthalene
AFG2	Other Reactive Aromatic Fragmentation Products
AFG3	Aromatic Fragmentation Products used in adjusted m-xylene mechanism
RNO3	Organic Nitrates
NPHE	Nitrophenols
PAN	Peroxy Acetyl Nitrate
PPN	Peroxy Propionyl Nitrate
GPAN	PAN Analogue formed from Glyoxal
PBZN	PAN Analogues formed from Aromatic Aldehydes
-OOH	Operator Representing Hydroperoxy Groups
Non-Reacting Species	
CO2	Carbon Dioxide
-C	"Lost Carbon"
-N	"Lost Nitrogen"
H2	Hydrogen
Steady State Species and Operators.	
HO.	Hydroxyl Radicals
O	Ground State Oxygen Atoms
O*1D2	Excited Oxygen Atoms
RO2-R.	Peroxy Radical Operator representing NO to NO_2 conversion with HO_2 formation.
RO2-N.	Peroxy Radical Operator representing NO consumption with organic nitrate formation.
RO2-NP.	Peroxy Radical Operator representing NO consumption with nitrophenol formation
R2O2.	Peroxy Radical Operator representing NO to NO_2 conversion.
CCO-O2.	Peroxy Acetyl Radicals
C2CO-O2.	Peroxy Propionyl Radicals
HCOCO-O2.	Peroxyacyl Radical formed from Glyoxal
BZ-CO-O2.	Peroxyacyl Radical formed from Aromatic Aldehydes
HOCOO.	Intermediate formed in Formaldehyde + HO_2 reaction
BZ-O.	Phenoxy Radicals
BZ(NO2)-O.	Nitratophenoxy Radicals
HOCOO.	Radical Intermediate formed in the HO_2 + Formaldehyde system.
(HCHO2)	Excited Criegee biradicals formed from $=CH_2$ groups
(CCHO2)	Excited Criegee biradicals formed from $=CHCH_3$ groups
(RCHO2)	Excited Criegee biradicals formed from =CHR groups, where R not CH_3
(C(C)CO2)	Excited Criegee biradicals formed from $=C(CH_3)_2$ groups
(C(R)CO2)	Excited Criegee biradicals formed from $=C(CH_3)R$ or CR_2 groups
(BZCHO2)	Excited Criegee biradicals formed from styrenes

Table A-1, (continued)

Name	Description
Hydrocarbon species represented explicitly	
CH4	Methane (EKMA simulations only)
ETHANE	Ethane (Ethane reactivity simulations only)
N-C4	n-Butane (Chamber simulations only)
N-C6	n-Hexane (Chamber simulations only)
N-C8	n-Octane (Chamber simulations only)
ETHE	Ethene
ISOP	Isoprene (EKMA Simulations only)
APIN	α-Pinene (EKMA Simulations only)
UNKN	Unknown biogenics. (EKMA Simulations only)
PROPENE	Propene (Chamber simulations only)
T-2-BUTE	trans-2-Butene (Chamber simulations only)
TOLUENE	Toluene (Chamber simulations only)
M-XYLENE	m-Xylene (Chamber simulations only)
Lumped alkane and aromatic species used to represent the Base ROG mixture in the EKMA model simulations.	
AAR1	Alkanes and aromatics with $k_{OH} < 5x10^3$ ppm^{-1} min^{-1}
AAR2	Alkanes and aromatics with k_{OH} between $5x10^3$ and $1.5x10^4$ ppm^{-1} min^{-1}
AAR3	Alkanes and aromatics with $k_{OH} > 1.5x10^4$ ppm^{-1} min^{-1}
Lumped higher alkenes used to represent the Base ROG mixture in the EKMA model simulations	
OLE2	Alkenes with $k_{OH} < 7x10^4$ ppm^{-1} min^{-1} (Primarily terminal alkenes.)
OLE3	Alkenes with $k_{OH} > 7x10^4$ ppm^{-1} min^{-1} (Primary internal alkenes.)

Table A-2. Listing of SAPRC-93 mechanism as used to in the base case simulations.

Rxn. Label	Kinetic Parameters [a] k(300)	A	Ea	B	Reactions [b]
Inorganic Reactions					
1	(Phot. Set = NO2)				NO2 + HV = NO + O
2	2.16E-05	2.16E-05	0.00	-4.30	O + O2 + M = O3 + M
3A	1.42E+04	9.54E+03	-0.24	-1.00	O + NO2 = NO + O2
3B	2.28E+03	(Falloff Kinetics)			O + NO2 = NO3 + M
	k0 =	3.23E-03	0.00	-4.00	
	kINF =	3.23E+04	0.00	-1.00	
		F= 0.60	n= 1.00		
4	2.76E+01	2.94E+03	2.78	-1.00	O3 + NO = NO2 + O2
5	4.94E-02	2.06E+02	4.97	-1.00	O3 + NO2 = O2 + NO3
6	4.11E+04	2.49E+04	-0.30	-1.00	NO + NO3 = #2 NO2
7	6.90E-10	1.19E-10	-1.05	-2.00	NO + NO + O2 = #2 NO2
8	1.84E+03	(Falloff Kinetics)			NO2 + NO3 = N2O5
	k0 =	7.90E-02	0.00	-6.30	
	kINF =	2.20E+03	0.00	-1.50	
		F= 0.60	n= 1.00		
9	2.26E-03	3.72E+13	22.26	1.00	N2O5 + #RCON8 = NO2 + NO3
10	1.47E-06	1.47E-06	0.00	-1.00	N2O5 + H2O = #2 HNO3
11	6.13E-01	3.67E+01	2.44	-1.00	NO2 + NO3 = NO + NO2 + O2
12A	(Phot. Set = NO3NO)				NO3 + HV = NO + O2
12B	(Phot. Set = NO3NO2)				NO3 + HV = NO2 + O
13A	(Phot. Set = O3O3P)				O3 + HV = O + O2
13B	(Phot. Set = O3O1D)				O3 + HV = O*1D2 + O2
14	3.23E+05	3.23E+05	0.00	-1.00	O*1D2 + H2O = #2 HO.
15	4.29E+04	2.82E+04	-0.25	-1.00	O*1D2 + M = O + M
16	7.05E+03	(Falloff Kinetics)			HO. + NO = HONO
	k0 =	2.51E-02	0.00	-4.60	
	kINF =	2.20E+04	0.00	-1.50	
		F= 0.60	n= 1.00		
17	(Phot. Set = HONO)				HONO + HV = HO. + NO
18	1.66E+04	(Falloff Kinetics)			HO. + NO2 = HNO3
	k0 =	9.34E-02	0.00	-5.20	
	kINF =	3.52E+04	0.00	-2.30	
		F= 0.60	n= 1.00		
19	1.51E+02	9.47E+00	-1.65	-1.00	HO. + HNO3 = H2O + NO3
21	3.52E+02	3.52E+02	0.00	-1.00	HO. + CO = HO2. + CO2
22	1.02E+02	2.35E+03	1.87	-1.00	HO. + O3 = HO2. + O2
23	1.21E+04	5.43E+03	-0.48	-1.00	HO2. + NO = HO. + NO2
24	2.00E+03	(Falloff Kinetics)			HO2. + NO2 = HNO4
	k0 =	6.46E-03	0.00	-5.20	
	kINF =	6.90E+03	0.00	-2.40	
		F= 0.60	n= 1.00		
25	3.24E-03	1.95E+13	21.66	1.00	HNO4 + #RCON24 = HO2. + NO2
27	6.77E+03	1.91E+03	-0.75	-1.00	HNO4 + HO. = H2O + NO2 + O2
28	3.05E+00	1.61E+01	0.99	-1.00	HO2. + O3 = HO. + #2 O2
29A	2.54E+03	3.23E+02	-1.23	-1.00	HO2. + HO2. = HO2H + O2
29B	1.80E-03	6.82E-05	-1.95	-2.00	HO2. + HO2. + M = HO2H + O2
29C	1.34E-01	1.11E-05	-5.60	-2.00	HO2. + HO2. + H2O = HO2H + O2 + H2O
29D	9.52E-02	2.37E-06	-6.32	-2.00	HO2. + HO2. + H2O = HO2H + O2 + H2O
30A	(Same k as Reaction 29A)				NO3 + HO2. = HNO3 + O2
30B	(Same k as Reaction 29B)				NO3 + HO2. + M = HNO3 + O2
30C	(Same k as Reaction 29C)				NO3 + HO2. + H2O = HNO3 + O2 + H2O
30D	(Same k as Reaction 29D)				NO3 + HO2. + H2O = HNO3 + O2 + H2O
31	(Phot. Set = H2O2)				HO2H + HV = #2 HO.
32	2.49E+03	4.84E+03	0.40	-1.00	HO2H + HO. = HO2. + H2O
33	1.45E+05	6.75E+04	-0.46	-1.00	HO. + HO2. = H2O + O2
Peroxy Radical Operators					
B1	1.13E+04	6.16E+03	-0.36	-1.00	RO2. + NO = NO
B2	3.31E+04	(Falloff Kinetics)			RCO3. + NO = NO
	k0 =	2.03E+01	0.00	-9.10	
	kINF =	3.87E+04	0.00	-1.90	
		F= 0.27	n= 1.00		
B4	1.52E+04	(Falloff Kinetics)			RCO3. + NO2 = NO2
	k0 =	9.23E+00	0.00	-9.10	
	kINF =	1.76E+04	0.00	-1.90	
		F= 0.30	n= 1.00		
B5	7.19E+03	4.99E+02	-1.59	-1.00	RO2. + HO2. = HO2. + RO2-HO2-PROD
B6	7.19E+03	4.99E+02	-1.59	-1.00	RCO3. + HO2. = HO2. + RO2-HO2-PROD
B8	1.47E+00	1.47E+00	0.00	-1.00	RO2. + RO2. = RO2-RO2-PROD
B9	1.60E+04	2.73E+03	-1.05	-1.00	RO2. + RCO3. = RO2-RO2-PROD
B10	2.40E+04	4.11E+03	-1.05	-1.00	RCO3. + RCO3. = RO2-RO2-PROD
B11	(Same k as Reaction B1)				RO2-R. + NO = NO2 + HO2.
B12	(Same k as Reaction B5)				RO2-R. + HO2. = -OOH
B13	(Same k as Reaction B8)				RO2-R. + RO2. = RO2. + #.5 HO2.
B14	(Same k as Reaction B9)				RO2-R. + RCO3. = RCO3. + #.5 HO2.

Table A-2 (continued)

Rxn. Label	Kinetic Parameters [a] k(300)	A	Ea	B	Reactions [b]
B19	(Same k as Reaction B1)				RO2-N. + NO = RNO3
B20	(Same k as Reaction B5)				RO2-N. + HO2. = -OOH + MEK + #1.5 -C
B21	(Same k as Reaction B8)				RO2-N. + RO2. = RO2. + #.5 HO2. + MEK + #1.5 -C
B22	(Same k as Reaction B9)				RO2-N. + RCO3. = RCO3. + #.5 HO2. + MEK + #1.5 -C
B15	(Same k as Reaction B1)				R2O2. + NO = NO2
B16	(Same k as Reaction B5)				R2O2. + HO2. =
B17	(Same k as Reaction B8)				R2O2. + RO2. = RO2.
B18	(Same k as Reaction B9)				R2O2. + RCO3. = RCO3.
B23	(Same k as Reaction B1)				RO2-XN. + NO = -N
B24	(Same k as Reaction B5)				RO2-XN. + HO2. = -OOH
B25	(Same k as Reaction B8)				RO2-XN. + RO2. = RO2. + #.5 HO2.
B26	(Same k as Reaction B9)				RO2-XN. + RCO3. = RCO3. + HO2.
G2	(Same k as Reaction B1)				RO2-NP. + NO = NPHE
G3	(Same k as Reaction B5)				RO2-NP. + HO2. = -OOH + #6 -C
G4	(Same k as Reaction B8)				RO2-NP. + RO2. = RO2. + #.5 HO2. + #6 -C
G5	(Same k as Reaction B9)				RO2-NP. + RCO3. = RCO3. + HO2. + #6 -C
Excited Criegee Biradicals					
RZ1	6.00E+01	(No T Dependence)			(HCHO2) = #.12 CO + #.18 CO2 + #.7 HCOOH + #.12 HO2. + #.12 HO.
RZ2	6.00E+01	(No T Dependence)			(CCHO2) = #.25 CCOOH + #.15 "CH4 + CO2" + #.6 HO. + #.3 "CCO-O2. + RCO3." + #.1 "RO2-R. + HCHO + CO + RO2."
RZ3	6.00E+01	(No T Dependence)			(RCHO2) = #.25 CCOOH + #.15 CO2 + #.6 HO. + #.3 "C2CO-O2. + RCO3." + #.1 "RO2-R. + CCHO + CO + RO2." + #.55 -C
RZ4	6.00E+01	(No T Dependence)			(C(C)CO2) = HO. + R2O2. + HCHO + CCO-O2. + RCO3. + RO2.
RZ5	6.00E+01	(No T Dependence)			(C(R)CO2) = HO. + CCO-O2. + CCHO + R2O2. + RCO3. + RO2.
RZ8	6.00E+01	(No T Dependence)			(BZCHO2) = #.5 O3OL-SB + #.5 "BZ-O. + R2O2. + CO + HO."
Lumped Hydroperoxide Group					
B7	(Phot. Set = CO2H)				-OOH + HV = HO2. + HO.
B7A	2.65E+03	1.73E+03	-0.25	-1.00	HO. + -OOH = HO.
B7B	5.45E+03	2.63E+03	-0.44	-1.00	HO. + -OOH = RO2-R. + RO2.
Formaldehyde					
C1	(Phot. Set = HCHONEWR)				HCHO + HV = #2 HO2. + CO
C2	(Phot. Set = HCHONEWM)				HCHO + HV = H2 + CO
C3	1.43E+04	1.65E+03	-1.29	1.00	HCHO + HO. = HO2. + CO + H2O
C4	1.14E+02	1.42E+01	-1.24	-1.00	HCHO + HO2. = HOCOO.
C4A	1.06E+04	1.44E+14	13.91	0.00	HOCOO. = HO2. + HCHO
C4B	(Same k as Reaction B1)				HOCOO. + NO = -C + NO2 + HO2.
C9	9.36E-01	4.11E+03	5.00	-1.00	HCHO + NO3 = HNO3 + HO2. + CO
Acetaldehyde and PAN					
C10	2.30E+04	8.15E+03	-0.62	-1.00	CCHO + HO. = CCO-O2. + H2O + RCO3.
C11A	(Phot. Set = CCHOR)				CCHO + HV = CO + HO2. + HCHO + RO2-R. + RO2.
C12	4.17E+00	2.05E+03	3.70	-1.00	CCHO + NO3 = HNO3 + CCO-O2. + RCO3.
C13	(Same k as Reaction B2)				CCO-O2. + NO = CO2 + NO2 + HCHO + RO2-R. + RO2.
C14	(Same k as Reaction B4)				CCO-O2. + NO2 = PAN
C15	(Same k as Reaction B6)				CCO-O2. + HO2. = -OOH + CO2 + HCHO
C16	(Same k as Reaction B9)				CCO-O2. + RO2. = RO2. + #.5 HO2. + CO2 + HCHO
C17	(Same k as Reaction B10)				CCO-O2. + RCO3. = RCO3. + HO2. + CO2 + HCHO
C18	3.90E-02	(Falloff Kinetics)			PAN = CCO-O2. + NO2 + RCO3.
	k0 =	7.19E+12	23.97	-1.00	
	kINF =	2.40E+18	27.08	0.00	
		F= 0.30	n= 1.00		
C3+ Aldehydes and PPN					
C25	2.89E+04	1.25E+04	-0.50	-1.00	RCHO + HO. = C2CO-O2. + RCO3.
C26	(Phot. Set = RCHO)				RCHO + HV = CCHO + RO2-R. + RO2. + CO + HO2.
C27	4.17E+00	2.05E+03	3.70	-1.00	NO3 + RCHO = HNO3 + C2CO-O2. + RCO3.
C28	(Same k as Reaction B2)				C2CO-O2. + NO = CCHO + RO2-R. + CO2 + NO2 + RO2.
C29	1.23E+04	1.23E+04	0.00	-1.00	C2CO-O2. + NO2 = PPN
C30	(Same k as Reaction B6)				C2CO-O2. + HO2. = -OOH + CCHO + CO2
C31	(Same k as Reaction B9)				C2CO-O2. + RO2. = RO2. + #.5 HO2. + CCHO + CO2
C32	(Same k as Reaction B10)				C2CO-O2. + RCO3. = RCO3. + HO2. + CCHO + CO2
C33	4.07E-02	9.60E+18	27.97	0.00	PPN = C2CO-O2. + NO2 + RCO3.

Table A-2 (continued)

Rxn. Label	Kinetic Parameters [a] k(300)	A	Ea	B	Reactions [b]
Acetone (standard mechanism)					
C38	3.28E+02	7.06E+02	0.46	1.00	ACET + HO. = R2O2. + HCHO + CCO-O2. + RCO3. + RO2.
C39	(Phot. Set = ACET-93C)				ACET + HV = CCO-O2. + HCHO + RO2-R. + RCO3. + RO2.
Acetone (adjusted mechanism)					
C38	3.28E+02	7.06E+02	0.46	1.00	ACET + HO. = R2O2. + HCHO + CCO-O2. + RCO3. + RO2.
C39x	(Phot. Set = ADJACET)				ACET + HV = CCO-O2. + HCHO + RO2-R. + RCO3. + RO2.
C4+ Ketones					
C44	1.70E+03	4.29E+02	-0.82	1.00	MEK + HO. = H2O + #.5 "CCHO + HCHO + CCO-O2. + C2CO-O2." + RCO3. + #1.5 "R2O2. + RO2."
C57	(Phot. Set = KETONE)				MEK + HV + #.1 = CCO-O2. + CCHO + RO2-R. + RCO3. + RO2.
Organic Nitrates					
C95	3.03E+03	3.22E+04	1.41	-1.00	RNO3 + HO. = NO2 + #.155 MEK + #1.05 RCHO + #.48 CCHO + #.16 HCHO + #.11 -C + #1.39 "R2O2. + RO2."
Glyoxal and GPAN					
C58A	(Phot. Set = GLYOXAL1)				GLY + HV = #.8 HO2. + #.45 HCHO + #1.55 CO
C58B	(Phot. Set = GLYOXAL2)				GLY + HV + #0.029 = #.13 HCHO + #1.87 CO
C59	1.67E+04	1.67E+04	0.00	-1.00	GLY + HO. = #.6 HO2. + #1.2 CO + #.4 "HCOCO-O2. + RCO3."
C60	(Same k as Reaction C12)				GLY + NO3 = HNO3 + #.6 HO2. + #1.2 CO + #.4 "HCOCO-O2. + RCO3."
C62	(Same k as Reaction B2)				HCOCO-O2. + NO = NO2 + CO2 + CO + HO2.
C63	(Same k as Reaction B4)				HCOCO-O2. + NO2 = GPAN
C65	(Same k as Reaction B6)				HCOCO-O2. + HO2. = -OOH + CO2 + CO
C66	(Same k as Reaction B9)				HCOCO-O2. + RO2. = RO2. + #.5 HO2. + CO2 + CO
C67	(Same k as Reaction B10)				HCOCO-O2. + RCO3. = RCO3. + HO2. + CO2 + CO
C64	(Same k as Reaction C18)				GPAN = HCOCO-O2. + NO2 + RCO3.
Methyl Glyoxal					
C68A	(Phot. Set = MEGLYOX1)				MGLY + HV = HO2. + CO + CCO-O2. + RCO3.
C68B	(Phot. Set = MEGLYOX2)				MGLY + HV + #.107 = HO2. + CO + CCO-O2. + RCO3.
C69	2.52E+04	2.52E+04	0.00	-1.00	MGLY + HO. = CO + CCO-O2. + RCO3.
C70	(Same k as Reaction C12)				MGLY + NO3 = HNO3 + CO + CCO-O2. + RCO3.
Phenol and cresols					
G46	3.86E+04	3.86E+04	0.00	-1.00	HO. + PHEN = #.15 RO2-NP. + #.85 RO2-R. + #.2 GLY + #4.7 -C + RO2.
G51	5.28E+03	5.28E+03	0.00	-1.00	NO3 + PHEN = HNO3 + BZ-O.
G52	6.16E+04	6.16E+04	0.00	-1.00	HO. + CRES = #.15 RO2-NP. + #.85 RO2-R. + #.2 MGLY + #5.5 -C + RO2.
G57	3.08E+04	3.08E+04	0.00	-1.00	NO3 + CRES = HNO3 + BZ-O. + -C
Benzaldehyde and PBzN					
G30	1.89E+04	1.89E+04	0.00	-1.00	BALD + HO. = BZ-CO-O2. + RCO3.
G31	(Phot. Set = BZCHO)				BALD + HV + #.05 = #7 -C
G32	3.83E+00	2.05E+03	3.75	-1.00	BALD + NO3 = HNO3 + BZ-CO-O2.
G33	(Same k as Reaction B2)				BZ-CO-O2. + NO = BZ-O. + CO2 + NO2 + R2O2. + RO2.
G34	1.23E+04	1.23E+04	0.00	-1.00	BZ-CO-O2. + NO2 = PBZN
G36	(Same k as Reaction B6)				BZ-CO-O2. + HO2. = -OOH + CO2 + PHEN
G37	(Same k as Reaction B9)				BZ-CO-O2. + RO2. = RO2. + #.5 HO2. + CO2 + PHEN
G38	(Same k as Reaction B10)				BZ-CO-O2. + RCO3. = RCO3. + HO2. + CO2 + PHEN
G35	1.30E-02	9.60E+16	25.90	0.00	PBZN = BZ-CO-O2. + NO2 + RCO3.
Nitrophenols					
G58	5.28E+03	5.28E+03	0.00	-1.00	NPHE + NO3 = HNO3 + BZ(NO2)-O.
G43	5.19E+04	1.91E+04	-0.60	-1.00	BZ-O. + NO2 = NPHE
G44	(Same k as Reaction B5)				BZ-O. + HO2. = PHEN
G45	6.00E-02	(No T Dependence)			BZ-O. = PHEN
G59	(Same k as Reaction G43)				BZ(NO2)-O. + NO2 = #2 -N + #6 -C
G60	(Same k as Reaction B5)				BZ(NO2)-O. + HO2. = NPHE
G61	(Same k as Reaction G45)				BZ(NO2)-O. = NPHE
Aromatic Fragmentation Products					
G7	1.67E+04	1.67E+04	0.00	-1.00	HO. + AFG1 = HCOCO-O2. + RCO3.
G8	(Phot. Set = ACROLEIN)				AFG1 + HV + #0.029 = HO2. + HCOCO-O2. + RCO3.

Table A-2 (continued)

Rxn. Label	Kinetic Parameters [a] k(300)	A	Ea	B	Reactions [b]
U2OH	2.52E+04	2.52E+04	0.00	-1.00	HO. + AFG2 = C2CO-O2. + RCO3.
U2HV	(Phot. Set = ACROLEIN)				AFG2 + HV + #0.615 = HO2. + CO + CCO-O2. + RCO3.
U3OH	2.52E+04	2.52E+04	0.00	-1.00	HO. + AFG3 = C2CO-O2. + RCO3.
U3HV	(Phot. Set = ACROLEIN)				AFG3 + HV + #0.022 = HO2. + CO + CCO-O2. + RCO3.
Methane – Used in EKMA Simulations					
RCH4	1.28E+01	9.18E+02	2.55	1.00	CH4 + HO. = HCHO + RO2-R. + RO2.
Ethane – Used for Ethane Reactivity Simulations					
OH01	2.74E-13	1.28E-12	0.92	2.00	ETHANE + HO. = RO2-R. + CCHO + RO2.
n-Butane – Used in Full Surrogate Experiment Simulations					
OH02	2.56E-12	1.36E-12	-0.38	2.00	N-C4 + HO. = #.076 RO2-N. + #.924 RO2-R. + #.397 R2O2. + #.001 HCHO + #.571 CCHO + #.14 RCHO + #.533 MEK + #-0.076 -C + #1.397 RO2.
n-Hexane – Used in Mini-Surrogate Experiment Simulations					
OH03	5.63E-12	1.35E-11	0.52	0.00	N-C6 + HO. = #.185 RO2-N. + #.815 RO2-R. + #.738 R2O2. + #.02 CCHO + #.105 RCHO + #1.134 MEK + #.186 -C + #1.738 RO2.
n-Octane – Used in Full Surrogate Experiment Simulations					
OH04	8.76E-12	3.15E-11	0.76	0.00	N-C8 + HO. = #.333 RO2-N. + #.667 RO2-R. + #.706 R2O2. + #.002 RCHO + #1.333 MEK + #.998 -C + #1.706 RO2.
Ethene					
OH05	8.43E-12	1.96E-12	-0.87	0.00	ETHENE + HO. = RO2-R. + RO2. + #1.56 HCHO + #.22 CCHO
O305	1.68E-18	9.14E-15	5.13	0.00	ETHENE + O3 = HCHO + (HCHO2)
N305	2.15E-16	5.43E-12	6.04	0.00	ETHENE + NO3 = R2O2. + RO2. + #2 HCHO + NO2
OA05	7.42E-13	1.04E-11	1.57	0.00	ETHENE + O = RO2-R. + HO2. + RO2. + HCHO + CO + #2 OLE-RI
Propene – Used in Full Surrogate Experiment Simulations					
OH06	2.60E-11	4.85E-12	-1.00	0.00	PROPENE + HO. = RO2-R. + RO2. + HCHO + CCHO
O306	1.05E-17	5.51E-15	3.73	0.00	PROPENE + O3 = #.6 HCHO + #.4 CCHO + #.4 (HCHO2) + #.6 (CCHO2)
N306	9.80E-15	4.85E-12	3.70	0.00	PROPENE + NO3 = R2O2. + RO2. + HCHO + CCHO + NO2
OA06	4.01E-12	1.18E-11	0.64	0.00	PROPENE + O = #.4 HO2. + #.5 RCHO + #.5 MEK + #-0.5 -C + #.4 OLE-RI
trans-2-Butene – Used in Full Surrogate Experiment Simulations					
OH07	6.30E-11	1.01E-11	-1.09	0.00	T-2-BUTE + HO. = RO2-R. + RO2. + #2 CCHO
O307	1.95E-16	6.64E-15	2.10	0.00	T-2-BUTE + O3 = CCHO + (CCHO2)
N307	3.92E-13	1.10E-13	-0.76	2.00	T-2-BUTE + NO3 = R2O2. + RO2. + #2 CCHO + NO2
OA07	2.34E-11	2.26E-11	-0.02	0.00	T-2-BUTE + O = #.4 HO2. + #.5 RCHO + #.5 MEK + #.5 -C + #.4 OLE-RI
Toluene – Used in Full Surrogate Experiment Simulations					
OH08	5.91E-12	1.81E-12	-0.70	0.00	TOLUENE + HO. = #.085 BALD + #.26 CRES + #.118 GLY + #.131 MGLY + #.49 AFG2 + #.74 RO2-R. + #.26 HO2. + #2.486 -C + #.74 RO2.
m-Xylene (Standard Mechanism) – Used in Full Surrogate Experiment Simulations					
OH09	2.36E-11	(No T Dependence)			M-XYLENE + HO. = #.04 BALD + #.18 CRES + #.108 GLY + #.37 MGLY + #.75 AFG2 + #.82 RO2-R. + #.18 HO2. + #2.884 -C + #.82 RO2.
m-Xylene (Adjusted Mechanism) – Used in Set 3 Mini-Surrogate Experiment Simulations (see Carter et al., 1993)					
OH09x	2.36E-11	(No T Dependence)			M-XYLENE + HO. = #.04 BALD + #.18 CRES + #.108 GLY + #.37 MGLY + #2 AFG3 + #.82 RO2-R. + #.18 HO2. + #-0.866 -C + #.82 RO2.
Isoprene (SAPRC-90 mechanism) – Used in EKMA Simulations					
ISOH	1.46E+05	3.73E+04	-0.81	-1.00	ISOP + HO. = RO2-R. + HCHO + RCHO + RO2. + -C
ISO3	2.20E-02	1.81E+01	4.00	-1.00	ISOP + O3 = #.5 HCHO + #.15 CCHO + #.5 RCHO + #.21 MEK + #.295 CO + #.285 O3OL-SB + #.165 HO2. + #.06 HO. + #.135 RO2-R. + #.135 RO2. + #1.565 -C + #.36 OLE-RI
ISN3	1.01E+03	4.45E+03	0.89	-1.00	ISOP + NO3 = NO2 + R2O2. + HCHO + RCHO + RO2. + -C
ISOA	8.81E+04	8.81E+04	0.00	-1.00	ISOP + O = #.4 HO2. + #.5 MEK + #.5 RCHO + #1.5 -C + #.4 OLE-RI
α-Pinene (SAPRC-90 mechanism) – Used in EKMA Simulations					
APOH	7.80E+04	1.78E+04	-0.88	-1.00	APIN + HO. = RO2-R. + RCHO + RO2. + #7 -C
APO3	1.47E-01	1.45E+00	1.37	-1.00	APIN + O3 = #.05 HCHO + #.2 CCHO + #.5 RCHO + #.61 MEK + #.075 CO + #.1 O3OL-SB + #.05 CCO-O2. + #.05 C2CO-O2. + #.1 RCO3. +

Table A-2 (continued)

Rxn. Label	Kinetic Parameters [a] k(300)	A	Ea	B	Reactions [b]
					#.105 HO2. + #.16 HO. + #.135 RO2-R. + #.15 R2O2. + #.285 RO2. + #5.285 -C + #.5 OLE-RI
APN3	8.95E+03	1.75E+03	-0.97	-1.00	APIN + NO3 = NO2 + R2O2. + RCHO + RO2. + #7 -C
APOA	4.40E+04	4.40E+04	0.00	-1.00	APIN + O = #.4 HO2. + #.5 MEK + #.5 RCHO + #6.5 -C + #.4 OLE-RI
Unknown Biogenics (Averaged parameters of α-pinene and β-pinene, SAPRC-90 mechanism) – Used in EKMA Simulations					
UNOH	9.64E+04	9.64E+04	0.00	-1.00	UNKN + HO. = RO2-R. + RO2. + #.5 HCHO + RCHO + #6.5 -C
UNO3	8.59E-02	8.59E-02	0.00	-1.00	UNKN + O3 = #.135 RO2-R. + #.135 HO2. + #.075 R2O2. + #.21 RO2. + #.025 CCO-O2. + #.025 C2CO-O2. + #.05 RCO3. + #.275 HCHO + #.175 CCHO + #.5 RCHO + #.41 MEK + #.185 CO + #5.925 -C + #.11 HO. + #.192 O3OL-SB + #.43 OLE-RI
UNN3	6.31E+03	6.31E+03	0.00	-1.00	UNKN + NO3 = R2O2. + RO2. + #.5 HCHO + RCHO + #6.5 -C + NO2
UNOA	4.26E+04	4.26E+04	0.00	-1.00	UNKN + O = #.4 HO2. + #.5 RCHO + #.5 MEK + #6.5 -C + #.4 OLE-RI
Representation of Alkanes and Aromatics the base ROG mixture in the EKMA simulations. [d,e]					
A1OH	2.90E+03	4.17E+03	0.22	0.00	AAR1 + HO. = #.917 RO2-R. + #.042 RO2-N. + #.007 RO2-XN. + #.034 HO2. + #.33 R2O2. + #1.295 RO2. + #.141 HCHO + #.315 CCHO + #.163 RCHO + #.254 ACET + #.25 MEK + #.024 CO + #.01 PHEN + #.065 GLY + #.077 AFG1 + #.078 -C
A2OH	8.75E+03	3.60E+03	-0.53	0.00	AAR2 + HO. = #.828 RO2-R. + #.109 RO2-N. + #.002 RO2-XN. + #.061 HO2. + #.635 R2O2. + #1.574 RO2. + #.013 HCHO + #.173 CCHO + #.205 RCHO + #.179 ACET + #.592 MEK + #.032 CO + #.007 CO2 + #.061 CRES + #.02 BALD + #.028 GLY + #.031 MGLY + #.115 AFG2 + #.917 -C
A3OH	4.30E+04	1.66E+04	-0.57	0.00	AAR3 + HO. = #.785 RO2-R. + #.079 RO2-N. + #.136 HO2. + #.198 R2O2. + #1.063 RO2. + #.003 HCHO + #.01 CCHO + #.046 RCHO + #.3 MEK + #.002 CO2 + #.136 CRES + #.027 BALD + #.046 GLY + #.36 MGLY + #.565 AFG2 + #3.376 -C
Representation of Anthropogenic C_{3+} Alkenes the base ROG mixture in the EKMA simulations. [d]					
O2OH	4.69E+04	3.28E+03	-1.59	0.00	OLE2 + HO. = #.859 RO2-R. + #.141 RO2-N. + RO2. + #.859 HCHO + #.252 CCHO + #.607 RCHO + #1.269 -C
O2O3	1.59E-02	2.10E+00	2.91	0.00	OLE2 + O3 = #.6 HCHO + #.635 RCHO + #.981 -C + #.4 (HCHO2) + #.529 (CCHO2) + #.071 (RCHO2)
O2N3	1.77E+01	3.28E+03	3.12	0.00	OLE2 + NO3 = R2O2. + RO2. + HCHO + #.294 CCHO + #.706 RCHO + #1.451 -C + NO2
O2OA	6.07E+03	6.67E+03	0.06	0.00	OLE2 + O = #.4 HO2. + #.5 RCHO + #.5 MEK + #1.657 -C + #.4 OLE-RI
O3OH	9.73E+04	7.33E+03	-1.54	0.00	OLE3 + HO. = #.875 RO2-R. + #.125 RO2-N. + RO2. + #.302 HCHO + #.609 CCHO + #.548 RCHO + #.104 ACET + #.079 MEK + #.053 BALD + #.852 -C
O3O3	2.30E-01	2.48E+00	1.42	0.00	OLE3 + O3 = #.24 HCHO + #.269 CCHO + #.373 RCHO + #.056 MEK + #.024 BALD + #.978 -C + #.106 (HCHO2) + #.427 (CCHO2) + #.253 (RCHO2) + #.143 (C(C)CO2 + #.035 (C(R)CO2 + #.036 (BZCHO2)
O3N3	1.53E+03	7.67E+02	-0.41	0.00	OLE3 + NO3 = R2O2. + RO2. + #.346 HCHO + #.696 CCHO + #.626 RCHO + #.119 ACET + #.091 MEK + #.06 BALD + #.883 -C + NO2
O3OA	3.37E+04	1.15E+04	-0.64	0.00	OLE3 + O = #.4 HO2. + #.5 RCHO + #.5 MEK + #2.14 -C + #.4 OLE-RI

[a] Except as noted, expression for rate constant is $k = A\ e^{Ea/RT}\ (T/300)^B$. Rate constants and A factor are in ppm, min units. Units of Ea is kcal $mole^{-1}$. "Phot Set" means this is a photolysis reaction, with the absorption coefficients and quantum yields given in Table A-5.

[b] Format of reaction listing same as used in documentation of the detailed mechanism (Carter 1990).

[c] "#RCONnn" as a reactant means that the rate constant for the reaction is obtained by multiplying the rate constant given by that for reaction "nn". Thus, the rate constant given is actually an equilibrium constant.

[d] Rate constants and product yield parameters based on the mixture of species in the base ROG mixture which are being represented.

[e] Lumping of alkanes with aromatics is not recommended for grid model simulations or for trajectory simulations where the composition of emitted ROG species vary with time. This is not the case with these EKMA simulations.

Table A-3. Absorption cross sections and quantum yields for photolysis reactions.

WL (nm)	Abs (cm^2)	QY	WL (nm)	Abs (cm^2)	QY	WL (nm)	Abs (cm^2)	QY	WL (nm)	Abs (cm^2)	QY	WL (nm)	Abs (cm^2)	QY
Photolysis File = NO2														
250.0	2.83E-20	1.000	255.0	1.45E-20	1.000	260.0	1.90E-20	1.000	265.0	2.05E-20	1.000	270.0	3.13E-20	1.000
275.0	4.02E-20	1.000	280.0	5.54E-20	1.000	285.0	6.99E-20	1.000	290.0	8.18E-20	0.999	295.0	9.67E-20	0.998
300.0	1.17E-19	0.997	305.0	1.66E-19	0.996	310.0	1.76E-19	0.995	315.0	2.25E-19	0.994	320.0	2.54E-19	0.993
325.0	2.79E-19	0.992	330.0	2.99E-19	0.991	335.0	3.45E-19	0.990	340.0	3.88E-19	0.989	345.0	4.07E-19	0.988
350.0	4.10E-19	0.987	355.0	5.13E-19	0.986	360.0	4.51E-19	0.984	365.0	5.78E-19	0.983	370.0	5.42E-19	0.981
375.0	5.35E-19	0.979	380.0	5.99E-19	0.975	381.0	5.98E-19	0.974	382.0	5.97E-19	0.973	383.0	5.96E-19	0.972
384.0	5.95E-19	0.971	385.0	5.94E-19	0.969	386.0	5.95E-19	0.967	387.0	5.96E-19	0.966	388.0	5.98E-19	0.964
389.0	5.99E-19	0.962	390.0	6.00E-19	0.960	391.0	5.98E-19	0.959	392.0	5.96E-19	0.957	393.0	5.93E-19	0.953
394.0	5.91E-19	0.950	395.0	5.89E-19	0.942	396.0	6.06E-19	0.922	397.0	6.24E-19	0.870	398.0	6.41E-19	0.820
399.0	6.59E-19	0.760	400.0	6.76E-19	0.695	401.0	6.67E-19	0.635	402.0	6.58E-19	0.560	403.0	6.50E-19	0.485
404.0	6.41E-19	0.425	405.0	6.32E-19	0.350	406.0	6.21E-19	0.290	407.0	6.10E-19	0.225	408.0	5.99E-19	0.185
409.0	5.88E-19	0.153	410.0	5.77E-19	0.130	411.0	5.88E-19	0.110	412.0	5.98E-19	0.094	413.0	6.09E-19	0.083
414.0	6.19E-19	0.070	415.0	6.30E-19	0.059	416.0	6.29E-19	0.048	417.0	6.27E-19	0.039	418.0	6.26E-19	0.030
419.0	6.24E-19	0.023	420.0	6.23E-19	0.018	421.0	6.18E-19	0.012	422.0	6.14E-19	0.008	423.0	6.09E-19	0.004
424.0	6.05E-19	0.000	425.0	6.00E-19	0.000									
Photolysis File = NO3NO														
585.0	2.77E-18	0.000	590.0	5.14E-18	0.250	595.0	4.08E-18	0.400	600.0	2.83E-18	0.250	605.0	3.45E-18	0.200
610.0	1.48E-18	0.200	615.0	1.96E-18	0.100	620.0	3.58E-18	0.100	625.0	9.25E-18	0.050	630.0	5.66E-18	0.050
635.0	1.45E-18	0.030	640.0	1.11E-18	0.000									
Photolysis File = NO3NO2														
400.0	0.00E+00	1.000	405.0	3.00E-20	1.000	410.0	4.00E-20	1.000	415.0	5.00E-20	1.000	420.0	8.00E-20	1.000
425.0	1.00E-19	1.000	430.0	1.30E-19	1.000	435.0	1.80E-19	1.000	440.0	1.90E-19	1.000	445.0	2.20E-19	1.000
450.0	2.80E-19	1.000	455.0	3.30E-19	1.000	460.0	3.70E-19	1.000	465.0	4.30E-19	1.000	470.0	5.10E-19	1.000
475.0	6.00E-19	1.000	480.0	6.40E-19	1.000	485.0	6.90E-19	1.000	490.0	8.80E-19	1.000	495.0	9.50E-19	1.000
500.0	1.01E-18	1.000	505.0	1.10E-18	1.000	510.0	1.32E-18	1.000	515.0	1.40E-18	1.000	520.0	1.45E-18	1.000
525.0	1.48E-18	1.000	530.0	1.94E-18	1.000	535.0	2.04E-18	1.000	540.0	1.81E-18	1.000	545.0	1.81E-18	1.000
550.0	2.36E-18	1.000	555.0	2.68E-18	1.000	560.0	3.07E-18	1.000	565.0	2.53E-18	1.000	570.0	2.54E-18	1.000
575.0	2.74E-18	1.000	580.0	3.05E-18	1.000	585.0	2.77E-18	1.000	590.0	5.14E-18	0.750	595.0	4.08E-18	0.600
600.0	2.83E-18	0.550	605.0	3.45E-18	0.400	610.0	1.45E-18	0.300	615.0	1.96E-18	0.250	620.0	3.58E-18	0.200
625.0	9.25E-18	0.150	630.0	5.66E-18	0.050	635.0	1.45E-18	0.000						
Photolysis File = O3O3P														
280.0	3.97E-18	0.100	281.0	3.60E-18	0.100	282.0	3.24E-18	0.100	283.0	3.01E-18	0.100	284.0	2.73E-18	0.100
285.0	2.44E-18	0.100	286.0	2.21E-18	0.100	287.0	2.01E-18	0.100	288.0	1.76E-18	0.100	289.0	1.58E-18	0.100
290.0	1.41E-18	0.100	291.0	1.26E-18	0.100	292.0	1.10E-18	0.100	293.0	9.89E-19	0.100	294.0	8.59E-19	0.100
295.0	7.70E-19	0.100	296.0	6.67E-19	0.100	297.0	5.84E-19	0.100	298.0	5.07E-19	0.100	299.0	4.52E-19	0.100
300.0	3.92E-19	0.100	301.0	3.42E-19	0.100	302.0	3.06E-19	0.100	303.0	2.60E-19	0.100	304.0	2.37E-19	0.100
305.0	2.01E-19	0.112	306.0	1.79E-19	0.149	307.0	1.56E-19	0.197	308.0	1.38E-19	0.259	309.0	1.25E-19	0.339
310.0	1.02E-19	0.437	311.0	9.17E-20	0.546	312.0	7.88E-20	0.652	313.0	6.77E-20	0.743	314.0	6.35E-20	0.816
315.0	5.10E-20	0.872	316.0	4.61E-20	0.916	317.0	4.17E-20	0.949	318.0	3.72E-20	0.976	319.0	2.69E-20	0.997
320.0	3.23E-20	1.000	330.0	6.70E-21	1.000	340.0	1.70E-21	1.000	350.0	4.00E-22	1.000	355.0	0.00E+00	1.000
400.0	0.00E+00	1.000	450.0	1.60E-22	1.000	500.0	1.34E-21	1.000	550.0	3.32E-21	1.000	600.0	5.06E-21	1.000
650.0	2.45E-21	1.000	700.0	8.70E-22	1.000	750.0	3.20E-22	1.000	800.0	1.60E-22	1.000	900.0	0.00E+00	1.000
Photolysis File = O3O1D														
280.0	3.97E-18	0.900	281.0	3.60E-18	0.900	282.0	3.24E-18	0.900	283.0	3.01E-18	0.900	284.0	2.73E-18	0.900
285.0	2.44E-18	0.900	286.0	2.21E-18	0.900	287.0	2.01E-18	0.900	288.0	1.76E-18	0.900	289.0	1.58E-18	0.900
290.0	1.41E-18	0.900	291.0	1.26E-18	0.900	292.0	1.10E-18	0.900	293.0	9.89E-19	0.900	294.0	8.59E-19	0.900
295.0	7.70E-19	0.900	296.0	6.67E-19	0.900	297.0	5.84E-19	0.900	298.0	5.07E-19	0.900	299.0	4.52E-19	0.900
300.0	3.92E-19	0.900	301.0	3.42E-19	0.900	302.0	3.06E-19	0.900	303.0	2.60E-19	0.900	304.0	2.37E-19	0.900
305.0	2.01E-19	0.888	306.0	1.79E-19	0.851	307.0	1.56E-19	0.803	308.0	1.38E-19	0.741	309.0	1.25E-19	0.661
310.0	1.02E-19	0.563	311.0	9.17E-20	0.454	312.0	7.88E-20	0.348	313.0	6.77E-20	0.257	314.0	6.35E-20	0.184
315.0	5.10E-20	0.128	316.0	4.61E-20	0.084	317.0	4.17E-20	0.051	318.0	3.72E-20	0.024	319.0	2.69E-20	0.003
320.0	3.23E-20	0.000												
Photolysis File = HONO														
311.0	0.00E+00	1.000	312.0	2.00E-21	1.000	313.0	4.20E-21	1.000	314.0	4.60E-21	1.000	315.0	4.20E-21	1.000
316.0	3.00E-21	1.000	317.0	4.60E-21	1.000	318.0	3.60E-20	1.000	319.0	6.10E-20	1.000	320.0	2.10E-20	1.000
321.0	4.27E-20	1.000	322.0	4.01E-20	1.000	323.0	3.93E-20	1.000	324.0	4.01E-20	1.000	325.0	4.04E-20	1.000
326.0	3.13E-20	1.000	327.0	4.12E-20	1.000	328.0	7.55E-20	1.000	329.0	6.64E-20	1.000	330.0	7.29E-20	1.000
331.0	8.70E-20	1.000	332.0	1.38E-19	1.000	333.0	5.91E-20	1.000	334.0	5.91E-20	1.000	335.0	6.45E-20	1.000
336.0	5.91E-20	1.000	337.0	4.58E-20	1.000	338.0	1.91E-19	1.000	339.0	1.63E-19	1.000	340.0	1.05E-19	1.000
341.0	8.70E-20	1.000	342.0	3.35E-19	1.000	343.0	2.01E-19	1.000	344.0	1.02E-19	1.000	345.0	8.54E-20	1.000
346.0	8.32E-20	1.000	347.0	8.20E-20	1.000	348.0	7.49E-20	1.000	349.0	7.13E-20	1.000	350.0	6.83E-20	1.000
351.0	1.74E-19	1.000	352.0	1.14E-19	1.000	353.0	3.71E-19	1.000	354.0	4.96E-19	1.000	355.0	2.46E-19	1.000
356.0	1.19E-19	1.000	357.0	9.35E-20	1.000	358.0	7.78E-20	1.000	359.0	7.29E-20	1.000	360.0	6.83E-20	1.000
361.0	6.90E-20	1.000	362.0	7.32E-20	1.000	363.0	9.00E-20	1.000	364.0	1.21E-19	1.000	365.0	1.33E-19	1.000
366.0	2.13E-19	1.000	367.0	3.52E-19	1.000	368.0	4.50E-19	1.000	369.0	2.93E-19	1.000	370.0	1.19E-19	1.000
371.0	9.46E-20	1.000	372.0	8.85E-20	1.000	373.0	7.44E-20	1.000	374.0	4.77E-20	1.000	375.0	2.70E-20	1.000
376.0	1.90E-20	1.000	377.0	1.50E-20	1.000	378.0	1.90E-20	1.000	379.0	5.80E-20	1.000	380.0	7.78E-20	1.000
381.0	1.14E-19	1.000	382.0	1.40E-19	1.000	383.0	1.72E-19	1.000	384.0	1.99E-19	1.000	385.0	1.90E-19	1.000
386.0	1.19E-19	1.000	387.0	5.65E-20	1.000	388.0	3.20E-20	1.000	389.0	1.90E-20	1.000	390.0	1.20E-20	1.000
391.0	5.00E-21	1.000	392.0	0.00E+00	1.000									
Photolysis File = H2O2														
250.0	8.30E-20	1.000	255.0	6.70E-20	1.000	260.0	5.20E-20	1.000	265.0	4.20E-20	1.000	270.0	3.20E-20	1.000
275.0	2.50E-20	1.000	280.0	2.00E-20	1.000	285.0	1.50E-20	1.000	290.0	1.13E-20	1.000	295.0	8.70E-21	1.000
300.0	6.60E-21	1.000	305.0	4.90E-21	1.000	310.0	3.70E-21	1.000	315.0	2.80E-21	1.000	320.0	2.00E-21	1.000
325.0	1.50E-21	1.000	330.0	1.20E-21	1.000	335.0	9.00E-22	1.000	340.0	7.00E-22	1.000	345.0	5.00E-22	1.000
350.0	3.00E-22	1.000	355.0	0.00E+00	1.000									

Table A-3. (continued)

WL (nm)	Abs (cm^2)	QY	WL (nm)	Abs (cm^2)	QY	WL (nm)	Abs (cm^2)	QY	WL (nm)	Abs (cm^2)	QY	WL (nm)	Abs (cm^2)	QY
Photolysis File = HCHONEWR														
280.0	2.49E-20	0.590	280.5	1.42E-20	0.596	281.0	1.51E-20	0.602	281.5	1.32E-20	0.608	282.0	9.73E-21	0.614
282.5	6.76E-21	0.620	283.0	5.82E-21	0.626	283.5	9.10E-21	0.632	284.0	3.71E-20	0.638	284.5	4.81E-20	0.644
285.0	3.95E-20	0.650	285.5	2.87E-20	0.656	286.0	2.24E-20	0.662	286.5	1.74E-20	0.668	287.0	1.13E-20	0.674
287.5	1.10E-20	0.680	288.0	2.62E-20	0.686	288.5	4.00E-20	0.692	289.0	3.55E-20	0.698	289.5	2.12E-20	0.704
290.0	1.07E-20	0.710	290.5	1.35E-20	0.713	291.0	1.99E-20	0.717	291.5	1.56E-20	0.721	292.0	8.65E-21	0.724
292.5	5.90E-21	0.727	293.0	1.11E-20	0.731	293.5	6.26E-20	0.735	294.0	7.40E-20	0.738	294.5	5.36E-20	0.741
295.0	4.17E-20	0.745	295.5	3.51E-20	0.749	296.0	2.70E-20	0.752	296.5	1.75E-20	0.755	297.0	1.16E-20	0.759
297.5	1.51E-20	0.763	298.0	3.69E-20	0.766	298.5	4.40E-20	0.769	299.0	3.44E-20	0.773	299.5	2.02E-20	0.776
300.0	1.06E-20	0.780	300.4	7.01E-21	0.780	300.6	8.63E-21	0.779	300.8	1.47E-20	0.779	301.0	2.01E-20	0.779
301.2	2.17E-20	0.779	301.4	1.96E-20	0.779	301.6	1.54E-20	0.778	301.8	1.26E-20	0.778	302.0	1.03E-20	0.778
302.2	8.53E-21	0.778	302.4	7.13E-21	0.778	302.6	6.61E-21	0.777	302.8	1.44E-20	0.777	303.0	3.18E-20	0.777
303.2	3.81E-20	0.777	303.4	5.57E-20	0.777	303.6	6.91E-20	0.776	303.8	6.58E-20	0.776	304.0	6.96E-20	0.776
304.2	5.79E-20	0.776	304.4	5.24E-20	0.776	304.6	4.30E-20	0.775	304.8	3.28E-20	0.775	305.0	3.60E-20	0.775
305.2	5.12E-20	0.775	305.4	4.77E-20	0.775	305.6	4.43E-20	0.774	305.8	4.60E-20	0.774	306.0	4.01E-20	0.774
306.2	3.28E-20	0.774	306.4	2.66E-20	0.774	306.6	2.42E-20	0.773	306.8	1.95E-20	0.773	307.0	1.58E-20	0.773
307.2	1.37E-20	0.773	307.4	1.19E-20	0.773	307.6	1.01E-20	0.772	307.8	9.01E-21	0.772	308.0	8.84E-21	0.772
308.2	2.08E-20	0.772	308.4	2.39E-20	0.772	308.6	3.08E-20	0.771	308.8	3.39E-20	0.771	309.0	3.18E-20	0.771
309.2	3.06E-20	0.771	309.4	2.84E-20	0.771	309.6	2.46E-20	0.770	309.8	1.95E-20	0.770	310.0	1.57E-20	0.770
310.2	1.26E-20	0.767	310.4	9.26E-21	0.764	310.6	7.71E-21	0.761	310.8	6.05E-21	0.758	311.0	5.13E-21	0.755
311.2	4.82E-21	0.752	311.4	4.54E-21	0.749	311.6	6.81E-21	0.746	311.8	1.04E-20	0.743	312.0	1.43E-20	0.740
312.2	1.47E-20	0.737	312.4	1.35E-20	0.734	312.6	1.13E-20	0.731	312.8	9.86E-21	0.728	313.0	7.82E-21	0.725
313.2	6.48E-21	0.722	313.4	1.07E-20	0.719	313.6	2.39E-20	0.716	313.8	3.80E-20	0.713	314.0	5.76E-20	0.710
314.2	6.14E-20	0.707	314.4	7.45E-20	0.704	314.6	5.78E-20	0.701	314.8	5.59E-20	0.698	315.0	4.91E-20	0.695
315.2	4.37E-20	0.692	315.4	3.92E-20	0.689	315.6	2.89E-20	0.686	315.8	2.82E-20	0.683	316.0	2.10E-20	0.680
316.2	1.66E-20	0.677	316.4	2.05E-20	0.674	316.6	4.38E-20	0.671	316.8	5.86E-20	0.668	317.0	6.28E-20	0.665
317.2	5.07E-20	0.662	317.4	4.33E-20	0.659	317.6	4.17E-20	0.656	317.8	3.11E-20	0.653	318.0	2.64E-20	0.650
318.2	2.24E-20	0.647	318.4	1.70E-20	0.644	318.6	1.24E-20	0.641	318.8	1.11E-20	0.638	319.0	7.70E-21	0.635
319.2	6.36E-21	0.632	319.4	5.36E-21	0.629	319.6	4.79E-21	0.626	319.8	6.48E-21	0.623	320.0	1.48E-20	0.620
320.2	1.47E-20	0.614	320.4	1.36E-20	0.608	320.6	1.69E-20	0.601	320.8	1.32E-20	0.595	321.0	1.49E-20	0.589
321.2	1.17E-20	0.583	321.4	1.15E-20	0.577	321.6	9.64E-21	0.570	321.8	7.26E-21	0.564	322.0	5.94E-21	0.558
322.2	4.13E-21	0.552	322.4	3.36E-21	0.546	322.6	2.39E-21	0.539	322.8	2.01E-21	0.533	323.0	1.76E-21	0.527
323.2	2.82E-21	0.521	323.4	4.65E-21	0.515	323.6	7.00E-21	0.508	323.8	7.80E-21	0.502	324.0	7.87E-21	0.496
324.2	6.59E-21	0.490	324.4	5.60E-21	0.484	324.6	4.66E-21	0.477	324.8	4.21E-21	0.471	325.0	7.77E-21	0.465
325.2	2.15E-20	0.459	325.4	3.75E-20	0.453	325.6	4.10E-20	0.446	325.8	6.47E-20	0.440	326.0	7.59E-20	0.434
326.2	6.51E-20	0.428	326.4	5.53E-20	0.422	326.6	5.76E-20	0.415	326.8	4.43E-20	0.409	327.0	3.44E-20	0.403
327.2	3.22E-20	0.397	327.4	2.13E-20	0.391	327.6	1.91E-20	0.384	327.8	1.42E-20	0.378	328.0	9.15E-21	0.372
328.2	6.79E-21	0.366	328.4	4.99E-21	0.360	328.6	4.77E-21	0.353	328.8	1.75E-20	0.347	329.0	3.27E-20	0.341
329.2	3.99E-20	0.335	329.4	5.13E-20	0.329	329.6	4.00E-20	0.322	329.8	3.61E-20	0.316	330.0	3.38E-20	0.310
330.2	3.08E-20	0.304	330.4	2.16E-20	0.298	330.6	2.09E-20	0.291	330.8	1.41E-20	0.285	331.0	9.95E-21	0.279
331.2	7.76E-21	0.273	331.4	6.16E-21	0.267	331.6	4.06E-21	0.260	331.8	3.03E-21	0.254	332.0	2.41E-21	0.248
332.2	1.74E-21	0.242	332.4	1.33E-21	0.236	332.6	2.70E-21	0.229	332.8	1.65E-21	0.223	333.0	1.17E-21	0.217
333.2	9.84E-22	0.211	333.4	8.52E-22	0.205	333.6	6.32E-22	0.198	333.8	5.21E-22	0.192	334.0	1.46E-21	0.186
334.2	1.80E-21	0.180	334.4	1.43E-21	0.174	334.6	1.03E-21	0.167	334.8	7.19E-22	0.161	335.0	4.84E-22	0.155
335.2	2.73E-22	0.149	335.4	1.34E-22	0.143	335.6	-1.62E-22	0.136	335.8	1.25E-22	0.130	336.0	4.47E-22	0.124
336.2	1.23E-21	0.118	336.4	2.02E-21	0.112	336.6	3.00E-21	0.105	336.8	2.40E-21	0.099	337.0	3.07E-21	0.093
337.2	2.29E-21	0.087	337.4	2.46E-21	0.081	337.6	2.92E-21	0.074	337.8	8.10E-21	0.068	338.0	1.82E-20	0.062
338.2	3.10E-20	0.056	338.4	3.24E-20	0.050	338.6	4.79E-20	0.043	338.8	5.25E-20	0.037	339.0	5.85E-20	0.031
339.2	4.33E-20	0.025	339.4	4.20E-20	0.019	339.6	3.99E-20	0.012	339.8	3.11E-20	0.006	340.0	2.72E-20	0.000
Photolysis File = HCHONEWM														
280.0	2.49E-20	0.350	280.5	1.42E-20	0.346	281.0	1.51E-20	0.341	281.5	1.32E-20	0.336	282.0	9.73E-21	0.332
282.5	6.76E-21	0.327	283.0	5.82E-21	0.323	283.5	9.10E-21	0.319	284.0	3.71E-20	0.314	284.5	4.81E-20	0.309
285.0	3.95E-20	0.305	285.5	2.87E-20	0.301	286.0	2.24E-20	0.296	286.5	1.74E-20	0.291	287.0	1.13E-20	0.287
287.5	1.10E-20	0.282	288.0	2.62E-20	0.278	288.5	4.00E-20	0.273	289.0	3.55E-20	0.269	289.5	2.12E-20	0.264
290.0	1.07E-20	0.260	290.5	1.35E-20	0.258	291.0	1.99E-20	0.256	291.5	1.56E-20	0.254	292.0	8.65E-21	0.252
292.5	5.90E-21	0.250	293.0	1.11E-20	0.248	293.5	6.26E-20	0.246	294.0	7.40E-20	0.244	294.5	5.36E-20	0.242
295.0	4.17E-20	0.240	295.5	3.51E-20	0.238	296.0	2.70E-20	0.236	296.5	1.75E-20	0.234	297.0	1.16E-20	0.232
297.5	1.51E-20	0.230	298.0	3.69E-20	0.228	298.5	4.40E-20	0.226	299.0	3.44E-20	0.224	299.5	2.02E-20	0.222
300.0	1.06E-20	0.220	300.4	7.01E-21	0.220	300.6	8.63E-21	0.221	300.8	1.47E-20	0.221	301.0	2.01E-20	0.221
301.2	2.17E-20	0.221	301.4	1.96E-20	0.221	301.6	1.54E-20	0.222	301.8	1.26E-20	0.222	302.0	1.03E-20	0.222
302.2	8.53E-21	0.222	302.4	7.13E-21	0.222	302.6	6.61E-21	0.223	302.8	1.44E-20	0.223	303.0	3.18E-20	0.223
303.2	3.81E-20	0.223	303.4	5.57E-20	0.223	303.6	6.91E-20	0.224	303.8	6.58E-20	0.224	304.0	6.96E-20	0.224
304.2	5.79E-20	0.224	304.4	5.24E-20	0.224	304.6	4.30E-20	0.225	304.8	3.28E-20	0.225	305.0	3.60E-20	0.225
305.2	5.12E-20	0.225	305.4	4.77E-20	0.225	305.6	4.43E-20	0.226	305.8	4.60E-20	0.226	306.0	4.01E-20	0.226
306.2	3.28E-20	0.226	306.4	2.66E-20	0.226	306.6	2.42E-20	0.227	306.8	1.95E-20	0.227	307.0	1.58E-20	0.227
307.2	1.37E-20	0.227	307.4	1.19E-20	0.227	307.6	1.01E-20	0.228	307.8	9.01E-21	0.228	308.0	8.84E-21	0.228
308.2	2.08E-20	0.228	308.4	2.39E-20	0.228	308.6	3.08E-20	0.229	308.8	3.39E-20	0.229	309.0	3.18E-20	0.229
309.2	3.06E-20	0.229	309.4	2.84E-20	0.229	309.6	2.46E-20	0.230	309.8	1.95E-20	0.230	310.0	1.57E-20	0.230
310.2	1.26E-20	0.233	310.4	9.26E-21	0.236	310.6	7.71E-21	0.239	310.8	6.05E-21	0.242	311.0	5.13E-21	0.245
311.2	4.82E-21	0.248	311.4	4.54E-21	0.251	311.6	6.81E-21	0.254	311.8	1.04E-20	0.257	312.0	1.43E-20	0.260
312.2	1.47E-20	0.263	312.4	1.35E-20	0.266	312.6	1.13E-20	0.269	312.8	9.86E-21	0.272	313.0	7.82E-21	0.275
313.2	6.48E-21	0.278	313.4	1.07E-20	0.281	313.6	2.39E-20	0.284	313.8	3.80E-20	0.287	314.0	5.76E-20	0.290
314.2	6.14E-20	0.293	314.4	7.45E-20	0.296	314.6	5.78E-20	0.299	314.8	5.59E-20	0.302	315.0	4.91E-20	0.305
315.2	4.37E-20	0.308	315.4	3.92E-20	0.311	315.6	2.89E-20	0.314	315.8	2.82E-20	0.317	316.0	2.10E-20	0.320
316.2	1.66E-20	0.323	316.4	2.05E-20	0.326	316.6	4.38E-20	0.329	316.8	5.86E-20	0.332	317.0	6.28E-20	0.335
317.2	5.07E-20	0.338	317.4	4.33E-20	0.341	317.6	4.17E-20	0.344	317.8	3.11E-20	0.347	318.0	2.64E-20	0.350
318.2	2.24E-20	0.353	318.4	1.70E-20	0.356	318.6	1.24E-20	0.359	318.8	1.11E-20	0.362	319.0	7.70E-21	0.365
319.2	6.36E-21	0.368	319.4	5.36E-21	0.371	319.6	4.79E-21	0.374	319.8	6.48E-21	0.377	320.0	1.48E-20	0.380
320.2	1.47E-20	0.386	320.4	1.36E-20	0.392	320.6	1.69E-20	0.399	320.8	1.32E-20	0.405	321.0	1.49E-20	0.411
321.2	1.17E-20	0.417	321.4	1.15E-20	0.423	321.6	9.64E-21	0.430	321.8	7.26E-21	0.436	322.0	5.94E-21	0.442
322.2	4.13E-21	0.448	322.4	3.36E-21	0.454	322.6	2.39E-21	0.461	322.8	2.01E-21	0.467	323.0	1.76E-21	0.473
323.2	2.82E-21	0.479	323.4	4.65E-21	0.485	323.6	7.00E-21	0.492	323.8	7.80E-21	0.498	324.0	7.87E-21	0.504
324.2	6.59E-21	0.510	324.4	5.60E-21	0.516	324.6	4.66E-21	0.523	324.8	4.21E-21	0.529	325.0	7.77E-21	0.535

Table A-3. (continued)

WL (nm)	Abs (cm^2)	QY	WL (nm)	Abs (cm^2)	QY	WL (nm)	Abs (cm^2)	QY	WL (nm)	Abs (cm^2)	QY	WL (nm)	Abs (cm^2)	QY
325.2	2.15E-20	0.541	325.4	3.75E-20	0.547	325.6	4.10E-20	0.554	325.8	6.47E-20	0.560	326.0	7.59E-20	0.566
326.2	6.51E-20	0.572	326.4	5.53E-20	0.578	326.6	5.76E-20	0.585	326.8	4.43E-20	0.591	327.0	3.44E-20	0.597
327.2	3.22E-20	0.603	327.4	2.13E-20	0.609	327.6	1.91E-20	0.616	327.8	1.42E-20	0.622	328.0	9.15E-21	0.628
328.2	6.79E-21	0.634	328.4	4.99E-21	0.640	328.6	4.77E-21	0.647	328.8	1.75E-20	0.653	329.0	3.27E-20	0.659
329.2	3.99E-20	0.665	329.4	5.13E-20	0.671	329.6	4.00E-20	0.678	329.8	3.61E-20	0.684	330.0	3.38E-20	0.690
330.2	3.08E-20	0.694	330.4	2.16E-20	0.699	330.6	2.09E-20	0.703	330.8	1.41E-20	0.708	331.0	9.95E-21	0.712
331.2	7.76E-21	0.717	331.4	6.16E-21	0.721	331.6	4.06E-21	0.726	331.8	3.03E-21	0.730	332.0	2.41E-21	0.735
332.2	1.74E-21	0.739	332.4	1.33E-21	0.744	332.6	2.70E-21	0.748	332.8	1.65E-21	0.753	333.0	1.17E-21	0.757
333.2	9.84E-22	0.762	333.4	8.52E-22	0.766	333.6	6.32E-22	0.771	333.8	5.21E-22	0.775	334.0	1.46E-21	0.780
334.2	1.80E-21	0.784	334.4	1.43E-21	0.789	334.6	1.03E-21	0.793	334.8	7.19E-22	0.798	335.0	4.84E-22	0.802
335.2	2.73E-22	0.798	335.4	1.34E-22	0.794	335.6	0.00E+00	0.790	335.8	1.25E-22	0.786	336.0	4.47E-22	0.782
336.2	1.23E-21	0.778	336.4	2.02E-21	0.773	336.6	3.00E-21	0.769	336.8	2.40E-21	0.764	337.0	3.07E-21	0.759
337.2	2.29E-21	0.754	337.4	2.46E-21	0.749	337.6	2.92E-21	0.745	337.8	8.10E-21	0.740	338.0	1.82E-20	0.734
338.2	3.10E-20	0.729	338.4	3.24E-20	0.724	338.6	4.79E-20	0.719	338.8	5.25E-20	0.714	339.0	5.85E-20	0.709
339.2	4.33E-20	0.703	339.4	4.20E-20	0.698	339.6	3.99E-20	0.693	339.8	3.11E-20	0.687	340.0	2.72E-20	0.682
340.2	1.99E-20	0.676	340.4	1.76E-20	0.671	340.6	1.39E-20	0.666	340.8	1.01E-20	0.660	341.0	6.57E-21	0.655
341.2	4.83E-21	0.649	341.4	3.47E-21	0.643	341.6	2.23E-21	0.638	341.8	1.55E-21	0.632	342.0	3.70E-21	0.627
342.2	4.64E-21	0.621	342.4	1.08E-20	0.616	342.6	1.14E-20	0.610	342.8	1.79E-20	0.604	343.0	2.33E-20	0.599
343.2	1.72E-20	0.593	343.4	1.55E-20	0.588	343.6	1.46E-20	0.582	343.8	1.38E-20	0.576	344.0	1.00E-20	0.571
344.2	8.26E-21	0.565	344.4	6.32E-21	0.559	344.6	4.28E-21	0.554	344.8	3.22E-21	0.548	345.0	2.54E-21	0.542
345.2	1.60E-21	0.537	345.4	1.15E-21	0.531	345.6	8.90E-22	0.525	345.8	6.50E-22	0.520	346.0	5.09E-22	0.514
346.2	5.15E-22	0.508	346.4	3.45E-22	0.503	346.6	3.18E-22	0.497	346.8	3.56E-22	0.491	347.0	3.24E-22	0.485
347.2	3.34E-22	0.480	347.4	2.88E-22	0.474	347.6	2.84E-22	0.468	347.8	9.37E-22	0.463	348.0	9.70E-22	0.457
348.2	7.60E-22	0.451	348.4	6.24E-22	0.446	348.6	4.99E-22	0.440	348.8	4.08E-22	0.434	349.0	3.39E-22	0.428
349.2	1.64E-22	0.423	349.4	1.49E-22	0.417	349.6	8.30E-23	0.411	349.8	2.52E-23	0.406	350.0	2.57E-23	0.400
350.2	0.00E+00	0.394	350.4	5.16E-23	0.389	350.6	0.00E+00	0.383	350.8	2.16E-23	0.377	351.0	7.07E-23	0.371
351.2	3.45E-23	0.366	351.4	1.97E-22	0.360	351.6	4.80E-22	0.354	351.8	3.13E-21	0.349	352.0	6.41E-21	0.343
352.2	8.38E-21	0.337	352.4	1.55E-20	0.331	352.6	1.86E-20	0.326	352.8	1.94E-20	0.320	353.0	2.78E-20	0.314
353.2	1.96E-20	0.309	353.4	1.67E-20	0.303	353.6	1.75E-20	0.297	353.8	1.63E-20	0.291	354.0	1.36E-20	0.286
354.2	1.07E-20	0.280	354.4	9.82E-21	0.274	354.6	8.66E-21	0.269	354.8	6.44E-21	0.263	355.0	4.84E-21	0.257
355.2	3.49E-21	0.251	355.4	2.41E-21	0.246	355.6	1.74E-21	0.240	355.8	1.11E-21	0.234	356.0	7.37E-22	0.229
356.2	4.17E-22	0.223	356.4	1.95E-22	0.217	356.6	1.50E-22	0.211	356.8	8.14E-23	0.206	357.0	0.00E+00	0.200
Photolysis File = CCHOR														
260.0	2.00E-20	0.310	270.0	3.40E-20	0.390	280.0	4.50E-20	0.580	290.0	4.90E-20	0.530	295.0	4.50E-20	0.480
300.0	4.30E-20	0.430	305.0	3.40E-20	0.370	315.0	2.10E-20	0.170	320.0	1.80E-20	0.100	325.0	1.10E-20	0.040
330.0	6.90E-21	0.000												
Photolysis File = RCHO														
280.0	5.26E-20	0.960	290.0	5.77E-20	0.910	300.0	5.05E-20	0.860	310.0	3.68E-20	0.600	320.0	1.66E-20	0.360
330.0	6.49E-21	0.200	340.0	1.44E-21	0.080	345.0	0.00E+00	0.020						
Photolysis File = ACET-93C (Standard Mechanism)														
250.0	2.37E-20	0.760	260.0	3.66E-20	0.800	270.0	4.63E-20	0.640	280.0	5.05E-20	0.550	290.0	4.21E-20	0.300
300.0	2.78E-20	0.150	310.0	1.44E-20	0.050	320.0	4.80E-21	0.026	330.0	8.00E-22	0.017	340.0	1.00E-22	0.000
350.0	3.00E-23	0.000	360.0	0.00E+00	0.000									
Photolysis File = ADJACET (Adjusted Mechanism)														
250.0	2.37E-20	0.760	260.0	3.66E-20	0.800	270.0	4.63E-20	0.640	280.0	5.05E-20	0.600	290.0	4.21E-20	0.600
300.0	2.78E-20	0.300	310.0	1.44E-20	0.005	320.0	4.80E-21	0.000	330.0	8.00E-22	0.000	340.0	1.00E-22	0.000
350.0	3.00E-23	0.000	360.0	0.00E+00	0.000									
Photolysis File = KETONE														
210.0	1.10E-21	0.100	220.0	1.20E-21	0.100	230.0	4.60E-21	0.100	240.0	1.30E-20	0.100	250.0	2.68E-20	0.100
260.0	4.21E-20	0.100	270.0	5.54E-20	0.100	280.0	5.92E-20	0.100	290.0	5.16E-20	0.100	300.0	3.44E-20	0.100
310.0	1.53E-20	0.100	320.0	4.60E-21	0.100	330.0	1.10E-21	0.100	340.0	0.00E+00	0.100			
Photolysis File = CO2H														
210.0	3.75E-19	1.000	220.0	2.20E-19	1.000	230.0	1.38E-19	1.000	240.0	8.80E-20	1.000	250.0	5.80E-20	1.000
260.0	3.80E-20	1.000	270.0	2.50E-20	1.000	280.0	1.50E-20	1.000	290.0	9.00E-21	1.000	300.0	5.80E-21	1.000
310.0	3.40E-21	1.000	320.0	1.90E-21	1.000	330.0	1.10E-21	1.000	340.0	6.00E-22	1.000	350.0	4.00E-22	1.000
360.0	0.00E+00	1.000												
Photolysis File = GLYOXAL1														
230.0	2.87E-21	1.000	235.0	2.87E-21	1.000	240.0	4.30E-21	1.000	245.0	5.73E-21	1.000	250.0	8.60E-21	1.000
255.0	1.15E-20	1.000	260.0	1.43E-20	1.000	265.0	1.86E-20	1.000	270.0	2.29E-20	1.000	275.0	2.58E-20	1.000
280.0	2.87E-20	1.000	285.0	3.30E-20	1.000	290.0	3.15E-20	1.000	295.0	3.30E-20	1.000	300.0	3.58E-20	1.000
305.0	2.72E-20	1.000	310.0	2.72E-20	1.000	312.5	2.87E-20	1.000	315.0	2.29E-20	1.000	320.0	1.43E-20	1.000
325.0	1.15E-20	1.000	327.5	1.43E-20	1.000	330.0	1.15E-20	1.000	335.0	2.87E-21	1.000	340.0	0.00E+00	1.000
Photolysis File = GLYOXAL2														
355.0	0.00E+00	0.029	360.0	2.29E-21	0.029	365.0	2.87E-21	0.029	370.0	8.03E-21	0.029	375.0	1.00E-20	0.029
380.0	1.72E-20	0.029	382.0	1.58E-20	0.029	384.0	1.49E-20	0.029	386.0	1.49E-20	0.029	388.0	2.87E-20	0.029
390.0	3.15E-20	0.029	391.0	3.24E-20	0.029	392.0	3.04E-20	0.029	393.0	2.23E-20	0.029	394.0	2.63E-20	0.029
395.0	3.04E-20	0.029	396.0	2.63E-20	0.029	397.0	2.43E-20	0.029	398.0	3.24E-20	0.029	399.0	3.04E-20	0.029
400.0	2.84E-20	0.029	401.0	3.24E-20	0.029	402.0	4.46E-20	0.029	403.0	5.27E-20	0.029	404.0	4.26E-20	0.029
405.0	3.04E-20	0.029	406.0	3.04E-20	0.029	407.0	2.84E-20	0.029	408.0	2.43E-20	0.029	409.0	2.84E-20	0.029
410.0	6.08E-20	0.029	411.0	5.07E-20	0.029	411.5	6.08E-20	0.029	412.0	4.86E-20	0.029	413.0	8.31E-20	0.029
413.5	6.48E-20	0.029	414.0	7.50E-20	0.029	414.5	8.11E-20	0.029	415.0	8.11E-20	0.029	415.5	6.89E-20	0.029
416.0	4.26E-20	0.029	417.0	4.86E-20	0.029	418.0	5.88E-20	0.029	419.0	6.69E-20	0.029	420.0	3.85E-20	0.029
421.0	5.67E-20	0.029	421.5	4.46E-20	0.029	422.0	5.27E-20	0.029	422.5	1.05E-19	0.029	423.0	8.51E-20	0.029
424.0	6.08E-20	0.029	425.0	7.29E-20	0.029	426.0	1.18E-19	0.029	426.5	1.30E-19	0.029	427.0	1.07E-19	0.029
428.0	1.66E-19	0.029	429.0	4.05E-20	0.029	430.0	5.07E-20	0.029	431.0	4.86E-20	0.029	432.0	4.05E-20	0.029
433.0	3.65E-20	0.029	434.0	4.05E-20	0.029	434.5	6.08E-20	0.029	435.0	5.07E-20	0.029	436.0	8.11E-20	0.029

Table A-3. (continued)

WL (nm)	Abs (cm^2)	QY	WL (nm)	Abs (cm^2)	QY	WL (nm)	Abs (cm^2)	QY	WL (nm)	Abs (cm^2)	QY	WL (nm)	Abs (cm^2)	QY
436.5	1.13E-19	0.029	437.0	5.27E-20	0.029	438.0	1.01E-19	0.029	438.5	1.38E-19	0.029	439.0	7.70E-20	0.029
440.0	2.47E-19	0.029	441.0	8.11E-20	0.029	442.0	6.08E-20	0.029	443.0	7.50E-20	0.029	444.0	9.32E-20	0.029
445.0	1.13E-19	0.029	446.0	5.27E-20	0.029	447.0	2.43E-20	0.029	448.0	2.84E-20	0.029	449.0	3.85E-20	0.029
450.0	6.08E-20	0.029	451.0	1.09E-19	0.029	451.5	9.32E-20	0.029	452.0	1.22E-19	0.029	453.0	2.39E-19	0.029
454.0	1.70E-19	0.029	455.0	3.40E-19	0.029	455.5	4.05E-19	0.029	456.0	1.01E-19	0.029	457.0	1.62E-20	0.029
458.0	1.22E-20	0.029	458.5	1.42E-20	0.029	459.0	4.05E-21	0.029	460.0	4.05E-21	0.029	460.5	6.08E-21	0.029
461.0	2.03E-21	0.029	462.0	0.00E+00	0.029									
Photolysis File = MEGLYOX1														
220.0	2.10E-21	1.000	225.0	2.10E-21	1.000	230.0	4.21E-21	1.000	235.0	7.57E-21	1.000	240.0	9.25E-21	1.000
245.0	8.41E-21	1.000	250.0	9.25E-21	1.000	255.0	9.25E-21	1.000	260.0	9.67E-21	1.000	265.0	1.05E-20	1.000
270.0	1.26E-20	1.000	275.0	1.43E-20	1.000	280.0	1.51E-20	1.000	285.0	1.43E-20	1.000	290.0	1.47E-20	1.000
295.0	1.18E-20	1.000	300.0	1.14E-20	1.000	305.0	9.25E-21	1.000	310.0	6.31E-21	1.000	315.0	5.47E-21	1.000
320.0	3.36E-21	1.000	325.0	1.68E-21	1.000	330.0	8.41E-22	1.000	335.0	0.00E+00	1.000			
Photolysis File = MEGLYOX2														
350.0	0.00E+00	1.000	354.0	4.21E-22	1.000	358.0	1.26E-21	1.000	360.0	2.10E-21	1.000	362.0	2.10E-21	1.000
364.0	2.94E-21	1.000	366.0	3.36E-21	1.000	368.0	4.21E-21	1.000	370.0	5.47E-21	1.000	372.0	5.89E-21	1.000
374.0	7.57E-21	1.000	376.0	7.99E-21	1.000	378.0	8.83E-21	1.000	380.0	1.01E-20	1.000	382.0	1.09E-20	1.000
384.0	1.35E-20	1.000	386.0	1.51E-20	1.000	388.0	1.72E-20	1.000	390.0	2.06E-20	1.000	392.0	2.10E-20	1.000
394.0	2.31E-20	1.000	396.0	2.48E-20	1.000	398.0	2.61E-20	1.000	400.0	2.78E-20	1.000	402.0	2.99E-20	1.000
404.0	3.20E-20	1.000	406.0	3.79E-20	1.000	408.0	3.95E-20	1.000	410.0	4.33E-20	1.000	412.0	4.71E-20	1.000
414.0	4.79E-20	1.000	416.0	4.88E-20	1.000	418.0	5.05E-20	1.000	420.0	5.21E-20	1.000	422.0	5.30E-20	1.000
424.0	5.17E-20	1.000	426.0	5.30E-20	1.000	428.0	5.21E-20	1.000	430.0	5.55E-20	1.000	432.0	5.13E-20	1.000
434.0	5.68E-20	1.000	436.0	6.22E-20	1.000	438.0	6.06E-20	1.000	440.0	5.47E-20	1.000	441.0	6.14E-20	1.000
442.0	5.47E-20	1.000	443.0	5.55E-20	1.000	443.5	6.81E-20	1.000	444.0	5.97E-20	1.000	445.0	5.13E-20	1.000
446.0	4.88E-20	1.000	447.0	5.72E-20	1.000	448.0	5.47E-20	1.000	449.0	6.56E-20	1.000	450.0	5.05E-20	1.000
451.0	3.03E-20	1.000	452.0	4.29E-20	1.000	453.0	2.78E-20	1.000	454.0	2.27E-20	1.000	456.0	1.77E-20	1.000
458.0	8.41E-21	1.000	460.0	4.21E-21	1.000	464.0	1.68E-21	1.000	468.0	0.00E+00	1.000			
Photolysis File = BZCHO														
299.0	1.78E-19	0.050	304.0	7.40E-20	0.050	306.0	6.91E-20	0.050	309.0	6.41E-20	0.050	313.0	6.91E-20	0.050
314.0	6.91E-20	0.050	318.0	6.41E-20	0.050	325.0	8.39E-20	0.050	332.0	7.65E-20	0.050	338.0	8.88E-20	0.050
342.0	8.88E-20	0.050	346.0	7.89E-20	0.050	349.0	7.89E-20	0.050	354.0	9.13E-20	0.050	355.0	8.14E-20	0.050
364.0	5.67E-20	0.050	368.0	6.66E-20	0.050	369.0	8.39E-20	0.050	370.0	8.39E-20	0.050	372.0	3.45E-20	0.050
374.0	3.21E-20	0.050	376.0	2.47E-20	0.050	377.0	2.47E-20	0.050	380.0	3.58E-20	0.050	382.0	9.90E-21	0.050
386.0	0.00E+00	0.050												
Photolysis File = ACROLEIN														
250.0	1.80E-21	1.000	252.0	2.05E-21	1.000	253.0	2.20E-21	1.000	254.0	2.32E-21	1.000	255.0	2.45E-21	1.000
256.0	2.56E-21	1.000	257.0	2.65E-21	1.000	258.0	2.74E-21	1.000	259.0	2.83E-21	1.000	260.0	2.98E-21	1.000
261.0	3.24E-21	1.000	262.0	3.47E-21	1.000	263.0	3.58E-21	1.000	264.0	3.93E-21	1.000	265.0	4.67E-21	1.000
266.0	5.10E-21	1.000	267.0	5.38E-21	1.000	268.0	5.73E-21	1.000	269.0	6.13E-21	1.000	270.0	6.64E-21	1.000
271.0	7.20E-21	1.000	272.0	7.77E-21	1.000	273.0	8.37E-21	1.000	274.0	8.94E-21	1.000	275.0	9.55E-21	1.000
276.0	1.04E-20	1.000	277.0	1.12E-20	1.000	278.0	1.19E-20	1.000	279.0	1.27E-20	1.000	280.0	1.27E-20	1.000
281.0	1.26E-20	1.000	282.0	1.26E-20	1.000	283.0	1.28E-20	1.000	284.0	1.33E-20	1.000	285.0	1.38E-20	1.000
286.0	1.44E-20	1.000	287.0	1.50E-20	1.000	288.0	1.57E-20	1.000	289.0	1.63E-20	1.000	290.0	1.71E-20	1.000
291.0	1.78E-20	1.000	292.0	1.86E-20	1.000	293.0	1.95E-20	1.000	294.0	2.05E-20	1.000	295.0	2.15E-20	1.000
296.0	2.26E-20	1.000	297.0	2.37E-20	1.000	298.0	2.48E-20	1.000	299.0	2.60E-20	1.000	300.0	2.73E-20	1.000
301.0	2.85E-20	1.000	302.0	2.99E-20	1.000	303.0	3.13E-20	1.000	304.0	3.27E-20	1.000	305.0	3.39E-20	1.000
306.0	3.51E-20	1.000	307.0	3.63E-20	1.000	308.0	3.77E-20	1.000	309.0	3.91E-20	1.000	310.0	4.07E-20	1.000
311.0	4.25E-20	1.000	312.0	4.39E-20	1.000	313.0	4.44E-20	1.000	314.0	4.50E-20	1.000	315.0	4.59E-20	1.000
316.0	4.75E-20	1.000	317.0	4.90E-20	1.000	318.0	5.05E-20	1.000	319.0	5.19E-20	1.000	320.0	5.31E-20	1.000
321.0	5.43E-20	1.000	322.0	5.52E-20	1.000	323.0	5.60E-20	1.000	324.0	5.67E-20	1.000	325.0	5.67E-20	1.000
326.0	5.62E-20	1.000	327.0	5.63E-20	1.000	328.0	5.71E-20	1.000	329.0	5.76E-20	1.000	330.0	5.80E-20	1.000
331.0	5.95E-20	1.000	332.0	6.23E-20	1.000	333.0	6.39E-20	1.000	334.0	6.38E-20	1.000	335.0	6.24E-20	1.000
336.0	6.01E-20	1.000	337.0	5.79E-20	1.000	338.0	5.63E-20	1.000	339.0	5.56E-20	1.000	340.0	5.52E-20	1.000
341.0	5.54E-20	1.000	342.0	5.53E-20	1.000	343.0	5.47E-20	1.000	344.0	5.41E-20	1.000	345.0	5.40E-20	1.000
346.0	5.48E-20	1.000	347.0	5.90E-20	1.000	348.0	6.08E-20	1.000	349.0	6.00E-20	1.000	350.0	5.53E-20	1.000
351.0	5.03E-20	1.000	352.0	4.50E-20	1.000	353.0	4.03E-20	1.000	354.0	3.75E-20	1.000	355.0	3.55E-20	1.000
356.0	3.45E-20	1.000	357.0	3.46E-20	1.000	358.0	3.49E-20	1.000	359.0	3.41E-20	1.000	360.0	3.23E-20	1.000
361.0	2.95E-20	1.000	362.0	2.81E-20	1.000	363.0	2.91E-20	1.000	364.0	3.25E-20	1.000	365.0	3.54E-20	1.000
366.0	3.30E-20	1.000	367.0	2.78E-20	1.000	368.0	2.15E-20	1.000	369.0	1.59E-20	1.000	370.0	1.19E-20	1.000
371.0	8.99E-21	1.000	372.0	7.22E-21	1.000	373.0	5.86E-21	1.000	374.0	4.69E-21	1.000	375.0	3.72E-21	1.000
376.0	3.57E-21	1.000	377.0	3.55E-21	1.000	378.0	2.83E-21	1.000	379.0	1.69E-21	1.000	380.0	8.29E-24	1.000
381.0	0.00E+00	1.000												